

POLITECNICO DI TORINO

Collegio di Ingegneria Meccanica, Aerospaziale, dell'Autoveicolo e della Produzione

Corso di Laurea Magistrale in Ingegneria Aerospaziale

Tesi di Laurea Magistrale

Design for Lagrangian Points Trajectories. A Complete Force Model Approach



Relatore

prof. Lorenzo Casalino

Candidato

Alessandro Benetton

Marzo 2018

Ai miei Genitori

A Michela

Summary

List of Figures	v
List of Tables	viii
Abstract	ix
1 Dynamics of the Three Body Problem	1
1.1 Historical introduction and basic laws of orbital mechanics	1
1.2 The N-Body Problem	2
1.3 Circular Restricted Three Body Problem	4
1.3.1 Pseudo Potential and Jacobi Constant	6
1.3.2 Libration Points	7
1.3.3 Linearized Solutions to the CR3BP	9
1.4 Lagrangian Points Orbits Applications	11
1.4.1 Earth-Moon System	11
1.4.2 Sun-Earth System	13
1.5 Astrodynamic Constants	19
2 CR3BP approach to Trajectory Construction	22
2.1 Computational Approach	23
2.1.1 Introduction to Numerical Integration Methods	24
2.1.2 Runge-Kutta Method	25
2.2 Quasi-Periodic Orbits	28
2.3 Transfer Phase	32
3 Complete Force Model	37
3.1 Perturbations to the CR3BP	37
3.1.1 Introducing The Elliptical Restricted Three Body Problem	38
3.1.2 Solar Radiation Pressure	40
3.1.3 Third Bodies Perturbations	41
3.2 Ephemerides Approach to Complete Force Field Design	42
3.2.1 SPICE Toolbox	44
3.2.2 Perturbations Effects	46
4 Complete Force Model Approach to Trajectory Optimization	49
4.1 Computational Approach	49
4.1.1 Dimensionalize the CR3BP Solution	50
4.1.2 Trajectory Arcs Construction	52
4.2 Algorithm Validation	56

5	Results	60
5.1	Trajectories Found	60
5.1.1	Nominal Periodic Orbit Selection	60
5.1.2	Variables domain	61
5.1.3	CR3BP Solution	63
5.1.4	Complete Force Model Solution	65
5.2	Response Surfaces based on preliminary DV budget	71
5.2.1	DV budget estimation	71
5.2.2	Building Response Surfaces	74
5.2.3	Final Optimization	80
5.3	STK Simulation	84
5.3.1	Result Validation	84
5.3.2	Analysis Report	89
5.3.3	Ignition Sequence Optimization	92
	Conclusions	x
	Bibliography	xi

List of Figures

1.1	N-body model representation	3
1.2	Geometric Schematization of the Restricted Three Body Problem	4
1.3	Zero velocity curves in the Earth-Moon system, shown in the synodic frame. The libration points are shown as red dots.	7
1.4	Libration Points, synodic reference frame. Earth-Moon system	8
1.5	Lissajous Orbit around L2 in the adimensionalized synodic frame, Earth-Moon system. $A_x=10000\text{km}$, $A_z=1000\text{km}$, propagation time 100 days	10
1.6	Sun-Earth System Representation	12
1.7	ARTEMIS's Artist's Impression	13
1.8	Herschel's Artist's Impression	14
1.9	Gaia's First Sky Map	15
1.10	Euclid Artist's Impression	16
1.11	SOHO Trajectory Representation	18
1.12	LISA Pathfinder's Journey to Space	19
2.1	Euler's Method Principle Representation	25
2.2	Initial Condition, Definition Process	29
2.3	Numerical QPO. $A_x=2e5$, $A_z=5e4$, $\phi=180\text{deg}$	29
2.4	Numerical QPO. $A_x=2e5$, $A_z=1e4$, $\phi=180\text{deg}$	30
2.5	Numerical QPO. $A_x=3e5$, $A_z=5e4$, $\phi=180\text{deg}$	30
2.6	Numerical QPO. $A_x=2e5$, $A_z=5e4$, $\phi=135\text{deg}$	31
2.7	Numerical QPO. $A_x=2e5$, $A_z=5e4$, $\phi=225\text{deg}$	31
2.8	Numerical QPO around L1. $A_x=2e5$, $A_z=5e4$, $\phi=0\text{deg}$	32
2.9	Transfer Trajectory. QPO: $A_x=2e5$, $A_z=5e4$, $\phi=180\text{deg}$	33
2.10	Transfer Trajectory. QPO: $A_x=2e5$, $A_z=1e4$, $\phi=180\text{deg}$	33
2.11	Transfer Trajectory. QPO: $A_x=3e5$, $A_z=5e4$, $\phi=180\text{deg}$	34
2.12	Transfer Trajectory. QPO: $A_x=2e5$, $A_z=5e4$, $\phi=135\text{deg}$	34
2.13	Transfer Trajectory. QPO: $A_x=2e5$, $A_z=5e4$, $\phi=225\text{deg}$	35
2.14	Transfer Trajectory. QPO around L1: $A_x=2e5$, $A_z=5e4$, $\phi=0\text{deg}$	35
3.1	Earth's Orbit Eccentricity and Semi-Major Axis Variation; 1 Year Time Span, from 01 Jan 2019 to 01 Jan 2020	39
3.2	Moon's Orbit Eccentricity and Semi-Major Axis Variation; 1 Year Time Span, from 01 Jan 2019 to 01 Jan 2020	39
3.3	Solar System Representation	42
3.4	J2000 Reference Frame Rappresentation	45
3.5	Propagators Confrontation. Distance [km] from H0 Trajectory	47

3.6	Terminal Section of Position Error Confrontation Curve	47
3.7	Propagators Confrontation. Velocity [m/s] (respect to the Earth)	47
3.8	Terminal Section of Velocity Error Confrontation Curve	48
3.9	H4 and H4Mod Propagators Confrontation. Distance Magnitude [km] from H0 Trajectory	48
4.1	Dimensionalization Comparison. Constant Sun-Earth Distance (shaded in red); Real Sun-Earth Distance (shaded in blue). Earth Centered Synodic Ref Frame.	50
4.2	Dimensionalization Comparison. Constant Sun-Earth Distance (shaded in red); Real Sun-Earth Distance (shaded in blue). Solar System Barycenter, J2000 Ref Frame.	51
4.3	Schematic Representation of a Single Step of the Iterative Cor- rection Process.	52
4.4	Final Corrected Trajectory Representation. CR3BP Trajectory at Variable Primary Distances Dimensionalization (shaded in blue), Complete Force Model Trajectory (shaded in red), Mesh Points (cyan dots). Earth Centered Synodic Ref Frame.	55
4.5	Reference Euclid Trajectory (RET). Earth Centered Synodic Ref- erence Frame	56
4.6	RET (shaded in blue). Computed CR3BP Trajectory (shaded in red)	57
4.7	STK representation of both RET and computed trajectory.	58
4.8	RET (shaded in blue). Final Corrected Trajectory (shaded in red)	59
5.1	Earth's Orbit around the Sun	62
5.2	Moon's Orbit around the Earth	62
5.3	Domain of Final Trajectory Variables	63
5.4	T200-050, Insertion Phase Angle in QPO 135, CR3BP propagation	64
5.5	T200-050, Insertion Phase Angle in QPO 180, CR3BP propagation	64
5.6	T200-050, Insertion Phase Angle in QPO 225, CR3BP propagation	65
5.7	Complete Force Field representation for a representative Epoch span, L1 and L2 positions are approximated and based on CR3BP	66
5.8	Mesh Points for T200-050 Trajectory, launch date 15 MAR 2019, Insertion Angle 180	67
5.9	Different views of T200-050 propagated considering the complete force model and different launch epoch values, insertion angle in QPO value 135	68
5.10	Different views of T200-050 propagated considering the complete force model and different launch epoch values, insertion angle in QPO value 180	69
5.11	Different views of T200-050 propagated considering the complete force model and different launch epoch values, insertion angle in QPO value 225	70
5.12	Graphical velocity discontinuity representation	71
5.13	Percentage weight of Sun-Earth combined gravitational effect over total force per unit of mass perceived by the probe, eval- uated according to the complete force model	73
5.14	Probe distance from Earth and Moon, spanning from 15 MAR 2019 16:00 to 26 MAR 2019 16:00	74

5.15	STK Visualization of relative positions of Earth, Moon and Probe at different mesh point epochs	76
5.16	Response Surface, Trajectory T200-050	77
5.17	Response Surface, Trajectory T200-010	78
5.18	Response Surface, Trajectory T300-050	79
5.19	Overall DV values for T200-050, insertion phase angle 180 degrees; launch epoch spans from 01 MAR 2019 to 01 APR 2019	81
5.20	Overall DV values for T200-050, insertion phase angle 135 degrees; launch epoch spans from 01 MAR 2019 to 01 APR 2019	82
5.21	Overall DV values for T200-050, insertion phase angle 180 degrees; launch epoch spans from 01 OCT 2019 to 01 NOV 2019	82
5.22	Overall DV values for T200-050, insertion phase angle 135 degrees; launch epoch spans from 01 OCT 2019 to 01 NOV 2019	83
5.23	Simulation of PT135 trajectory	85
5.24	Simulation of PT180 trajectory	86
5.25	Different Views of Simulated PT135 and PT180	87
5.26	Deviation between PT135 and the related simulated trajectory	89
5.27	Deviation between PT180 and the related simulated trajectory	90
5.28	Distances Values Evolution, PT135	90
5.29	Distances Values Evolution, PT180	91
5.30	Acceleration Values Evolution, PT135	91
5.31	Acceleration Values Evolution, PT180	92
5.32	Acceleration Values Evolution, enlarged visual; from this diagram it is possible to observe the initial drop	92

List of Tables

1.1	Planetary Constants	20
1.2	Lagrangian Points Dimensionless Coordinates	20
1.3	Lagrangian Points Coordinates	21
3.1	Earth's Orbit Keplerian Elements. Values validity: 1800 AD - 2050 AD	39
3.2	Moon's Orbit Keplerian Elements. Epoch: 01 Jan 2000 12:00:00.000	39
3.3	Euclid's spacecraft main characteristics	41
3.4	Kernels Contents	45
5.1	Estimated DV	72
5.2	Best solution found, Trajectory T200-050	80
5.3	Refined solutions achieved optimizing the launch epoch, Trajec- tory T200-050	83
5.4	DV Budget Validation, PT135	88
5.5	DV Budget Validation, PT180	89
5.6	DV Budget Comparison, PT135	93
5.7	DV Budget Comparison, PT180	94

Abstract

In the framework of the Circular Restricted Three Body Problem, this work aims to identify and design particular trajectories connecting the Earth and a family of quasi-periodic orbit around the collinear libration points in the Sun-Earth system. These particular periodic orbits represent the state of the art, in terms of trajectory design, concerning the majority of the space missions targeting tasks as the solar system observation, outer space observation or particular events observation (i.e. gravitational waves).

Firstly it has been developed a computational procedure to integrate the differential equations of motion deriving from the CR3BP model in an effort to design separately both the transfer phase to the QPO and the QPO itself. Then, aiming to define a much more close to reality force model, it has been taken in consideration many different perturbations. Simplifications regarding the circular and planar orbits of the primary bodies have been overcome considering the evolution in time of both Sun and Earth ephemerides respect to the solar system barycenter. In this sense, for the purpose of this research, it has been decided to directly solve the differential equations of motion for the generic probe given the position of other N bodies (contributions of both inner and outer solar system planets have been considered, obviously also the Moon gravitational field effect has been investigated). To obtain the final set of equations it has been added the solar radiation pressure contribution, considering a simple spherical model.

Finally, adopting the CR3BP trajectory as reference, the complete force model differential equations have been integrated with intent to revisit the baseline solution by minimizing the number and the overall cost of the necessary correction maneuvers. Many trajectories have been designed aiming to optimize the departure-from-the-Earth epoch and the geometric characteristics of the QPO insertion.

Chapter 1

Dynamics of the Three Body Problem

On Christmas Day, 1642, the year Galileo died, there was born in the Manor house of Woolsthorpe-by-Colsterworth a male infant so tiny that, as his mother told him in later years, he might have been put into a quart mug, and so frail that he had to wear a bolster around his neck to support his head. This unfortunate creature was entered in the parish register as 'Isaac son of Isaac and Hanna Newton'. There is no record that the wise men honored the occasion, yet this child was to alter the thought and habit of the world.

-James R.Newman[2]

1.1 Historical introduction and basic laws of orbital mechanics

Before Isaac Newton's birth, two men prepared the ground to his fundamental discoveries. These two scientist are the Dane Tycho Brahe and Johannes Von Kepler; Brahe put together an incredibly meticulous series of data regarding Mars' position and other planets, Kepler was gifted with the patience and innate mathematical perception needed to unlock the secrets hidden in Tycho's data. It's important to understand that since the time of Aristotle, planets were assumed to revolve in circular path or combinations of smaller circles moving on larger ones, but referring to the accurate research of Brahe, Kepler found immense difficulties in recognize such a theory as correct. From 1601 and 1606, Kepler tried to fit lots of geometrical curves to Brahe's Mars observation. After many years and attempts, finally in 1609 he grasped the solution to his problem and identified the elliptical nature of falling object's motion and published his first two laws of motion; the third came out in 1613:

- *First Law* - The orbit of each planet is an ellipse, with the Sun at focus.
- *Second Law* - The line joining the planet to the Sun sweeps out equal areas in equal times.
- *Third Law* - The square of the period of a planet is proportional to the cube of its mean distance from the Sun.

The three fundamental Kepler's laws describe only the aspect and the geometrical characteristics of planets motion, however there was still an unsolved riddle, the nature of this motion; few years later Isaac Newton unveiled the answer to the major question: 'why are the planets moving along such an elliptical path?'. During a 2-year closing period of the University of Cambridge, due to the plague, in 1666 the 23 years old Isaac Newton conceived the law of gravitation, the laws of motion and developed the fundamental concepts of the differential calculus. Anyway the entire scientific community learns about his discoveries only twenty years later, in 1685, Edmund Halley, consulting Newton in Cambridge about the planetary motion, casually disclosed the aforementioned Newton's researches. In 1687 sir Isaac Newton published his masterpiece, *The Mathematical Principles of Natural Philosophy* or more simply, the *Principia*, one of the main achievements of the human knowledge about physics.

In the first book of the *Principia* the famous three laws of motions are introduced:

- *First Law* - Every body continues in its state of rest or of uniform motion in a straight line unless it is compelled to change that state by forces impressed upon it.
- *Second Law* - The rate of change of momentum is proportional to the force impressed and is in the same direction as that force.
- *Third Law* - To every action there is always opposed and equal reaction.

It is possible to notice that the second law can be rewrote mathematically as follows:

$$\Sigma \mathbf{F} = m\ddot{\mathbf{r}} \quad (1.1)$$

Where $\Sigma \mathbf{F}$ refers to the sum of all the forces perceived by the point mass m , resulting in an acceleration of the mass itself, $\ddot{\mathbf{r}}$, measured in an inertial reference frame. Besides the three fundamental laws of motion, Isaac Newton formulated the law of gravity asserting that two bodies attract each other with a force directly proportional to the product of their masses and inversely proportional to the square of the distance between them. Using the vector notation, this law can be expressed as follow:

$$\mathbf{F}_g = -\frac{GMm}{r^2} \frac{\mathbf{r}}{r} \quad (1.2)$$

Where \mathbf{F}_g is the force on mass m due to mass M and \mathbf{r} is the vector from M to m . G refers to the *Universal Gravitational Constant*. Applying equation (1.2) to equation (1.1), it is possible to develop the equation of motion of planets and satellites.

1.2 The N-Body Problem

During its motion, a body (i.e. a satellite, a probe or a celestial body) is being affected by many gravitational forces and could experience other forces of different nature, as example, for the purpose of this research, the solar radiation pressure. It is possible to refer to this model considering a system of n -bodies

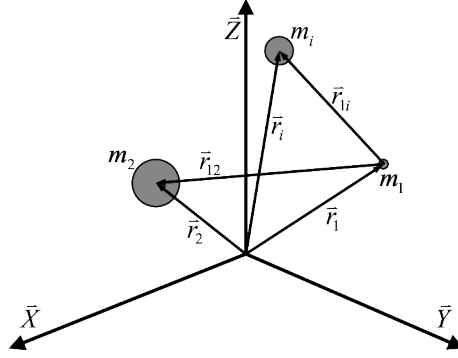


Figure 1.1: N-body model representation

$(m_1, m_2, \dots, m_i, \dots, m_N)$, m_i is the body whose motion is the objective of the analysis. Figure 1.1 enlightens schematically the characteristics of the N-body model. It is aiming to determine how this body move through the force field experiencing all the gravitational forces related to aforementioned point masses, without neglecting additional forces. The resulting equation motion is a vector sum of all gravitational forces and other external. The first step is to choose an inertial reference frame in which, during the time of analysis, all the position vectors of involved bodies are known. Applying the Newton's law of universal gravitation (1.2), it is possible to explicate the formulation of force \mathbf{F}_{gn} excited by the n^{th} body on m_i , the body whose motion it is trying to evaluate

$$\mathbf{F}_{gn} = -\frac{Gm_i m_n}{r_{ni}^3} \mathbf{r}_{ni} \quad (1.3)$$

Where the distance vector between the n^{th} body and m_i has been expressed as

$$\mathbf{r}_{ni} = \mathbf{r}_i - \mathbf{r}_n \quad (1.4)$$

Thus the sum vector of all the gravitational forces acting on body m_i may be written as

$$\mathbf{F}_g = -\frac{Gm_i m_1}{r_{1i}^3} \mathbf{r}_{1i} - \frac{Gm_i m_2}{r_{2i}^3} \mathbf{r}_{2i} - \dots - \frac{Gm_i m_n}{r_{ni}^3} \mathbf{r}_{ni} \quad (1.5)$$

Obviously in the equation (1.5) the contribution relative to the attraction force excited by the i^{th} body on itself. Using the summation notation the equation (1.5) could be explicated as

$$\mathbf{F}_g = -Gm_i \sum_{j=1, j \neq i}^n \frac{m_j}{r_{ji}^3} \mathbf{r}_{ij} \quad (1.6)$$

Assuming that the mass of the i^{th} body remains constant, it is possible to write the formulation of the i^{th} body acceleration vector as

$$\ddot{\mathbf{r}}_i = \frac{\mathbf{F}_{TOTAL}}{m_i} \quad (1.7)$$

Where \mathbf{F}_{TOTAL} represents the sum of the gravitational forces acting on the i^{th} body, equation (1.6), and the other external forces. For the purpose of this

research will be considered the effect of the solar radiation pressure and the effect of Earth's oblateness, Chapter 3. It will be used a numerical integration method to achieve a numerical solution to the differential equations of motion (1.7).

1.3 Circular Restricted Three Body Problem

The formulation of the CR3BP presented in this Chapter, follows the work of Victor Szebehely, one of the key figure in the development of the Apollo program. His text, *Theory of Orbits*, is considered the definitive text about the restricted three body problem; further explanations of the formulation of equations of motion here presented could be found far more detailed in his publication [4].

The restricted three body problem has to be considered as a simplification of the N-body problem. This model takes into account only three bodies, a primary and a secondary body (collectively termed the primaries) and a third characterized by a mass negligible respect to the others; this third body has to be considered as the generic probe whose motion it is trying to identify. Figure

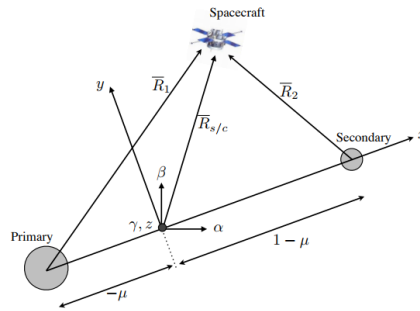


Figure 1.2: Geometric Schematization of the Restricted Three Body Problem

1.2 schematically shows the geometrical representation of the restricted three body problem model. It has been assumed that the primaries are subject to the Keplerian laws of motion and each of them describe a circular orbit around the barycenter of the system; according to the assumption of the third body negligible mass respect to the others, the system barycenter could be evaluated considering only the primary bodies. Then it is possible to analyze the motion of the generic spacecraft, the third body, in a non-inertial frame of reference which rotates about the center of mass of the system; such a reference frame is defined as a synodic or rotating reference frame. Referring to Figure 1.2 an inertial coordinate system α, β, γ is centered at the barycenter. Synodic frame is denoted by the x, y, z axes and again it is centered at the barycenter. X-axis points from the origin of the system considered to the secondary body. Z-axis is directed as the angular momentum of the system, then the Y-axis completes the right-hand coordinate frame. The motion could be considered as planar in the x-y plane.

Once the system has been modeled, the next step is to adimensionalize the parameters characterizing the model. It is very useful, studying the restricted three body problem, to take into account some dimensionless quantities. The normalization process is implemented such in a way that the sum of the masses, the distance between the primaries and the gravitational parameter are equal to one; the orbital period is normalized to a value of 2π . The aforementioned parameters are normalized using a quantity related to the mass values of the primary and expressed as follows

$$\mu = \frac{m_2}{m_1 + m_2} \quad (1.8)$$

Where m_2 ; m_1 are respectively the mass values of the secondary and the primary bodies. So the dimensionless quantities are:

- Sum of primaries masses (total mass of the system): $m_1+m_2=1$
- Mass value of the primary body: $m_1=1-\mu$
- Mass value of the secondary body: $m_2=\mu$
- Distance between primaries: 1
- Position of the primary body: $[-\mu \ 0]$
- Position of the secondary body: $[1-\mu \ 0]$
- Gravitational Parameter: 1
- Orbital Period: 2π

Now it is possible to explicate the equations of motions relative to the restricted three body problem. Using the notation adopted in Figure 1.2, the equation (1.6) may be written as

$$\sum \mathbf{F} = m_3 \ddot{\mathbf{R}}_{s/c} = -G \frac{m_3 m_1}{R_{31}^3} \mathbf{R}_{31} - G \frac{m_3 m_2}{R_{32}^3} \mathbf{R}_{32} \quad (1.9)$$

Adimensionalizing the equation by the mass parameter μ , it is possible to write the formulation of the acceleration vector of the third body in the inertial frame as

$$\ddot{\mathbf{R}}_{s/c}^I = -\frac{1-\mu}{R_1^3} \mathbf{R}_1 - \frac{\mu}{R_2^3} \mathbf{R}_2 \quad (1.10)$$

Where parameters R_1 and R_2 are referred to the distance of the primary and secondary masses from the third.

$$\begin{aligned} R_1^2 &= (x + \mu)^2 + y^2 + z^2 \\ R_2^2 &= (x - 1 + \mu)^2 + y^2 + z^2 \end{aligned} \quad (1.11)$$

It is possible to express the velocity of the spacecraft in the inertial reference frame through the velocity evaluated in the synodic frame. Will be introduced the angular velocity which is adimensionalized to unit, $\omega^{\text{IxR}} = \hat{\gamma} = \hat{z}$. The equations of spacecraft velocity may be written as

$$\dot{\mathbf{R}}_{s/c}^R = (\dot{x} - y)\hat{x} + (x + \dot{y})\hat{y} \quad (1.12)$$

$$\dot{\mathbf{R}}_{s/c}^I = \dot{\mathbf{R}}_{s/c}^R + \omega^{IxR} \times \mathbf{R}_{s/c} \quad (1.13)$$

It is possible to combine equations (1.13) and (1.12), then, differentiating the result, it is obtained this formulation of spacecraft acceleration

$$\dot{\mathbf{R}}_{s/c}^R = (\ddot{x} - 2\dot{y} - x)\hat{x} + (\ddot{y} + 2\dot{x} - y)\hat{y} + \ddot{z}\hat{z} \quad (1.14)$$

The equation (1.14) may be written, combining it with equation (1.10), splitting the three components of acceleration

$$\begin{aligned} \ddot{x} &= 2\dot{y} + x - (1 - \mu)\frac{x+\mu}{R_1^3} - \mu\frac{x-1+\mu}{R_2^3} \\ \ddot{y} &= -2\dot{x} + y - (1 - \mu)\frac{y}{R_1^3} - \mu\frac{y}{R_2^3} \\ \ddot{z} &= -(1 - \mu)\frac{z}{R_1^3} - \mu\frac{z}{R_2^3} \end{aligned} \quad (1.15)$$

These last three equations represent the adimensionalized equations of motion expressed in the synodic reference frame.

1.3.1 Pseudo Potential and Jacobi Constant

It will now introduced a pseudo-potential quantity Ω , which will be further useful to analyze extensively the CR3BP. it will be identified three components of the pseudo-potential, respectively along x, y and z direction. To evaluate the potential it is necessary to integrate the left sides of equation of motion (1.15) with respect to x, y and z. Thus the pseudo-potential Ω may be written as

$$\begin{aligned} \Omega_x &= \frac{x^2}{2} + \frac{1-\mu}{R_1} + \frac{\mu}{R_2} + f(y, z) \\ \Omega_y &= \frac{y^2}{2} + \frac{1-\mu}{R_1} + \frac{\mu}{R_2} + f(x, z) \\ \Omega_z &= \frac{1-\mu}{R_1} + \frac{\mu}{R_2} + f(x, y) \end{aligned} \quad (1.16)$$

Equations (1.16) may be combined and rearranged to express the formulation of the pseudo-potential as a function of position of the generic particle and parameter μ

$$\Omega = \frac{1}{2}(x^2 + y^2) + \frac{1 - \mu}{R_1} + \frac{\mu}{R_2} \quad (1.17)$$

Once the expression of the potential has been found, it is possible to write the equations of motion in terms of potential itself

$$\begin{aligned} \ddot{x} &= 2\dot{y} + \frac{\partial\Omega}{\partial x} \\ \ddot{y} &= -2\dot{x} + \frac{\partial\Omega}{\partial y} \\ \ddot{z} &= \frac{\partial\Omega}{\partial z} \end{aligned} \quad (1.18)$$

Or in a differential form

$$\ddot{x}\dot{x} + \ddot{y}\dot{y} + \ddot{z}\dot{z} = \frac{\partial\Omega}{\partial x}\dot{x} + \frac{\partial\Omega}{\partial y}\dot{y} + \frac{\partial\Omega}{\partial z}\dot{z} \quad (1.19)$$

Integrating the equation (1.19) with time, a constant of integration has been introduced. It is possible to refer to this constant, C , as the Jacobi Constant

$$\dot{x}^2 + \dot{y}^2 + \dot{z}^2 = 2\Omega - C \quad (1.20)$$

Or in terms of velocity and position evaluated in the rotating reference frame

$$C = 2\Omega - V^2 \quad (1.21)$$

Considering a generic particle in motion through the system delineated by the restricted three body model, a certain value of pseudo-potential Ω and velocity may be assigned to it. Once these parameters have been fixed, the value of the Jacobi constant limits the motion of the particle to certain regions. The forbidden regions could be found generating the zero-velocity curves. Considering equation (1.21), setting the velocity value to zero, it is possible to map these resultant zero-velocity curves for positions near to the primary bodies. The motion of an object with a specified Jacobi constant is bound within its zero-velocity curve and can only cross the boundaries under some non-conservative force, such as thrusting. Figure 1.3 enlightens the zero-velocity curves, considering only the motion of the third body in the x-y plane, for the Earth-Moon CR3BP.

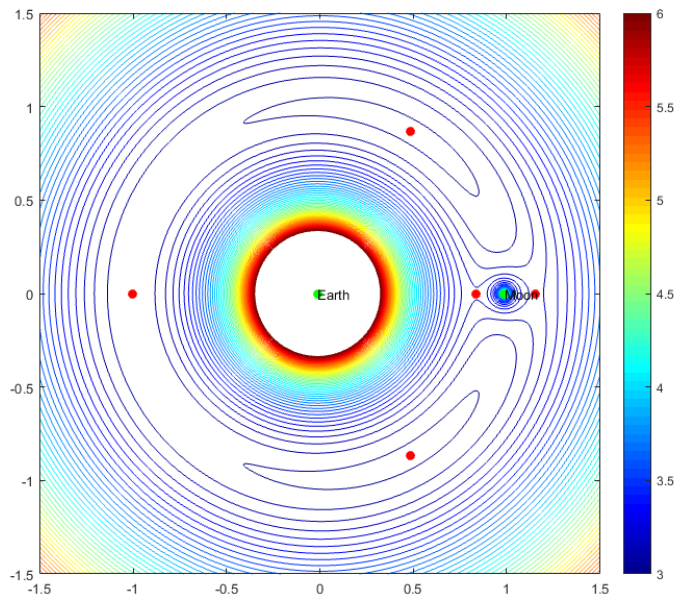


Figure 1.3: Zero velocity curves in the Earth-Moon system, shown in the synodic frame. The libration points are shown as red dots.

1.3.2 Libration Points

Inside the system described by the CR3BP it is possible to find five equilibrium points, these are defined as libration points or Lagrangian points. At the libration points the gravitational forces acting on the third body are balanced by the centripetal acceleration. Thus, considering the equations of motion (1.15), setting the synodic velocity and acceleration to zero, if the body of negligible

mass moves in the x-y plane, two equations come out

$$\begin{aligned} x - (1 - \mu) \frac{x+m\mu}{R_1^3} - \mu \frac{x-1+\mu}{R_2^3} &= 0 \\ y - (1 - \mu) \frac{y}{R_1^3} - \mu \frac{y}{R_2^3} &= 0 \end{aligned} \tag{1.22}$$

In order to find the first three solutions to this system of equations, y is set to zero, the first of (1.22) become a quintic equation and solving for x yields the three collinear libration points. Evaluating both the first and the second equation of (1.22) also the fourth and fifth libration points emerge; in particular these points are defined as the equilateral libration points, cause they form an equilateral triangle with the primaries. Collinear libration points lie on x-axis and conventionally L1 is placed between the primary and the secondary, L2, whose distance form the secondary is the same of L1, is placed beyond the secondary and L3 is placed on the fra side of the primary along the negative direction of x-axis. Figure 1.4 shows a schematic representation of Lagrangian points positions in Earth-Moon system. If a generic third body is placed exactly

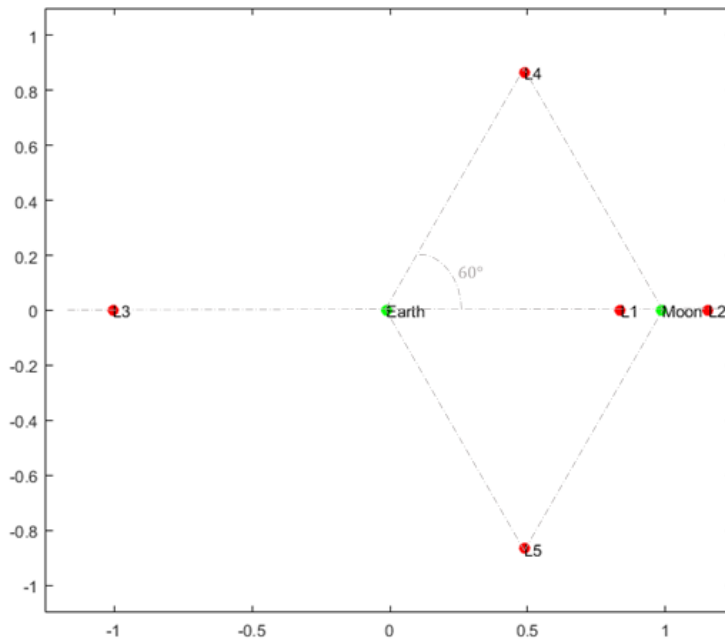


Figure 1.4: Libration Points, synodic reference frame. Earth-Moon system

at the libration points with initial velocity in the synodic frame equal to zero, it would remain stationary relative to the motion of primary and secondary body. Nevertheless, linearizing the equation of motions near Lagrangian points enlightens that the three collinear points are unstable. Besides, observing Figure 1.3 it is possible to see that these three equilibrium points are placed in saddle points in the graph. Particles positioned in collinear points will drift away under the effect of minimal perturbations. Instead the equilateral triangle libration

points, L4 and L5, are stable, in fact, looking to the zero-velocity curves, they are surrounded by contours. Mathematically L4 and L5 are stable until the inequality $\mu < 0.0385$ is satisfied, however considering both the Earth-Moon system and Sun-Earth system, this relation is fully satisfied. Section 1.5 will report values of Lagrangian points position and μ , considering both the CR3BP Earth-Moon system and the CR3BP Sun-Earth system.

1.3.3 Linearized Solutions to the CR3BP

It's aiming now to find solutions to aforementioned equations of motion. The purpose of such an operation is to find suitable orbits around the collinear libration point; in particular the focus will point on L1 and L2, due to the scientific relevance of these points. First of all it is useful to linearize these equations in the proximity of the equilibrium point considered. Referring to the libration point coordinates in the synodic frame as (x_0, y_0, z_0) , a new dimensionless constant may be introduced

$$K = \frac{1 - \mu}{(x_0 + \mu)^3} + \frac{\mu}{(x_0 - 1 + \mu)^3} \quad (1.23)$$

Considering (1.23), the linearized equations of motion may be rewritten as

$$\begin{aligned} \ddot{x} - 2\dot{y} &= V_{xx}x \\ \ddot{y} + 2\dot{x} &= V_{yy}y \\ \ddot{z} &= V_{zz}z, \end{aligned} \quad (1.24)$$

Where three new terms have been introduced

$$\begin{aligned} V_{xx} &= 2K + 1 \\ V_{yy} &= 1 - K \\ V_{zz} &= -K \end{aligned} \quad (1.25)$$

Dividing the system in two parts, the in-plane subsystem (first couple of equations (1.24)) and out-of-plane equation (third equation (1.24)), and then applying the eigenvalue research method, two characteristic equations emerge and may be written, introducing the eigenvalue λ , as

$$\begin{aligned} \lambda^4 + (4 - V_{xx} - V_{yy})\lambda^2 + V_{xx}V_{yy} &= 0 \\ \lambda^2 - V_{zz} &= 0 \end{aligned} \quad (1.26)$$

Relative to the selected libration point, two important constants are obtained

$$\begin{aligned} \omega &= \frac{1}{\sqrt{2}} \sqrt{2 - K + \sqrt{9K^2 - 8K}} \\ \lambda &= \pm \frac{1}{\sqrt{2}} \sqrt{K - 2 + \sqrt{9K^2 - 8K}} \end{aligned} \quad (1.27)$$

It is now possible to formulate a solution for the system (1.24). Such a solution expresses the evolution in time of the three components of both position and velocity, regarding the third body moving in the binary system of primaries.

It has been obtained an harmonic solution, coefficients and phase angles definition process will identify different families of periodic orbits. State vector components, as a function of time, may be written as follows

$$\begin{aligned}
 x(t) &= A_1 e^{\lambda t} + A_2 e^{-\lambda t} + A_x \cos(\omega t + \phi) \\
 y(t) &= c_1 A_1 e^{\lambda t} - c_1 A_2 e^{-\lambda t} - A_y \sin(\omega t + \phi) \\
 z(t) &= A_z \cos(\omega_z t + \psi) \\
 u(t) &= A_1 \lambda e^{\lambda t} - A_2 \lambda e^{-\lambda t} - A_x \omega \sin(\omega t + \phi) \\
 v(t) &= c_1 A_1 \lambda e^{\lambda t} + c_1 A_2 \lambda e^{-\lambda t} - A_y \omega \cos(\omega t + \phi) \\
 w(t) &= -A_z \omega_z \sin(\omega_z t + \psi)
 \end{aligned} \tag{1.28}$$

Where A_1 and A_2 are the instability's amplitude and A_x, A_y and A_z are the stable amplitude of the characteristic ellipse. Three dimensionless constants have been introduced

$$\begin{aligned}
 \omega_z &= \sqrt{K} \\
 c_1 &= \frac{\lambda^2 - 2K - 1}{2\lambda} \\
 c_2 &= \frac{\omega^2 + 2K + 1}{2\omega}
 \end{aligned} \tag{1.29}$$

From system (1.28), setting instability amplitude values to zero, Lissajous periodic orbits are obtained. Lissajous orbits actually are the most relevant periodic orbit involved in scientific mission and with these simplifications the problem is easier to resolve, considering the reduced number of amplitude as inputs. Furthermore the y-axis amplitude could be expressed as a function of the x-axis amplitude

$$A_y = c_2 A_x \tag{1.30}$$

Obviously this type of solution is not feasible in real applications, many perturbations have to be taken in consideration during the trajectory design procedure. As a matter of fact, for the purpose of this research quasi-periodic orbits will

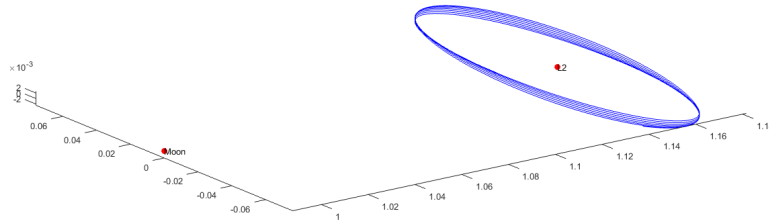


Figure 1.5: Lissajous Orbit around L2 in the adimensionalized synodic frame, Earth-Moon system. $A_x=10000\text{km}$, $A_z=1000\text{km}$, propagation time 100 days

be considered; these orbits are the result of a numeric integration operation of

the equations of motion (1.15), so they represent a numerical solution to the CR3BP. Instead Lissajous orbits are an analytical solution to the CR3BP, however, further in this research, they will be adopted as a benchmark to produce final quasi-periodic orbits around the libration point considered.

1.4 Lagrangian Points Orbits Applications

The Lagrangian points colonization provides many opportunities concerning the human space exploration and scientific research. Practically, engineers focus is pointed to the libration points situated in the Earth-Moon system and in the Sun-Earth system. In addition, moving through the libration points space, from and to the primaries, would significantly reduce the DV (velocity change) requirements.

Placing outposts in the collinear points L1 and L2 of the Earth-Moon system would guarantee many advantages concerning the space exploration. As an example the L1 point, due to its locked position between Earth and Moon, could be an excellent location to supervise, manage and coordinate communications between the Earth and any nearside lunar mission. It could also serve as a useful station to provide maintenance and upkeep to spaceships involved in Lunar exploration; reach the Moon surface from L1 requires few hours, thus an L1 outpost would provide a fundamental support in case of emergency. The L2 point instead is completely shielded from the Earth radiation, it could be an excellent location to place radio telescopes, due to the much less interference perceived in such a position. However an hypothetical station located on the lunar farside surface would fulfill same purposes. Considering the unstable nature of collinear points, any mission concerning these locations must provide active station-keeping operations. L4 and L5 are stable and could be used as waypoints to the cislunar space exploration.

Considering the state of the art of space exploration, much more interest is pointed to the Sun-Earth system; in particular the L1 and L2 Lagrangian points provides perfect locations for solar observations purposes, L1 is in constant sunlight, and to observe deep-space and outer planets, L2 is perpetually shadowed by the Earth. Again the stability of L4 and L5 could provide excellent location to expand launch opportunities for outer planets missions. Further in this Chapter the focus will be pointed on accomplished or planned missions to Sun-Earth collinear libration points, whose scientific interest is constantly growing.

1.4.1 Earth-Moon System

Compared to the amount of space mission involving both L1 and L2 libration point in the Sun-Earth system, the quantity of spacecrafts exploring libration points in the Earth-Moon system is slightly lower. Few probes were been placed in periodic orbit around near Moon libration points, two of them are NASA's spacecraft THEMIS B and THEMIS C. These are part of The Time History of Events and Macroscale Interactions during Substorms (THEMIS), a NASA constellation composed by 5 satellites. The objective of this mission began in February 2007 was to study energy releases from the Earth's magnetosphere.

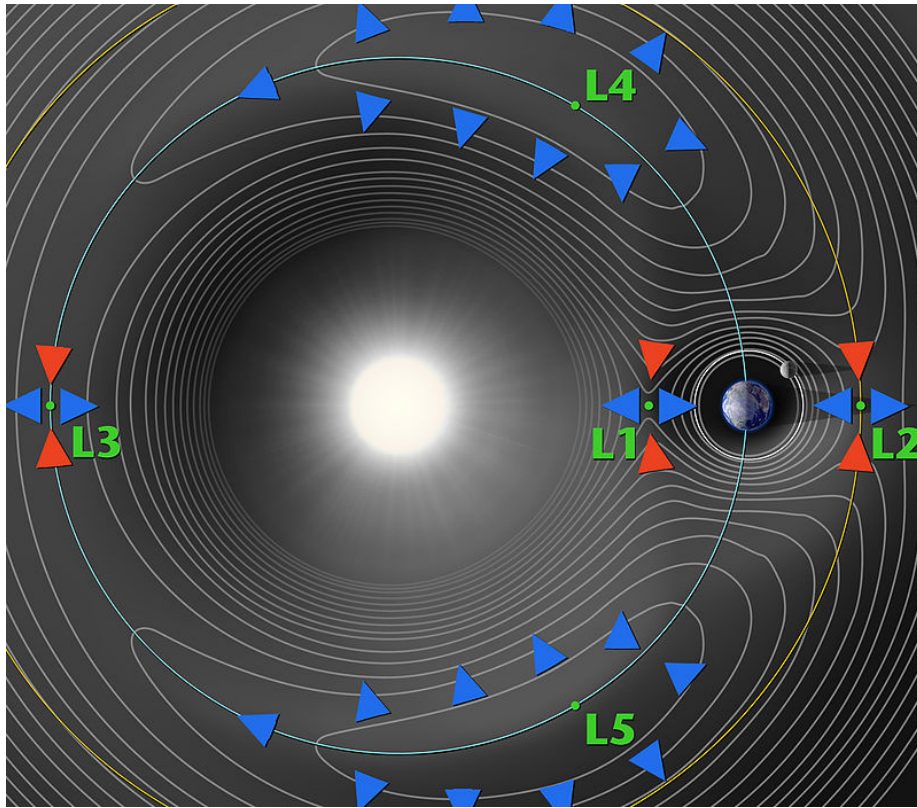


Figure 1.6: Sun-Earth System Representation

On May 19, 2008 the Space Sciences Laboratory (SSL) at Berkeley announced NASA had extended the THEMIS mission to the year 2012. Two satellites, THEMIS B and THEMIS C, were moved into lunar orbit, this mission was named ARTEMIS. ARTEMIS P1, previously THEMIS B, in early 2010, performed two Lunar flybys and an Earth flyby, later it approached an insertion in a Lissajous-type orbit around Lunar L2. ARTEMIS P2 (THEMIS C) completed a Lunar flyby and performed three deep-space maneuvers before the insertion in its Lissajous orbit around Lunar L2. As of August 2017, both lunar probes are in stable orbits, and the health of all instruments and the spacecraft remains very good. However ARTEMIS P1 and P2 were first spacecrafts to achieve a periodic orbit, Lissajous like, around Lunar Lagrangian points.

Launched in on January 24 1990, Hiten was the first Japanese Lunar probe. Hiten had to be placed into an high elliptical orbit, swinging close to the Moon, but an ignition deficit occurred and the spacecraft didn't reach its nominal altitude. Thanks to the work of Edward Belbruno and James Miller of the Jet Propulsion Laboratory the deficiency was corrected and Hiten continued its mission. Belbruno and Miller designed a trajectory based on the *Weak Stability Boundary Theory*. This course would result in the probe being captured into temporary lunar orbit using zero delta-v, such a trajectory is defined as ballistic transfer. Definitively, Hiten was the first spacecraft to demonstrate the feasibility of a low energy trajectory. Once Hiten performed its nominal mission, it

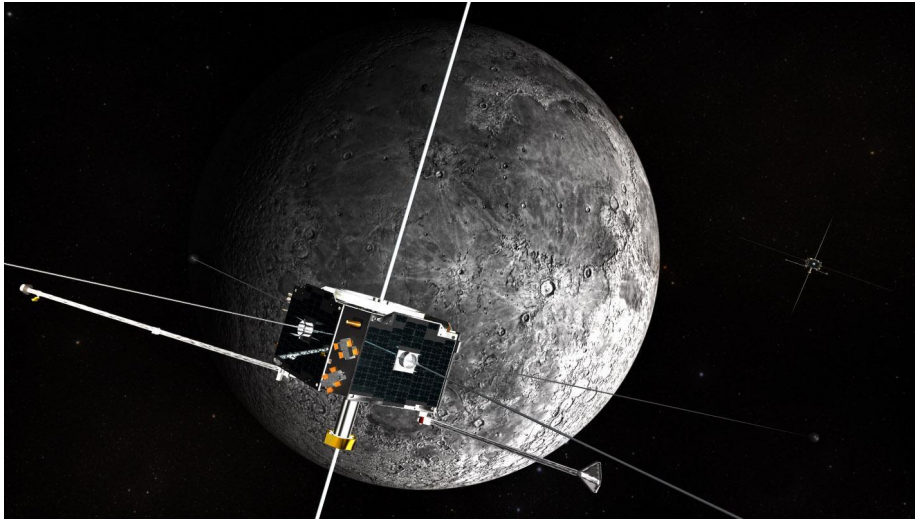


Figure 1.7: ARTEMIS's Artist's Impression

was placed in a looping orbit swinging through Lunar L4 and L5 searching in these regions for trapped particles. What Hiten was searching for are the Kordylewski clouds, large concentrations of dust particles that may exist at Lunar L4 and L5. There is still debate as to whether they actually exist, due to their extreme faintness. It is supposed that these particles clouds may be transient phenomena, as a matter of fact that inner planets of our Solar System perturb the stability of L4 and L5 in the Earth-Moon system.

1.4.2 Sun-Earth System

In this Section will be exposed a brief overview of the most interesting missions involving Lagrangian points L1 and L2 in the Sun-Earth system. Trajectories employed in such missions will be taken into account as benchmark results for the purpose of this research.

Herschel

At the moment that this research is written, the Herschel Space Observatory is the largest infrared space observatory. Equipped with a 3.5 meter diameter reflecting telescope and instruments cooled to close to absolute zero, Herschel observes at wavelengths that have never previously been explored. In recent years the infrared astronomy unveiled a large number of galaxies and also surprisingly discovered a large amount of water vapor which fulfill our galaxy, the Milky Way. Furthermore, thanks to the in-space infrared observation, free from Earth's atmosphere restrictions, it has been possible for the astronomers to discover planetary systems and to understand a large scale of events occurring in the early Universe, like the birth of galaxies. [13]

After a roughly 50-day journey from Earth, Herschel entered its operational orbit around the second Lagrange point of the Sun-Earth system (L2), for a nominal mission lifetime of three years. Herschel mission began on 14 May

2009, launched together with ESA's Planck Spacecraft from Kourou, French Guiana. The two probes moved to the Lagrangian L2, 1.5 million km away from the Earth, independently and reached different operative orbits. After the completion of the transfer orbit, Herschel reached its orbit around L2 in the Sun-Earth system, a large Lissajous orbit of large amplitude (700000 km). Lissajous orbits are the natural motion of a satellite around a collinear libration point in a two-body system and require less momentum change to be expended for station keeping than halo orbits, where the satellite follows a simple circular or elliptical path about the libration point. Herschel orbit was characterized by a period of 178 and an excursion above and below the ecliptic plane of 500000 km. Due to the unstable nature of orbits around collinear libration points, several correction maneuvers had to be planned about every month.

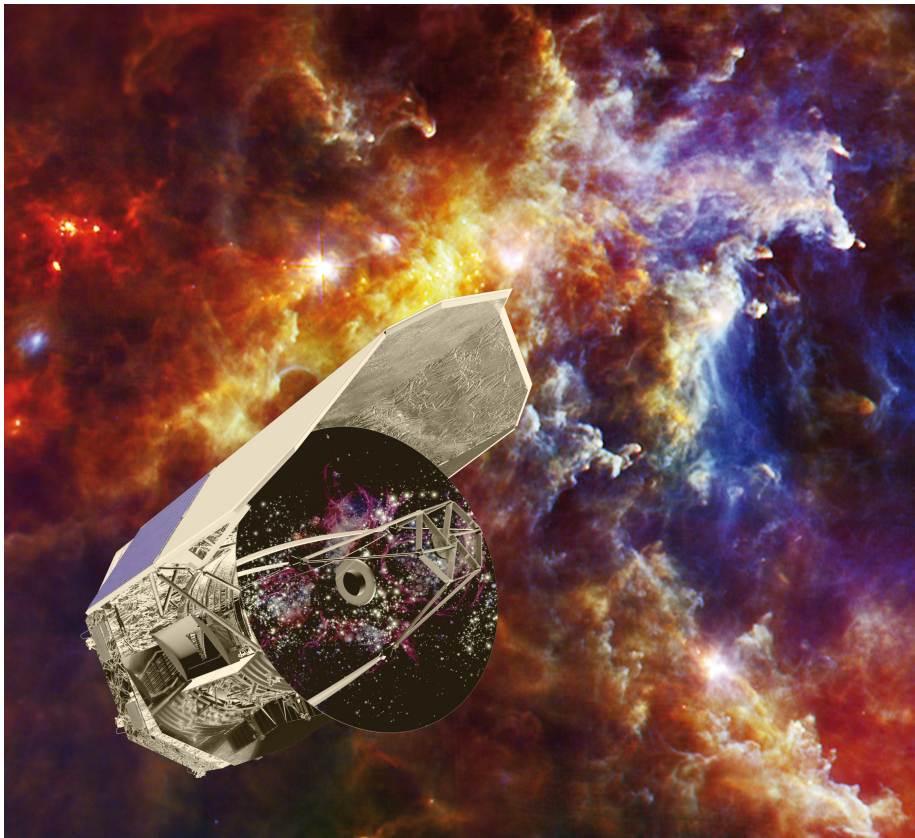


Figure 1.8: Herschel's Artist's Impression

Infrared observation requirements had driven the choice of an around-L2 orbit, as a matter of fact that a near Earth orbit is too much affected by Earth thermal influx. Furthermore, a quasi-periodic orbit around a libration point in the Earth-Moon system would have permitted to reach low temperatures necessary to Herschel observations, but in such an orbit both the Earth and the Moon would have not been very far from the telescope line-of-sight. Thus the chosen Lissajous orbit around L2 in the Sun-Earth system resulted as the optimal trajectory to guarantee satisfying performances of payload. Herschel's operations

were concluded on 17 June 2013, after that the spacecraft were switched off and placed in his final heliocentric orbit for the post-operation phase.

Gaia

Gaia is an ongoing mission, its goal is to produce the most precise three-dimensional map of our galaxy, the Milky Way, surveying an unprecedented one per cent of 100 billion stars composing the galaxy's population. During the mapping operation, Gaia will measure the motion of each star that it can detect. Stars are moving around the center of the galaxy, this motion was imparted upon each star during its birth. Analyzing stars motion, astronomers can peer back in time, understanding the galaxy's birth. By constructing such an ambitious map, astronomers will be able to study the formation of the Milky Way. During its operation phase, Gaia will observe at least 70 times each one of its one billion source. The astrometry concept influencing Gaia's development has been demonstrated by the Hypparcos mission. This measurement principle is based on subsequent observations of star sources in two fields of view. For this purpose the spacecraft rotates slowly, keeping constant its angular rate value at 1deg per minute around a selected axis perpendicular to the two fields of view planes. With a basic angle of 106.5deg separating the astrometric fields of view, objects transit in the second field of view 106.5 minutes after crossing the first one. Gaia's payload is composed by a single integrated instrument

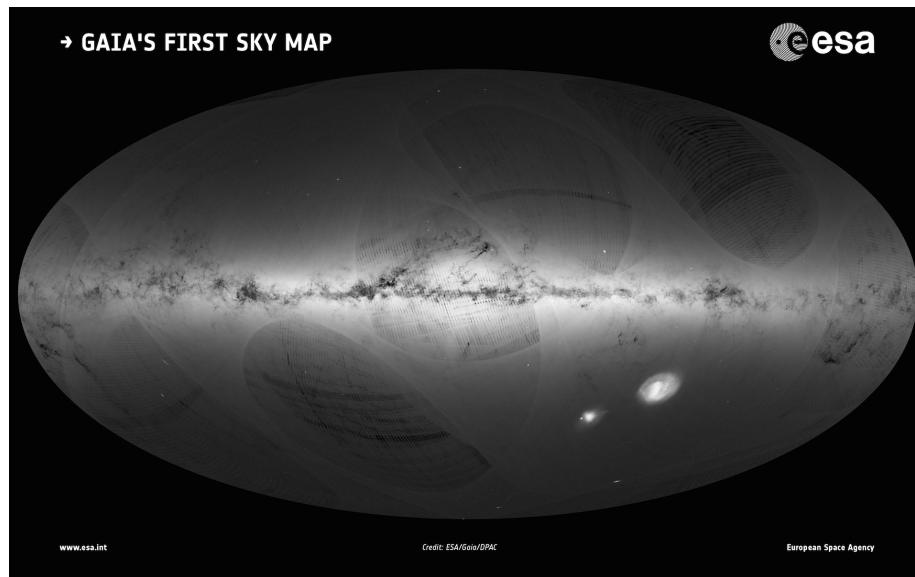


Figure 1.9: Gaia's First Sky Map

which performs three different functions: spectrometry, fotometry and astrometry. By detecting stars position and recording them brightness, together with the incredible accuracy of astrometric measurements, scientists will be able to discover planets belonging to faraway planetary systems, asteroids in our Solar System, icy bodies in the outer Solar System, brown dwarfs and far-distant supernovae and quasars. Gaia's possibilities are enormous, this makes its scientific

return unique.

The spacecraft was launched from Kourou, French Guiana, on 19 December 2013, by a Soyuz-Fregat launcher. The assembly Fregat-Gaia was placed in a parking orbit, then the Fregat boost injected Gaia on its transfer trajectory to the Sun-Earth system Lagrangian point L2. Gaia operational orbit is a Lissajous-type periodic orbit. The orbit has a period of about 180 days and is characterized by amplitude values of 340000 km and 90000 km. Such an orbit provides a stable thermal and low radiation environment, furthermore, the absence of Sun, Earth and Moon from the instrumental field of view, guarantees very high observing efficiency. Gaia' operational phase is planned to last about 5 years and may be extended by one year [12].

Euclid

Protons, electrons, neutrons and atoms, the ordinary matter, almost constitute the entire Universe. This is the largely accepted theory about Universe's composition for a long time. About thirty years ago, astronomers overcame this idea, as a matter of fact, in the intervening years, the emerging picture of Universe's composition changed drastically. Now it is assumed that the aforementioned ordinary matter represents only the 4%, the mass-energy budget is drastically dominated by two other components: *dark energy* and *dark matter*.

Euclid is a planned ESA mission to map the geometry of the dark Universe. The mission will investigate the distance-redshift relationship and the evolution of cosmic structures. It achieves this by measuring shapes and redshifts of galaxies and clusters of galaxies out to redshifts ~ 2 , or equivalently to a look-back time of 10 billion years. It will therefore cover the entire period over which dark energy played a significant role in accelerating the expansion [11]. Euclid will represent an unprecedented source of knowledge of regarding Uni-

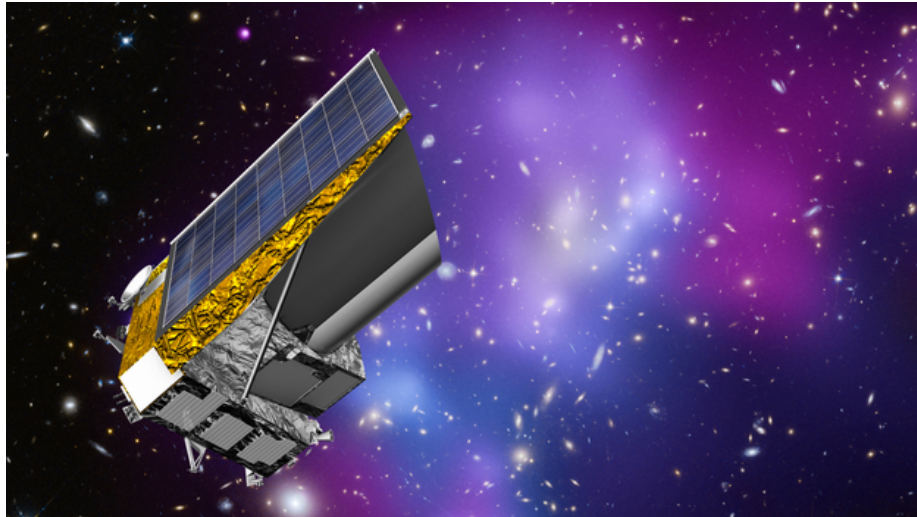


Figure 1.10: Euclid Artist's Impression

verse comprehension and composition, supporting the astronomical community research and impacting upon all branches of astronomy. As a matter of fact it

would produce a large amount of data and spectral images of almost half of the entire sky. Euclid will be a discovery machine on an unprecedented scale, and may well be the major feeder for more detailed studies both with ground-based facilities and future satellites.

Euclid will start his journey from the Europe's Spaceport in French Guiana, carried by a Soyuz launch vehicle. The transfer trajectory aims to the insertion in a large amplitude Halo orbit around L2 in the Sun-Earth system and it will last about 30 days. At the insertion on the quasi-periodic orbit no maneuvers are predicted. The designed Halo orbit is characterized by an amplitude of $\sim 1e6$ km around L2; this orbit is selected to provide best conditions to operate. First of all a good radiation environment is guarantee, essential to sensitive detectors operations, furthermore Euclid's orbit has very stable observing conditions, which are sufficiently far away from the disturbing Earth-Moon system. Lastly, station-keeping maneuvers are planned every 30 days, a good trade off between low-budget necessities and scientific requirements.

James Webb Telescope

The James Webb Telescope (JWST) has been developed in coordination between three space agencies, NASA, ESA and CSA. Scheduled to launch in October 2018, it will take the heritage of the Hubble telescope. With his capabilities, the JWST will investigate the Universe aiming to observe many events and objects distant in time and space, trying to detect particular phenomena as the formation of the first galaxies. Current ground and space based instruments are unable to reach performances of the James Webb Telescope. JWST will have the ability to see high-redshift objects, much more distant and old than any other source previously observed. Considering the JWST as a successor of Hubble and not its replacement, Hubble will keep in life until JWST will be completely operative. As a matter of fact The JWST has been designed to collect images in deeper infrared than Hubble moving beyond the observation capabilities of the Spitzer Space Telescope and the Infrared Space Observatory. The JWST will be placed in an Halo orbit around L2 in the Sun-Earth system, its operative lifetime is planned to last five years. Differently from the Hubble telescope, the JSWT will be placed far away from the Earth, thus astronauts will be obviously unable to perform maintenance on the telescope.

SOHO

The Solar Heliospheric Observatory (SOHO) is stationed in an Halo orbit around L1 in the Sun-Earth system, in such a position, the observatory enjoys an uninterrupted view of the Sun and its activity. It is the second mission orbiting L1 to observe the SUN (the first was ISEE-3. Scientists all around the world use images and data provided by SOHO and predict bad space weather affecting our own planet. SOHO investigate both the Sun interior through its surface and its incredibly storming atmosphere. Discoveries include complex currents of gas flowing beneath the visible surface, and rapid changes in the pattern of magnetic fields. In the atmosphere SOHO sees non-stop explosions and also remarkable shock waves and tornadoes [15]. SOHO represents an international cooperation between NASA and ESA, Europe's industry built the spacecraft for ESA, including nine instruments of the twelve composing SOHO's payload,

NASA instead launched the spacecraft and perform communications and continuous operations. The spacecraft was launched in 1995, due to the large success of the mission, its operational lifetime was extended from 1998 to 2018. It is

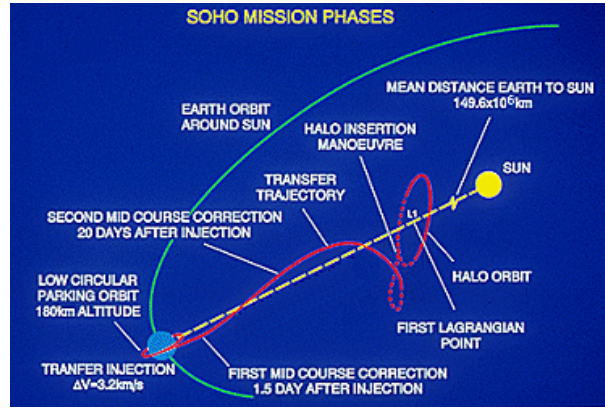


Figure 1.11: SOHO Trajectory Representation

important to notice that the enlargement of the mission due to perfect orbit insertion with low fuel consumption. Despite problems regarding gyros failures and a four months period of SOHO disappearance in 1998, scientists and engineers had successfully kept the instruments and the spacecraft itself operative and well performing. SOHO's trajectory to L1 is characterized by a direct transfer, it was launched on December 2, 1995, carried by an Atlas II launcher. The observatory orbits around L1 in Halo orbit characterized by an x-axis amplitude of $\sim 200000 \text{ km}$ and a z-axis amplitude of $\sim 120000 \text{ km}$. It cycles L1 twice a year approximately due to its orbit duration of 178 days. SOHO is permanently outside of the magneto-sphere, appropriate for the in situ sampling of the solar wind and particles and its particular orbit allows uninterrupted observation of the Sun, appropriate for all the investigations. [10].

Lisa Pathfinder

Lisa Pathfinder is a probe designed to test the technology needed to develop in future in space gravitational waves detectors. Gravitational waves are ripples in space-time predicted for the first time by A.Einstein in his *General Theory of Relativity*. Detecting these waves could increase scientists knowledge about General Relativity. Whilst ground-based detectors are already being used to try to identify high-frequency gravitational waves, a space-based mission would try to pick up frequencies from 10^{-4} Hz to 10^{-1} Hz . This corresponds to galactic-scale events such as the coalescence of supermassive black holes. LISA was launched from Kourou in French Guiana, carried by Vega launcher on December 3 2015. The launcher placed LISA in an elliptical parking orbit (perigee 200 km, apogee 1540 km), then, once the final stage of Vega was jettisoned, LISA started a transfer phase characterized by six maneuvers planned to raise the apogee and performed by the onboard thrusters. After the completion of the apogee-raising phase, LISA moved to its nominal orbit around L1 in the Sun-Earth system. This operational orbit is a Lissajous-like quasi-periodic trajectory, characterized by amplitude values of $500000 \text{ km} \times 800000 \text{ km}$ around Lagrangian L1. Such

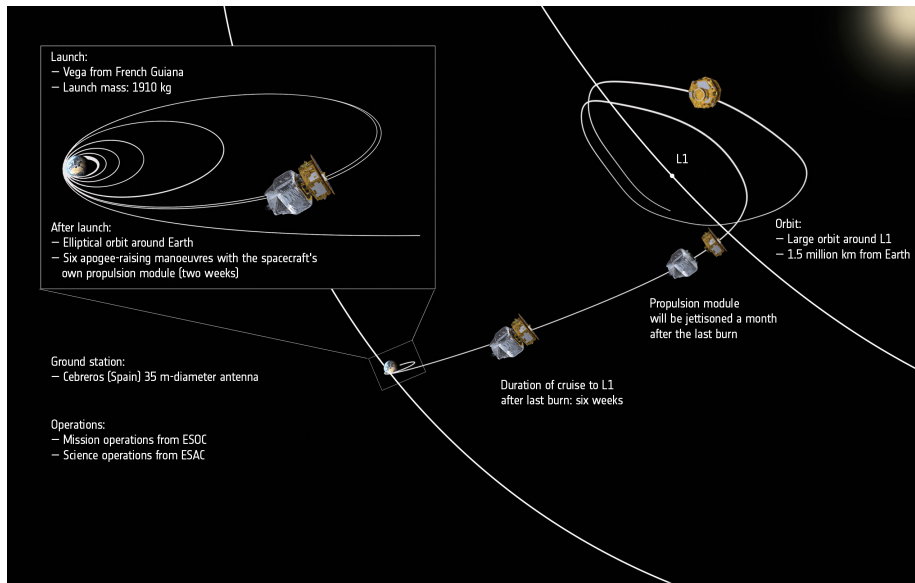


Figure 1.12: LISA Pathfinder's Journey to Space

an orbit guarantee a sufficiently far distance from main massive bodies, whose gravitational fields may induce tidal forces on the spacecraft. Moreover LISA's orbit has constant illumination from the Sun and fulfills thermal and gravitational stability requirements concerning spacecraft operations. After sixteen months of science operations, LISA Pathfinder completed successfully its mission on 30 June 2017, demonstrating the technology to build ESA's future space observatory of gravitational waves. Unfortunately, just before LISA started its operations, precisely on September 15, 2016, high-frequency gravitational waves coming from two collapsing black holes had been firstly detected with the Advanced Laser Interferometer Gravitational-Wave Observatory (LIGO) [14]. However, considering LISA Pathfinder's achievements, LISA will be the first space-based gravitational wave observatory. It will consist of three different spacecrafts separated by 2.5 million km in a triangular formation, following the Earth's in his revolution motion. Launch is expected to be in 2034.

1.5 Astrodynamics Constants

In this Section are reported all the astrodynamics constants values considered during the development of this research. Successively, considering the aforementioned parameters, evaluated dimensionless mass parameter μ and Lagrangian points positions, concerning both the Earth-Moon system and Sun-Earth system are shown. Values reported are rounded to the 4th decimal digit. First of all, for what concerns the main astronomical constants, it has been assumed following values:

- *Gravitational Constant* - $6.6726e-20 \text{ km}^3/\text{kgs}^2$.
- *Astronomical Unit, Sun-Earth Reference Distance* - $1.4960e8 \text{ km}$

Body	Radius [km]	Mass [kg]	Grav. Par. μ [km ³ s ⁻²]
Sun	6.9600e5	1.9899e30	1.3271e11
Earth	6.3781e3	5.9737e24	3.9860e5
Moon	1.7374e3	7.3477e22	4.9028e3
Mercury	2.4397e3	3.3018e23	2.2032e4
Venus	6.0518e3	4.8686e24	3.2486e5
Mars	3.3962e3	6.4186e23	4.2828e4
Jupiter	7.1492e4	1.8990e27	1.2671e8
Saturn	6.0268e4	5.6860e26	3.7941e7
Uranus	2.5559e4	8.6841e25	5.7945e6
Neptune	2.4764e4	1.0246e26	6.8365e6
Pluto	1.1950e3	1.3033e22	8.6961e2

Table 1.1: Planetary Constants

- *Earth-Moon Reference Distance* - 3.8440e5 km
- *Speed Of Light* - 3.0000e8 m/s²
- *Solar Constant* - 1367 W/m²

Table 1.1 highlights planetary constants values considered carrying out the analysis concerning the entire Solar System gravitational field. These values are computed by means of Spice Toolkit which provides access to all planets and principal bodies ephemerides. For what concerns Spice usage, to obtain all the object's ephemerides and physics parameters, following generic kernels have been used:

- *Spacecraft and Planet Kernel, SPK* - de430.bsp
- *Leapseconds Kernel, LSK* - naif0012.tls.pc
- *GM and Mass Kernel* - gmde431.tpc

Focusing on the precise location of Lagrangian points in both Earth-Moon system and Sun-Earth system, firstly dimensionless mass parameters are introduced

- *Earth-Moon System* - $\mu=0.012150584$
- *Sun-Earth System* - $\mu=3.0035e-6$

Point	EM (x)	EM (y)	SE (x)	SE (y)
L1	0.836915	0	0.990027	0
L2	1.155682	0	1.010034	0
L3	-1.005063	0	-1.000001	0
L4	0.500000	0.866025	0.500000	0.866025
L5	0.500000	-0.866025	0.500000	-0.866025

Table 1.2: Lagrangian Points Dimensionless Coordinates

Once mass parameters are determined, coordinates of libration points are evaluated and listed in Table 1.2, then these values are dimensionalized using aforementioned distance values, results are reported in Table 1.3 (SE refers to coordinates of Lagrangian points relative to the Sun-Earth system, EM To coordinates of Lagrangian points relative to the Earth-Moon system).

Point	EM (x)	EM (y)	SE (x)	SE (y)
L1	3.217102e5	0	1.481059e8	0
L2	4.442442e5	0	1.510989e8	0
L3	-3.866958e5	0	-1.495941e8	0
L4	1.922000e5	3.329002e5	7.479655e7	1.295522e8
L5	1.922000e5	-3.329002e5	7.479655e7	-1.295522e8

Table 1.3: Lagrangian Points Coordinates

Chapter 2

CR3BP approach to Trajectory Construction

In this Chapter it will be explained the strategy adopted to build, throughout the application of a numerical integration process, quasi-periodic orbits around targeted libration points. Moreover the focus will be pointed on transfer trajectories whose purpose is to connect the Earth and the quasi-periodic orbits, QPO, just built. These procedures rely so far on the Circular Restricted Three Body Problem force model. According to what has been written in Section 1.4, design operations are oriented to find trajectories in the Sun-Earth system, libration points in such a binary model are object to a greater scientific and engineering interest.

This chapter concerns the first design step aiming to compute an hypothetical trajectory whose usefulness is to connect the Earth and a Lagrangian point in both Earth-Moon system and Sun-Earth system. The focus will point on the Sun-Earth system, nevertheless the entire process is completely scalable to the Earth-Moon system; however it is also necessary to notice that, relate the design process to the Earth-Moon system means that the desired trajectory will connect the primary body (the Earth) to the libration points which are closer to the secondary (the Moon). Such an approach is much more complicated due to the necessity of passing closer to the secondary mass, whose gravitational field could heavily affect the motion of the hypothetical spacecraft, the third mass. Instead, considering the Sun-Earth system, it is aiming to design a trajectory to move from the secondary mass (the Earth) to the libration points L1 and L2, avoiding any close approach to the primary mass (the Sun).

Firstly it will be explained the computational approach adopted to correctly design all the supposed trajectories, then, considering a distinction of two different sections characterizing these trajectories, it will be reported the methodology to design each subdivision. These sections are the *Quasi-Periodic Orbit, QPO*, the proper scientific orbit around the considered libration point, and the *Transfer Phase*, which connect the Earth to the QPO. In this sense it will be clear all the causes which have led to the decision of differentiate the design method for the Transfer Phase and the QPO. Even though both sections are designed using the numerical integration of the differential equations of motion, the Transfer

Phase is characterized by a 'backwards' numerical integration, instead of a classical integration process used to design the QPOs. Both the numerical methods will be analyzed in the next Section. All the code implemented to design and analyze each trajectory is written in *Mathworks' MATLAB* environment.

2.1 Computational Approach

In order to design every kind of trajectory, solving the circular restricted three body problem, it is necessary to identify a suitable numerical method which could provide a solution to differential equations of motion (1.15). The equations are now reported for practical reasons

$$\begin{aligned}\ddot{x} &= 2\dot{y} + x - (1 - \mu)\frac{x+\mu}{R_1^3} - \mu\frac{x-1+\mu}{R_2^3} \\ \ddot{y} &= -2\dot{x} + y - (1 - \mu)\frac{y}{R_1^3} - \mu\frac{y}{R_2^3} \\ \ddot{z} &= -(1 - \mu)\frac{z}{R_1^3} - \mu\frac{z}{R_2^3}\end{aligned}\tag{2.1}$$

Practically a numerical integration method has been adopted to solve (2.1) and compute the third body state vector, position and velocity values, as function of time.

Differential equations could be adopted to describe all sort of systems which are subject to change. Applications span through nearly all science and engineering study fields, nevertheless differential equations are suitable to describe many systems regarding economics, biology, social science, etc. Moreover adopted differential equations could be very complex, in addition the systems described are so large, thus it could be difficult rather than impossible to find a purely analytical solution. In this sense, numerical methods could be useful to find solutions to the differential equations considered. For practical purposes, a numerical approximation could be often considered sufficient, the algorithm that will be further presented can be used to compute this approximation. For the sake of completeness it is necessary to take notice of another method to achieve a solution of differential equations, in fact techniques from calculus could be used to obtain a series expansion of the solution.

It is now necessary to introduce the definition of the generic first-order differential equation as an *initial value problem* of the form

$$\begin{aligned}\dot{y}(t) &= f(t, y(t)) \\ y(t_0) &= y_0\end{aligned}\tag{2.2}$$

Where y_0 is a given vector which represents the initial value or the initial condition. Previously it is been referred to the differential equation as *first order* differential equation. Such a definition refers to the fact that in the considered equation appears only the first derivative of y , higher order derivatives are completely absent. Without loss of generality it is possible, while debating this issue, to refer only to the aforementioned first order differential equations. In fact higher-order systems may be reduced to the first order case introducing new variables and creating a larger system of first order differential equations. Thus introducing a generic second order equation

$$\ddot{y} = -y\tag{2.3}$$

It may be rewritten as a system of first order differential equations

$$\begin{aligned}\dot{y} &= z \\ \dot{z} &= -y\end{aligned}\tag{2.4}$$

Now recalling the system (2.1) it is clearly observable that such a system contains second order differential equations. Thus it is possible to convert this system, introducing three new variables, to a first order differential equations system. It may be written as

$$\begin{aligned}\dot{x} &= u \\ \dot{y} &= v \\ \dot{z} &= w \\ \dot{u} &= 2v + x - (1 - \mu)\frac{x+\mu}{R_1^3} - \mu\frac{x-1+\mu}{R_2^3} \\ \dot{v} &= -2u + y - (1 - \mu)\frac{y}{R_1^3} - \mu\frac{y}{R_2^3} \\ \dot{w} &= -(1 - \mu)\frac{z}{R_1^3} - \mu\frac{z}{R_2^3}\end{aligned}\tag{2.5}$$

Inside the system (2.5) only first order derivatives of the six variables x, y, z, u, v, w appear. The aforementioned variables set represents the state vector, at a defined time point, t , of the hypothetical third body moving through the main bodies binary system. It is now clear that the initial condition, necessary to apply the considered numerical method, is identified by the precise state vector measured at a selected epoch, from which the propagation of the trajectory will start.

2.1.1 Introduction to Numerical Integration Methods

What does *numerical integration* means? Using this method it is possible to compute, from a selected and completely defined initial condition, y_0 , each successive point, y_1, y_2, y_3 , etc., that satisfy the evolution (2.2). Thus an algorithm computes as much precise as possible or required the value of y_{n+1} given the value of y_n . It is now briefly presented some basic numerical methods including Euler, Heun and Midpoint methods.

Euler Method

The Euler method is very simple to apply; considering the generic first order differential equation (2.2), Euler's formula may be written as

$$y_{n+1} = y_n + \Delta t \cdot f(t_n, y_n)\tag{2.6}$$

Given a user specified time step, Δt , Euler's formula permits to directly evaluate y_{n+1} computing only the derivative value at t_n . However such a method is not recommended to use, it is not so accurate especially if compared to other methods and using the same time step. The major imprecision is due to the fact that the derivative varies between t_n and $t_n + \Delta t$, but such a method relies only on the evaluation of the derivative value at t_n . Considering a smaller time step would reduce the error. Figure 2.1 shows a representation of the Euler's method principle.

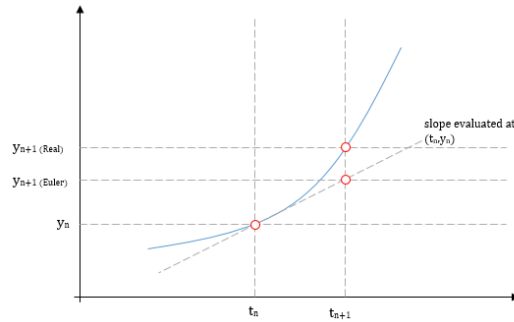


Figure 2.1: Euler's Method Principle Representation

Heun Method

The Heun method's principle is more complex than the Euler's. Practically the derivative isn't evaluated at the starting point t_n ; a better estimation is given evaluating the slope as the average value between the derivatives at the starting point, t_n , and at the end point, t_{n+1} . The Heun's formula may be written as (always referring to generic first order differential equation (2.2))

$$y_{n+1} = y_n + \frac{\Delta t}{2} \cdot (f(t_{n+1}, y_{n+1}) + f(t_n, y_n)) \quad (2.7)$$

Where the derivative at the end point is evaluated using the Euler's method and t_{n+1} corresponds to $t_n + \Delta t$. Such an algorithm could be considered as an improvement of the Euler's method and it is a simple example of a *predictor-corrector* algorithm.

Midpoint Method

Lastly it is presented the Midpoint Method which basically use the aforementioned Euler's method to evaluate the slope at $\Delta t/2$ and further evaluate the value of y_{n+1} using this slope value. The Midpoint's formula may be expressed as follows

$$\begin{aligned} k_1 &= f(t_n, y_n) \\ k_2 &= f\left(t_n + \frac{\Delta t}{2}, y_n + \frac{\Delta t}{2} k_1\right) \\ y_{n+1} &= y_n + \Delta k_2 \end{aligned} \quad (2.8)$$

2.1.2 Runge-Kutta Method

Further in this Section it will be outlined the basic principle of the Runge-Kutta numerical method. Focus on such a numerical method is justified by the fact that the computational process, designed to solve the system of differential equations of motion (2.5), is based on an explicit Runge-Kutta (4,5) formula, the Dormand-Prince pair [6].

It is common to refer to *The Runge-Kutta Method* to indicate the most widely used numerical method belonging to family of Runge-Kutta methods: the fourth-order Runge-Kutta Method also known as *RK4*. It is now reported the principle of this method in order to introduce the family of explicit RK

methods, a generalization of the aforementioned RK4. Recalling the general definition of the differential equation (2.2), the 4th order Runge-Kutta's formula may be written as

$$y_{n+1} = y_n + \Delta t \cdot \left(\frac{1}{6}k_1 + \frac{1}{3}k_2 + \frac{1}{3}k_3 + \frac{1}{6}k_4 \right) \quad (2.9)$$

Where it has been defined k_1 , k_2 , k_3 and k_4 as follows

$$\begin{aligned} k_1 &= f(t_n, y_n) \\ k_2 &= f\left(t_n + \frac{\Delta t}{2}, y_n + \frac{\Delta t}{2}k_1\right) \\ k_3 &= f\left(t_n + \frac{\Delta t}{2}, y_n + \frac{\Delta t}{2}k_2\right) \\ k_4 &= f(t_n + \Delta t, y_n + \Delta tk_3) \end{aligned} \quad (2.10)$$

Thus it is possible to express the RK4 approximation of y_{n+1} as the sum of y_n plus the weighted average of four increments. These increments are calculated by multiplying the time step Δ by four different estimated slope values, specified by the function f . In particular it may be written

- k_1 is related to the slope evaluated at the starting point using the Euler's method
- k_2 is related to the slope evaluated at the midpoint. The y value at the midpoint $\Delta t/2$ is evaluated considering $y + k_1h/2$
- k_3 is related to the slope evaluated at the midpoint. The y value at the midpoint $\Delta t/2$ is evaluated considering $y + k_2h/2$
- k_4 is related to the slope evaluated at the end of the interval. The y value at the end point Δt is evaluated considering $y + k_3h$

As it has been previously said, the RK4 method could be generalized to define the family of explicit Runge-Kutta methods. The generic formula may be written as follows

$$y_{n+1} = y_n + \Delta t \sum_{i=1}^s b_i k_i \quad (2.11)$$

Where slope values k may be expressed as

$$\begin{aligned} k_1 &= f(t_n, y_n) \\ k_2 &= f(t_n + c_2\Delta t, y_n + \Delta t(a_{21}k_1)) \\ k_3 &= f(t_n + c_3\Delta t, y_n + \Delta t(a_{31}k_1 + a_{32}k_2)) \\ &\dots \\ k_s &= f(t_n + c_s\Delta t, y_n + \Delta t(a_{s1}k_1 + a_{s2}k_2 + \dots + a_{s,s-1}k_{s-1})) \end{aligned} \quad (2.12)$$

In the expression of the slope values (2.12) and in the generic Runge-Kutta formula, (2.11), it has been introduced three groups of coefficients (s represents the number of stages considered)

- The matrix $[a_{ij}]$ for $1 \leq j \leq s$ is known as the *Runge-Kutta matrix*
- Coefficients b_i for $i=1,2,\dots,s$ are known as the *weights*

- Coefficients c_i for $i=2,3,\dots,s$ are known as the nodes

It is necessary to notice that the RK method is considered consistent only if

$$\sum_{j=1}^{i-1} a_{ij} = c_i \quad \text{for } i = 2, 3, \dots, s \quad (2.13)$$

Aforementioned coefficients may be rearranged using the *Butcher Tableau*

$$\begin{array}{c|cccccc} 0 & & & & & & \\ c_2 & a_{21} & & & & & \\ c_3 & a_{31} & a_{32} & & & & \\ \dots & \dots & & & & & \\ c_s & a_{s1} & a_{s2} & \dots & a_{s,s-1} & & \\ \hline & b_1 & b_2 & \dots & b_{s-1} & b_s & \end{array} \quad (2.14)$$

The implemented code, used to solve system of differential equations of motion (2.5), MATLAB's built in function, *ode45*, is based on the *Dormand-Prince Method* an adaptive Runge-Kutta (4,5) method. An adaptive method is used with a view to optimize the time span considered and adopt for each step the optimal time step. In particular a Runge-Kutta adaptive method exploits two methods, one with an higher order than the other, on the same Butcher Tableau. Thus the time step is modified until the error between the two methods is lower than the absolute error required. Several techniques are provided to correctly evaluate how to scale efficiently the time step. The Dormand-Prince pair is based on the evaluation of seven different slope values, k_1, k_2, \dots, k_7 , these values are used in two different linear combinations to find two approximations of the next point, a 5th order approximation and a 4th order approximation. The Butcher Tableau of the Dormand-Prince pair may be written as follows

$$\begin{array}{c|ccccccc} 0 & & & & & & & \\ \frac{1}{5} & \frac{1}{5} & & & & & & \\ \frac{3}{10} & \frac{3}{40} & \frac{9}{40} & & & & & \\ \frac{4}{5} & \frac{44}{45} & -\frac{56}{15} & \frac{32}{9} & & & & \\ \frac{8}{9} & \frac{19372}{6561} & -\frac{26360}{2187} & \frac{64448}{6561} & -\frac{212}{729} & & & \\ 1 & \frac{9017}{3168} & -\frac{355}{33} & \frac{46732}{5247} & \frac{49}{176} & -\frac{5103}{18656} & & \\ 1 & \frac{35}{384} & 0 & \frac{500}{1113} & \frac{125}{192} & -\frac{2187}{6784} & \frac{11}{84} & \\ \hline & \frac{5179}{57600} & 0 & \frac{7571}{16695} & \frac{393}{640} & -\frac{92097}{339200} & \frac{187}{2100} & \frac{1}{40} \\ & \frac{35}{384} & 0 & \frac{500}{113} & \frac{125}{192} & -\frac{2187}{6784} & \frac{11}{84} & 0 \end{array} \quad (2.15)$$

Where the first row of b coefficients represents the 4th order approximation of the solution, the second row represents the 5th order approximation. Throughout the design process of each trajectory, different absolute error requirements have been imposed. This has been done to better balance precision requirements, characterizing some particular aspect of the design process, and overall computational costs.

'Backwards' Numerical Integration

Section 2.3 will focus on the design process of the Transfer Phase. Due to the extreme sensitivity, to even slightly variations of the initial conditions, of such a problem, it could result much easier to set an arbitrary point on the quasi-periodic orbit considered and try to reach the Earth. Thus it is necessary to adopt a 'backwards' numerical integration strategy, considering the state vector of the aforementioned point on QPO as the initial condition of the system of differential equations of motion. Then a decreasing time span will be adopted to easy compute a sufficiently accurate numerical approximation of the solution. Again such a process is easily applicable using the MATLAB's *ode45* solver. Considering what it has just been said reasons it has been chosen to design QPOs before the transfer phase are completely clear, the first point of the selected quasi-periodic orbit will be adopted as 'initial' condition to numerical integrate backwards the transfer phase.

2.2 Quasi-Periodic Orbits

The arrival quasi-periodic orbit could be considered as the most relevant part of the supposed final trajectory. QPO's selection is driven by scientific stakeholders necessities and requirements. Different geometric characteristics could be chosen, nevertheless the time of propagation and maintenance on such an orbit is an important parameter which could affect the entire mission. Lastly and more important, different mission objectives could be accomplished orbiting around different libration points in different binary systems. Again recalling considerations made in Section 1.4, the focus will point on collinear libration points in the Sun-Earth system, with particular emphasis to L2.

Generically design attempts are made to aim to the analytical solution of the circular restricted three body problem, 1.3.3. All the periodic orbits resulting from the analytical solution of the CR3BP could be considered as the nominal solution to which it is trying to reach out. Practically, due to the assumptions and simplifications made to derive the analytical equations, the numerical solution, computed applying the aforementioned numerical methods to the system of differential equations of motion, (2.5), will diverge from the analytical solution. Such a solution highlights the theoretical existence of many different families of periodic orbits, in reality these orbits aren't achievable, thus it is necessary to almost find, according to the numerical solution, quasi-periodic orbits around the selected libration point.

It is now illustrated the practical process adopted to find the quasi-periodic orbits. First of all it has to be computed the analytical periodic orbits, thus a process of geometrical characteristics definition has to be accomplished. In the case of this particular treatment, the focus will point on the Lissajous periodic orbits, so X-axis and Z-axis amplitude have to be defined along with the phase angle values and the time of propagation. Once an analytical periodic orbit has been computed, it will be considered as reference to build the final quasi-periodic orbit. Previously in this Chapter, it has been underlined the need to choose an initial condition to properly solve, using numerical integration methods, the system of differential equations of motion which characterize the CR3BP. Thus

the first point of the selected analytical periodic orbit will be considered to be the initial condition used to solve the aforementioned ODE's system.

Solving the equations of motion using as initial condition the first point of the analytical periodic orbit will result in an orbit whose path drastically diverge from the reference periodic solution. Thus, to obtain a quasi-periodic orbit, it is necessary to even slightly vary the initial condition, in terms of velocity components, until a quasi-periodic orbit around the libration point is obtained. This orbit will be the hypothetical arrival QPO, to whom the transfer phase will connect. Figure 2.2 briefly shows the process of initial condition

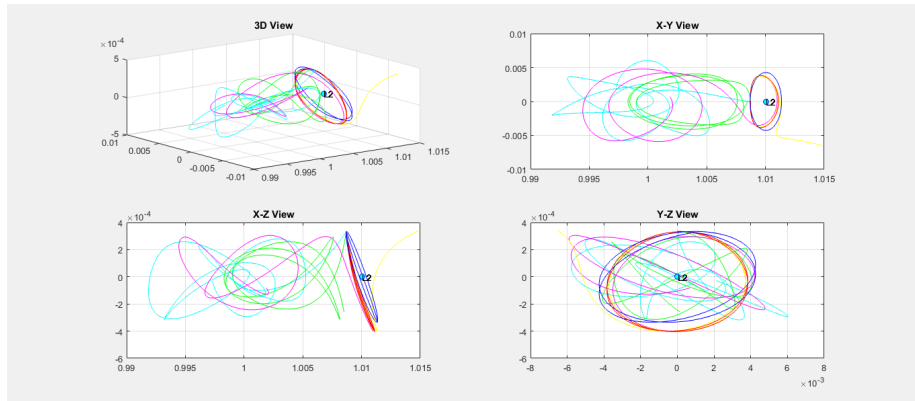


Figure 2.2: Initial Condition, Definition Process

definition. Five different solution of the equations of motion are reported, each one derives from different initial condition values (only velocity components variations are considered). These values are variations of the initial condition of the analytical Lissajous periodic orbit of $2e5$ km X-Axis amplitude, A_x , $5e4$ km Z-Axis amplitude, A_z , and 180 deg phase angle, ϕ ; such an orbit has been propagated for 360 days. The numerical QPO shaded in red could be considered

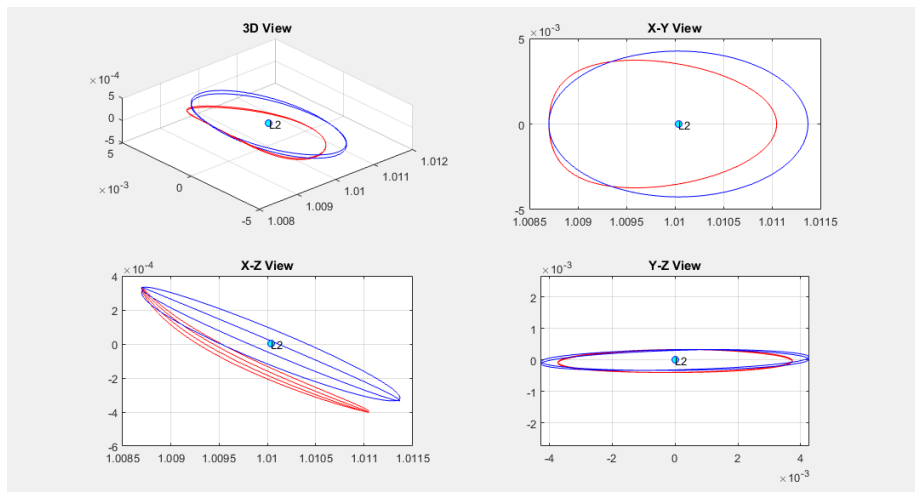


Figure 2.3: Numerical QPO. $A_x=2e5$, $A_z=5e4$, $\phi=180$ deg

as an acceptable result.

It is now reported a confrontation of different numerical solutions characterized by different amplitude values; each orbit has been propagated for 360 days. Figure 2.3 shows in detail the QPO based on the Lissajous orbit of, A_x equal to $2e5$, A_z equal to $5e4$, ϕ equal to 180deg . Variations to this trajectory are reported on Figure 2.4 and Figure 2.5.

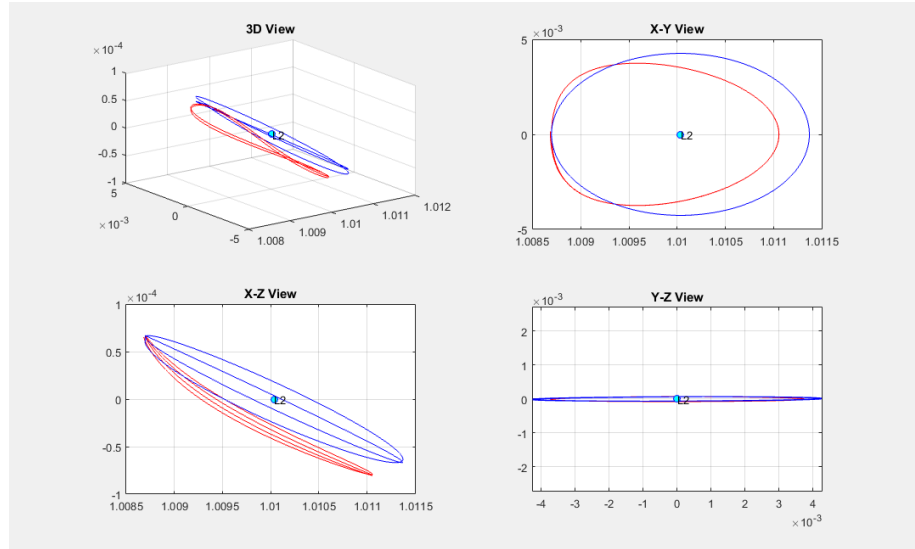


Figure 2.4: Numerical QPO. $A_x=2e5$, $A_z=1e4$, $\phi=180\text{deg}$

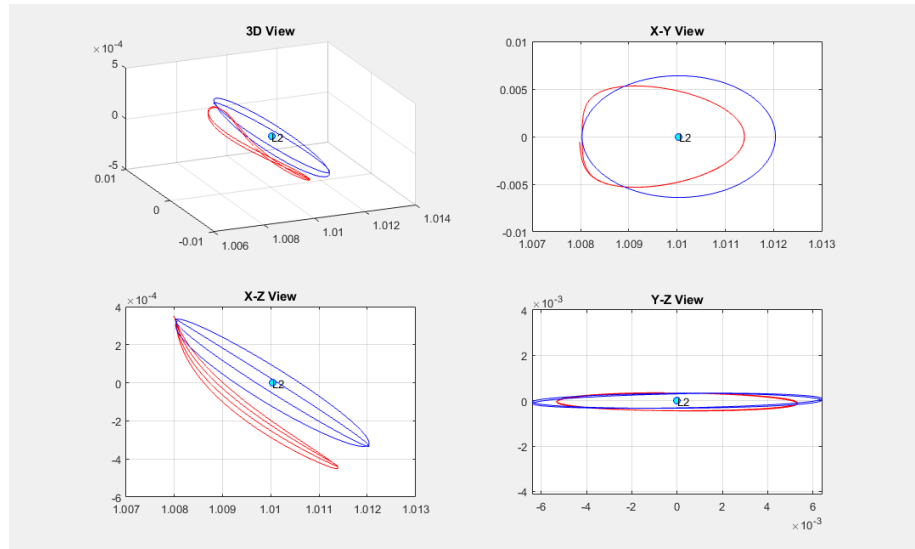


Figure 2.5: Numerical QPO. $A_x=3e5$, $A_z=5e4$, $\phi=180\text{deg}$

From Figure 2.3, 2.4 and Figure 2.5 it can be seen that no significant differences arise varying amplitude values; shapes of the numerical solutions remain

similar. A different analysis is provided modifying the value of the phase angle, ϕ . Setting A_x equal to $2e5$ km and A_z equal to $5e4$, Figure 2.6 and Figure 2.7 report QPO with different ϕ values.

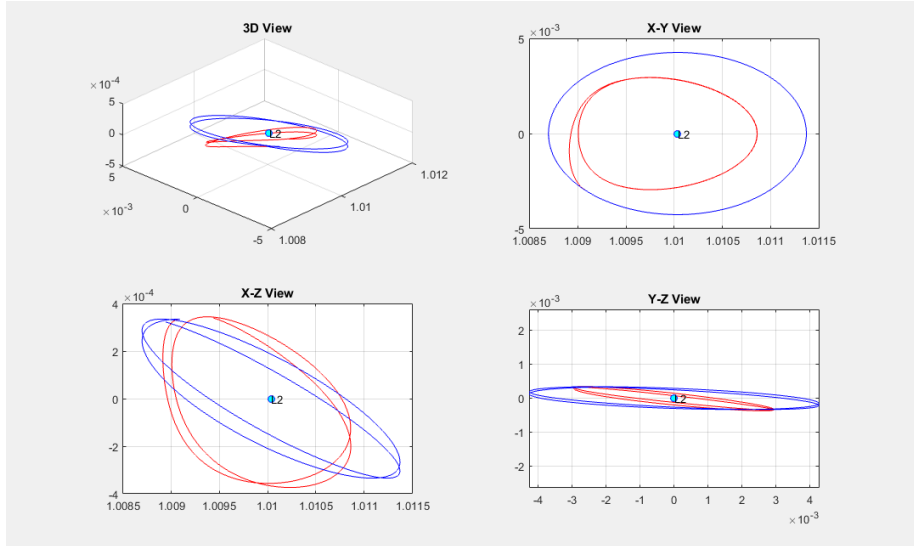


Figure 2.6: Numerical QPO. $A_x=2e5$, $A_z=5e4$, $\phi=135\text{deg}$

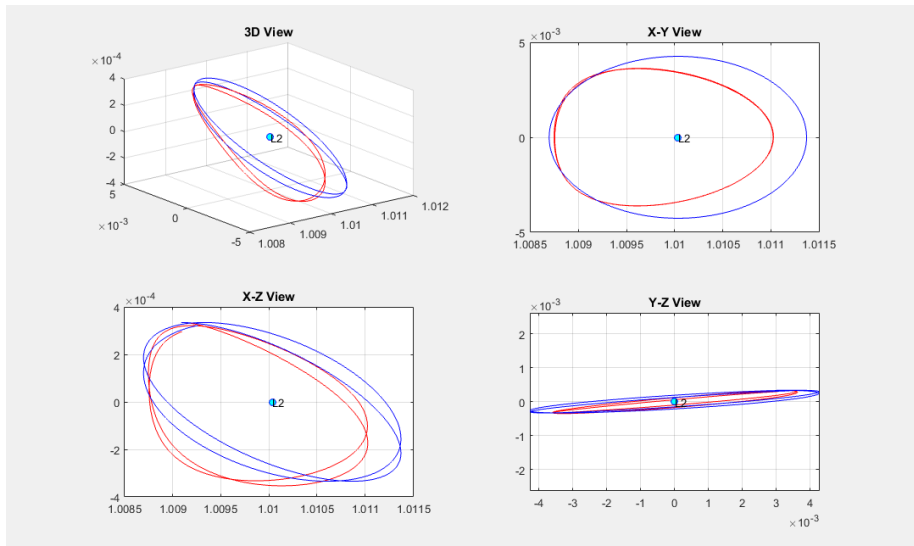


Figure 2.7: Numerical QPO. $A_x=2e5$, $A_z=5e4$, $\phi=225\text{deg}$

Analyzing orbits resulting from different ϕ values it could be noticed substantial differences in terms of shape and orientation. This aspect is very significant and furthermore it is important to consider that the definition of the phase angle value will strictly affect the design process of the transfer phase, fixing the arrival condition characteristic of such a phase. Further in this research it will

be highlighted that the phase angle value, ϕ , represents a critical parameter to be considered in order to design an optimal and satisfying trajectory to a Lagrangian point, including the corresponding quasi-periodic orbit around it.

For the sake of completeness, Figure 2.8 show a numerical quasi-periodic orbit around the Sun-Earth Lagrangian point L1. No significant differences could be detected by comparing it with the corresponding QPO around L2, Figure 2.3. Further considerations made about transfer to and orbit around L2 could be reported to L1 trajectories, without loss of generality.

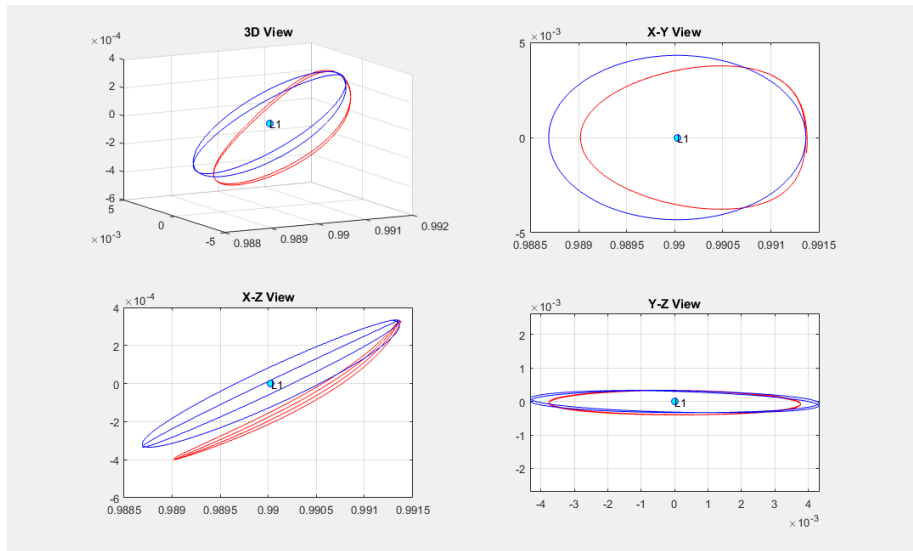


Figure 2.8: Numerical QPO around L1. $A_x=2e5$, $A_z=5e4$, $\phi=0deg$

2.3 Transfer Phase

All that's left now, once the arrival QPO has been defined, is to properly design a transfer trajectory to connect such an orbit, around the libration point, to the Earth. Previously it has been said that the state vector, of the first point of the quasi-periodic orbit, would be considered as the initial condition to solve, always through numerical methods, the system of differential equations of motion, thus finding the aforementioned transfer trajectory. Obviously, operating a process of backwards numerical integration, it is necessary to adopt a decreasing time span, so the state vector at the arrival in QPO becomes the 'initial' state of the transfer phase traveled backwards.

Operationally it must be defined a propagation time limit by which the transfer phase has to be accomplished. Then initial state vector could be propagated backwards in time until the trajectory reach its minimum distance from the Earth, at that point the numerical integration process is stopped; an hypothetical transfer trajectory has been designed. The transfer phase design shall be optimized for the achievement of a sufficiently close approach to the Earth, precisely it is aiming to find a transfer trajectory which starts from an altitude

value, over the Earth surface, no higher than $4e4$ km. As it has already been done designing the numerical quasi-periodic orbits, to better design a satisfying the transfer phase, it is necessary to act on the velocity components of the initial state vector. The optimal trajectory, in terms of closer as possible approach to the Earth, could be found just slightly modifying the initial condition.

No parameters have to be set in order to design any transfer phase, preliminary initial condition values are determined by the choice of the quasi-periodic orbit. Figure 2.9, Figure 2.10 and Figure 2.11 show different transfer phases evaluated for three QPOs, which differ from each other only in X-Axis and Z-Axis amplitude. All the Figures report the analytical periodic orbit shaded in blue, not the numerical QPO, for representation clarity's sake.

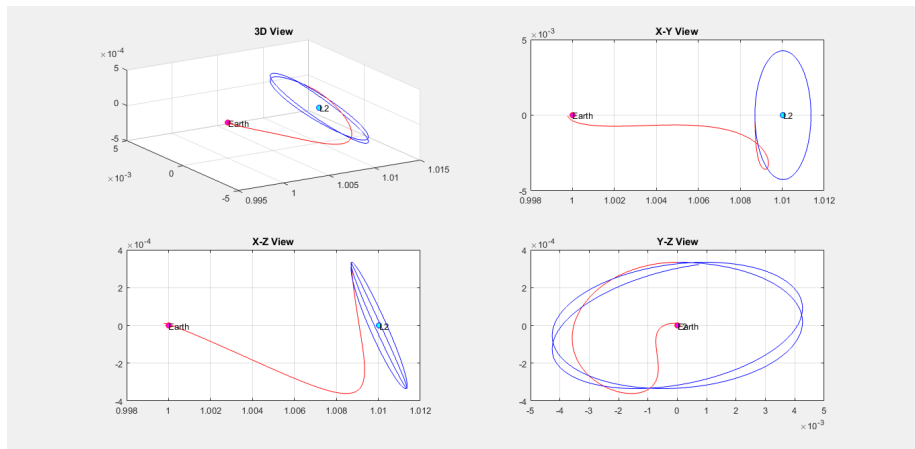


Figure 2.9: Transfer Trajectory. QPO: $A_x=2e5$, $A_z=5e4$, $\phi=180deg$

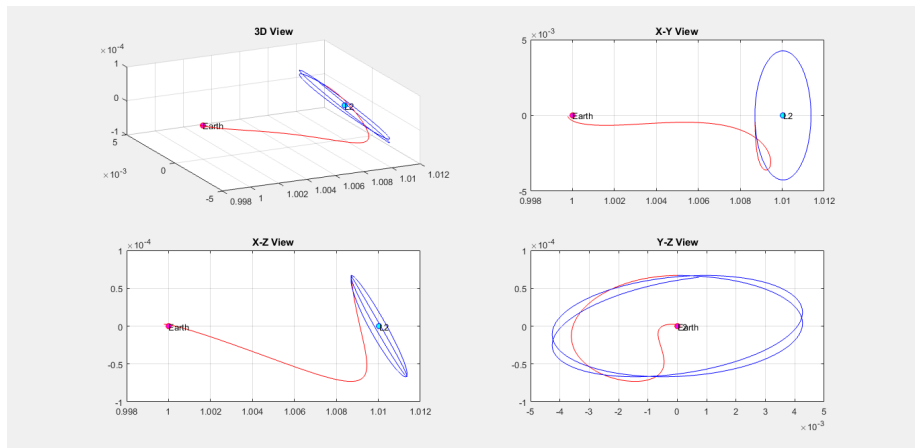


Figure 2.10: Transfer Trajectory. QPO: $A_x=2e5$, $A_z=1e4$, $\phi=180deg$

Analyzing Figure 2.9, Figure 2.10 and Figure 2.11, it could be noticed that no significant differences could be detected in the shape pattern of the transfer trajectories. Amplitudes variations of QPOs slightly affect geometrical characteristics of the transfer phase. Instead Figure 2.12 and Figure 2.13 show two

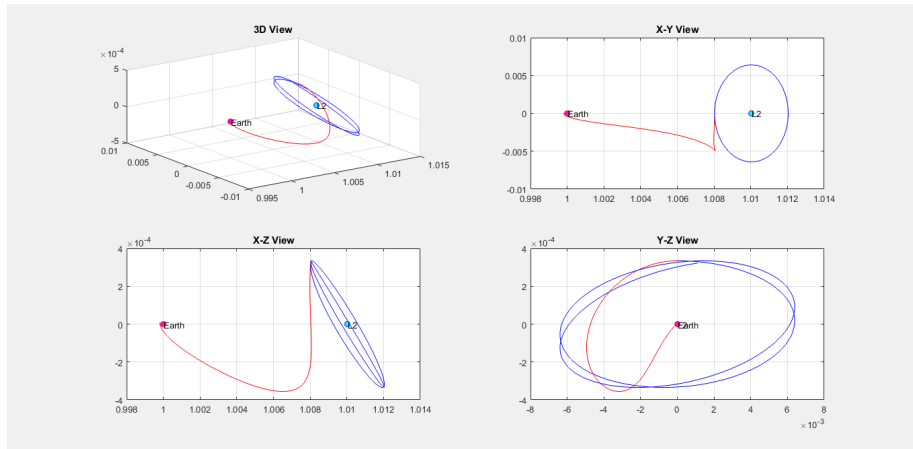


Figure 2.11: Transfer Trajectory. QPO: $A_x=3e5$, $A_z=5e4$, $\phi=180\text{deg}$

much more transfer trajectories deriving from QPOs of X-Axis amplitude equal to $2e5$ km and Z-Axis amplitude equal to $2e5$ km and Z-Axis amplitude equal to $5e4$ km, which differ from the one depicted in Figure 2.9 only in phase angle value, ϕ .

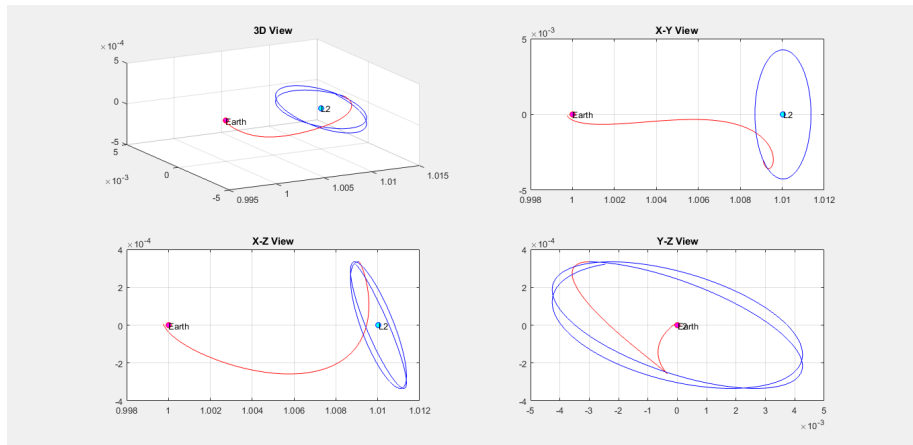


Figure 2.12: Transfer Trajectory. QPO: $A_x=2e5$, $A_z=5e4$, $\phi=135\text{deg}$

More differences arise varying the phase angle value, highlighting a similar to the QPO design behaviour. Again the ϕ value seems to be the predominant variable designing even the transfer phase. Further in this dissertation, observing that this geometric characteristic uniquely define the connection between the transfer phase and the QPO, it will refer to the ϕ angle as the *Insertion Phase Angle* or much easier as the *Insertion Angle*.

It's important to notice that the connection point has just been considered to be initial condition for both QPO and Transfer Phase (in this case it is better to refer to such a state vector as the arrival condition), thus it has been modified twice to meet both QPO and Transfer Phase design requirements and constraints. So this aspect could result in an instant variation of velocity, in

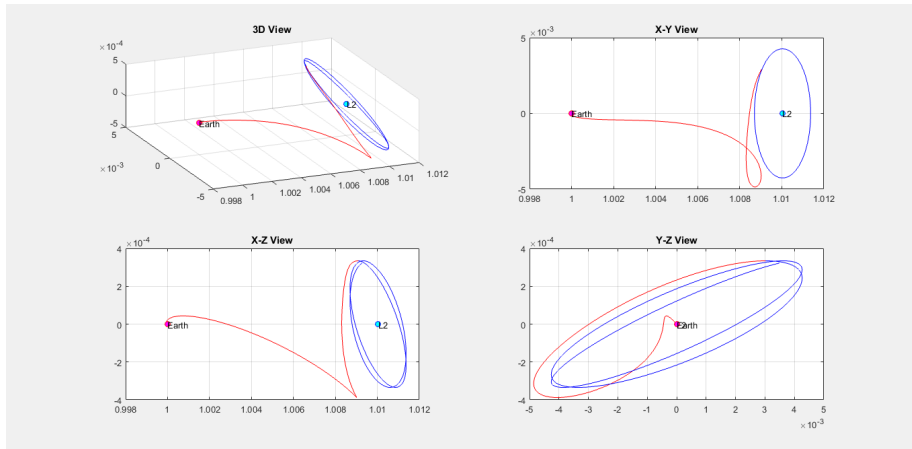


Figure 2.13: Transfer Trajectory. QPO: $A_x=2e5$, $A_z=5e4$, $\phi=225\text{deg}$

terms of module and direction, at the aforementioned junction point. Nevertheless this DV does not pose a problem for the trajectory design process, it shouldn't be taken into account for further analysis. In fact, the trajectory designed according to the CR3BP model will be used only as reference to go over considering the complete force model. Chapter 4 illustrates how the CR3BP Trajectory will be used as reference path, only in terms of position state vector, to define a new Trajectory propagated according to the complete force model, Chapter 3. In this sense, velocity values will not be considered.

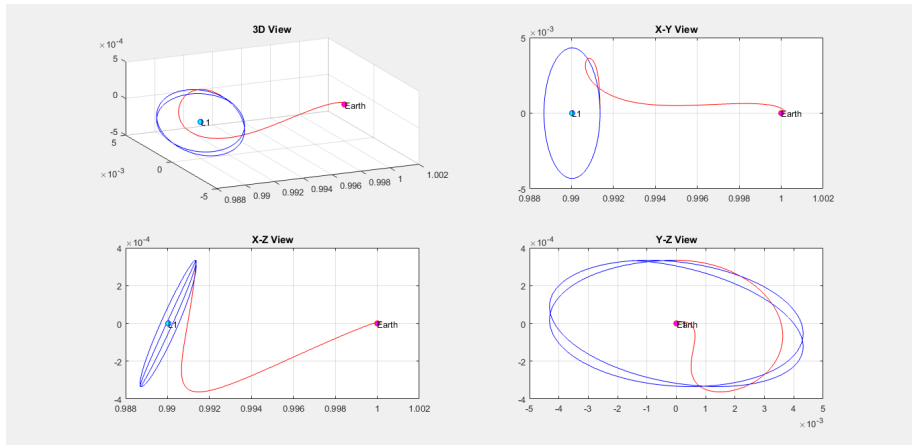


Figure 2.14: Transfer Trajectory. QPO around L1: $A_x=2e5$, $A_z=5e4$, $\phi=0\text{deg}$

For the sake of completeness, Figure 2.14 show a transfer trajectory to an analytical periodic orbit around the Sun-Earth Lagrangian point L1. No significant differences could be detected by comparing it with the corresponding trajectory to a QPO around L2 depicted in Figure 2.9. The only aspect worthy of consideration is that the transfer trajectory mainly propagates in the region of positive y values. This is obviously justifiable considering that it is assuming to travel the QPO in a clockwise direction, moreover the transfer trajectory

approaches the QPO from the right, thus the resulting trajectory pattern is completely consistent. Further considerations made about transfer to and orbit around L2 could be reported to L1 trajectories, without loss of generality.

Lastly, some examples about the trajectory design process complete results, according to the CR3BP, are provided in Section 5.1.

Chapter 3

Complete Force Model

Neptune existence was predicted before the planet itself was discovered. On November 10, 1845, Urban Le Verrier, French mathematician, presented a memoir regarding the motion of Uranus. His calculations highlighted errors in Uranus orbit calculation, supposing the existence of an external and unknown body whose presence could have perturbed the planet's path. On August 31, 1846, Le Verrier presented another memoir, now giving the mass and orbit of the new body. He finally sent his results by post to Johann Gottfried Galle at the Berlin Observatory. Neptune was discovered just after midnight, on September 24 after less than an hour of searching and less than 1 degree from the position Le Verrier had predicted. Further continuous observations had confirmed the calculation of Neptune's orbit made by La Verrier, thus Galle replied to the French mathematician: "the planet whose place you have computed really exists".

3.1 Perturbations to the CR3BP

Basically the CR3BP model predicts the motion of a generic body of negligible mass, respectively to the entire mass of the system, under the gravitational fields influence produced by two primary bodies. Besides these bodies are orbiting in a circular path around the barycenter of the three mass system and their motion is considered planar. Such a three body system could depict, with a rather acceptable tolerance, many coupled bodies mutual motion inside the Solar System. Common examples are the Sun-Earth system and the Earth-Moon system, whose applications have been yet highlighted in Chapter 1, systems coupling the Sun and one of the solar system planet, or even a three body system involving Jupiter or Saturn and one of their moons. However many perturbations have to be taken into account if the aim is to design a much more accurate trajectory in such a two main bodies gravitational field. Going forward through this Section three main perturbations to the circular restricted three body problem will be highlighted. First of all the elliptical restricted three body problem will be introduced, thus it will be shown how the eccentricity of the primaries orbits could be taken into account, then it will be discussed the influence of the main 'third perturbing bodies' in the solar system and finally the effect of the solar radiation pressure will be considered adopting an appropriate spherical model.

3.1.1 Introducing The Elliptical Restricted Three Body Problem

The main fault of the approximation induced by the adoption of the circular restricted three body problem is its low reliability to treat long-term motion regarding the majority of dynamical systems characterizing the celestial mechanics. There is a preponderant feature which lead to this significant fault, the eccentricity of the orbits of both primaries. To consider these bodies orbiting along an elliptical path around the system barycenter, spreads significant effects in determining the correct third body's motion. Introducing elliptic orbits for primaries motion generalizes the CR3BP and improves its applicability. Following the work of V. Szebehely and G. E. O. Giacaglia [3] it will be extended the applicability of the CR3BP increasing its reliability in long-term dynamic systems analysis; the set of equations relative to the elliptical problem may be written as

$$\begin{aligned}\xi'' - 2\eta' &= w_\xi \\ \eta'' + 2\xi' &= w_\eta\end{aligned}\tag{3.1}$$

In the equations of motion (3.1) primes indicate derivatives respect to the true anomaly of the secondary body, referring for example to the Sun-Earth system, f represents the Earth's true anomaly value along Earth's orbit around the Sun. Then ξ and η are the synodic Cartesian rectangular dimensionless coordinates of the third body in a non uniformly rotating system. This couple of coordinates is obtained dividing the dimensional (ξ^*, η^*) by the variable distance between the primaries. Thus it may be written

$$\zeta = \frac{1 + e \cos f}{a(1 - e^2)} \zeta^*\tag{3.2}$$

Where $\zeta = \xi + \eta$, $\zeta^* = \xi^* + \eta^*$, $i^2 = -1$, a is the semi-axis major of the secondary elliptic orbit and e is the eccentricity of both primaries orbits. Lastly w may be expressed as

$$w(\rho_1, \rho_2) = (1 + e \cos f)^{-1} \Omega(\rho_1, \rho_2)\tag{3.3}$$

Where

$$\begin{aligned}\rho_1(\xi, \eta) &= r_1(\xi, \eta) \\ \rho_2(\xi, \eta) &= r_2(\xi, \eta)\end{aligned}\tag{3.4}$$

From equations (3.1), (3.2), (3.3) and (3.4) it is possible to notice that setting the eccentricity value, e , to zero, otherwise considering circular orbits for the primaries, the equations of motions relative to the elliptical problem become equal to those relative to the circular restricted three body problem. The CR3BP could be considered as a particular and simplified case from the elliptical model.

Table 3.1 and Table 3.2 report keplerian elements regarding both Earth's and Moon orbit [16]. As comparison to the Earth' orbit, considering the entire Solar System, Mercury is the planet which presents the highest eccentricity value, 0,20564 (Pluto, whose planetary status had been demoted, has an eccentricity of 0,24883), instead Venus and Neptune orbits have lower eccentricity values, 0,00678 and 0,00859 respectively; the Moon has the most eccentric orbit considering the large moons of the Solar System. These values are obviously

Eccentricity [rad]	Rate [rad/Cy]	SemiMajor Axis [AU]	Rate [AU/Cy]
0.01671123	-0.00004392	1.00000261	0.00000562

Table 3.1: Earth's Orbit Keplerian Elements. Values validity: 1800 AD - 2050 AD

Eccentricity [rad]	Semi-Major Axis [km]	Inclination [deg]	Period [days]
0.0554	384400	5.16	27.322

Table 3.2: Moon's Orbit Keplerian Elements. Epoch: 01 Jan 2000 12:00:00.000

referred to the present configuration of the Solar System; secular perturbations tend to modify planets and satellites orbit along long-term periods.

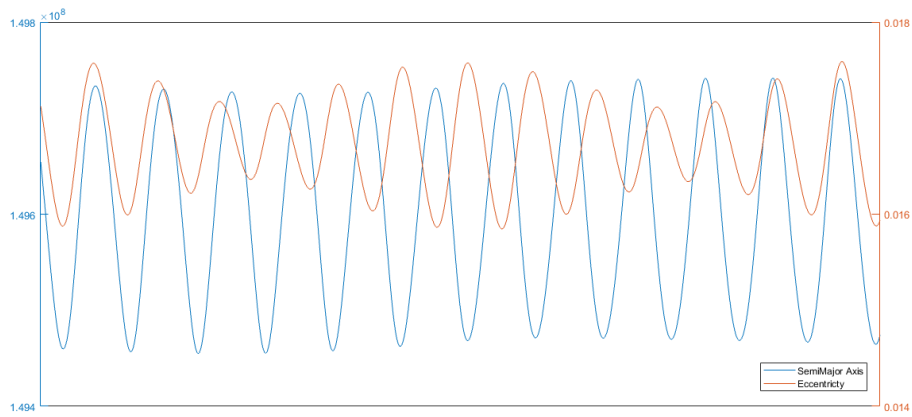


Figure 3.1: Earth's Orbit Eccentricity and Semi-Major Axis Variation; 1 Year Time Span, from 01 Jan 2019 to 01 Jan 2020

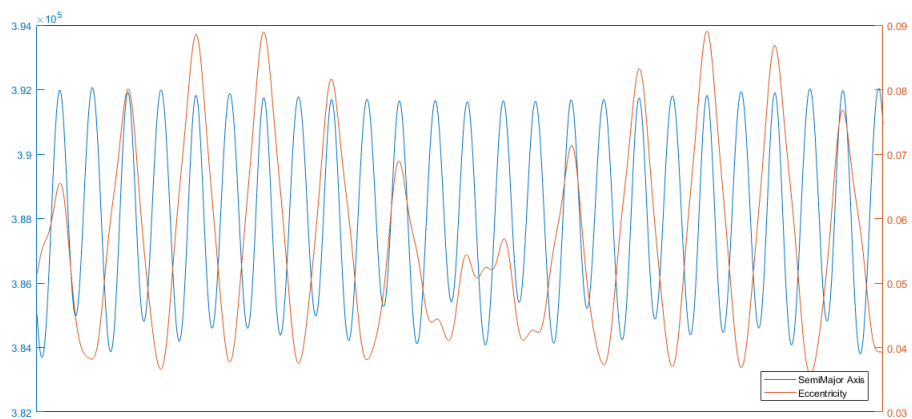


Figure 3.2: Moon's Orbit Eccentricity and Semi-Major Axis Variation; 1 Year Time Span, from 01 Jan 2019 to 01 Jan 2020

Such a refined elliptical model application permits to drive a more accurate evaluation of an hypothetical long-term motion of the third body through the primaries system. However it has yet to be considered a simplified model. Aiming to accomplish an accurate trajectory design involving such unstable regions of space like those around Lagrangian points, it is necessary, for example, to overcome restrictions imposed by considering primaries orbits planar; moreover eccentricity and semi-major axis values, even if only slightly, are not constants in time Figure 3.1 and Figure 3.2 show variations of eccentricity and semi-major axis values along a one year time span; keplerian elements are evaluated using ephemerides sources 3.2 . Thus, considering the much more complex implementation of the elliptical equations of motion, for the purpose of this research, to design the baseline trajectory has been considered the classical CR3BP model. In Section 3.2 will be introduced the ephemerides based approach to the force field modeling operation, so designing the final trajectory, the circular orbit assumption will be overcome easily considering the exactly state vector of each body which perturbs the motion of the hypothetical spacecraft. Considering final trajectory results coming from both a CR3BP and an Elliptical Restricted Three Body Problem preliminary design, no significant variations have been found, so considering the aforementioned difficulty of implementation, the application of CR3BP to preliminary mark the desired trajectory is justified.

3.1.2 Solar Radiation Pressure

Introducing the nature of such a dynamical perturbation due to the effect of the solar radiation pressure, it's important to understand the behaviour of a photon which collides with a generic body. Interacting with a solid surface, a photon of light would exchange its momentum whose amount corresponds to the photon energy value divided by the velocity of light. The surface reached by the aforementioned photon perceives a radiation pressure, equal to the vector difference between the incident and reflected momentum flux. It is possible to refer to the Solar radiation as a continuous flux of particles originated from the Sun. Solar radiation isn't the only source of electromagnetic radiation, others are the radiation pressure due to the Earth albedo, the Earth infrared radiation and the spacecraft's own thermal emission. However these sources could be neglected considering the purpose of this research.

Implementing the perturbation driven by the solar radiation pressure, a simple spherical model, or 'cannonball' model, has been taken in consideration. Such a model assumes that the hypothetical spacecraft is an invariant sphere characterized by constant thermo-optical properties, thus it is necessary to define a cross-sectional area exposed permanently and continuously to the Sun and a coefficient of reflectivity, C_R . For what concerns this research, it has been assumed that the complete trajectory designed is free from umbra and penumbra regions or rather it is always in complete sunlight. The coefficient of reflectivity, C_R , as defined by David A. Vallado [9], indicates how and in what measure the hypothetical spacecraft reflects the incoming Sun radiation; values of C_R spans from 0 to 2. Setting the coefficient of reflectivity equal to 0 corresponds to assume that the spacecraft is translucent to incoming radiation, non of the radiative force is transferred to the body. If the spacecraft behaves as a black body, the coefficient has to be set equal to the unit value, 1; in this case all the incoming radiation is absorbed and re-radiated, all of the radiative force

is transferred to the spacecraft. Lastly, considering a coefficient of 2 highlights that the spacecraft behaves as a flat mirror perpendicularly oriented respect to the incoming solar radiation; all the radiation itself is reflected, the spacecraft perceives twice the radiation force. So considering such a spherical model, the equation of the force due to the solar radiation pressure may be written as

$$\mathbf{a} = -\frac{\Phi A}{mc} C_R \frac{\mathbf{s}}{s^3} \quad (3.5)$$

- \mathbf{F} is the acceleration due to the solar radiation pressure on the sphere modeled spacecraft
- Φ is the Solar Flux expressed in W/m^2
- A is the cross-sectional area of the spacecraft expressed in m^2
- c is the speed of light expressed in m/s
- m is the mass of the spacecraft expressed in kg
- C_R is the coefficient of reflectivity
- \mathbf{s} is the distance between the spacecraft and the Sun expressed in m

Considering what it has just been said, such a perturbation, related to the effect of the solar radiation upon the hypothetical probe, is directly dependent by the physical and geometrical properties of the probe itself. Thus in order to evaluate the additional acceleration, due to the incoming Sun radiation, it is necessary to define a preliminary shape of the spacecraft traveling along the designed trajectory. Taking as reference the nature of this research, it has been considered justifiable to adopt ESA Euclid's spacecraft characteristics, Section 1.4, to evaluate the perturbation driven by the solar radiation. Table 3.3 reports all the data useful to compute the additional acceleration. Moreover considering

Surface Area [m^2]	Coefficient of Reflectivity C_R	Mass [kg]
16	1.1	2100

Table 3.3: Euclid's spacecraft main characteristics

Euclid's spacecraft as reference model to compute the solar radiation pressure component of the complete force field is useful to validate the force model itself. In Chapter 4 a validation of the designed force model is presented; the cross-validation is in fact based on a discarded Euclid's trajectory.

3.1.3 Third Bodies Perturbations

In Chapter 1 main features of such a dynamical model like the circular restricted three body model have been discussed; moreover, previously in this chapter, it has been cleared up the relevance of overcoming restrictions imposed by considering primaries orbits circular and planar. Lastly it has been highlighted the nature of an additional perturbation driven by the solar radiation pressure, thus, in order to design an accurate and reliable force model, to propagate all the

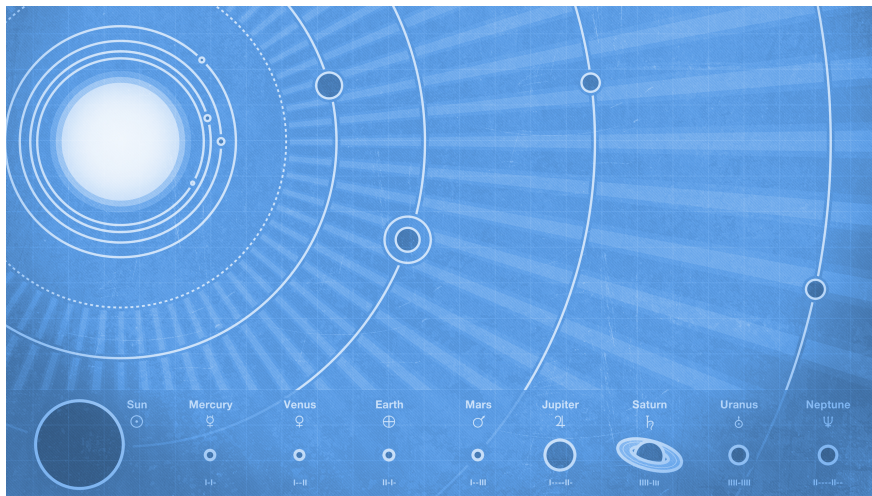


Figure 3.3: Solar System Representation. *Credit to Adam Dorman*

analyzed trajectories, it is necessary to take into account another type of perturbation, gravitational attraction due to the presence of external third bodies. Modeling the complete force field, through which it has been assumed that the hypothetical spacecraft is moving, gravitational fields of all the Solar System planets have been considered, besides Pluto perturbation has been included. Moreover it has been made necessary to take notice of Moon's gravitational field, whose influence, along the early transfer-to-Lagrangian phase, acts upon spacecraft trajectory above all other perturbations considered; Section 5.2 will be highlighted the relevance of such a third body perturbation.

To evaluate all the gravitational fields included in the complete force model, it has been assumed a simplified spherical model.

3.2 Ephemerides Approach to Complete Force Field Design

Ascertained that the CR3BP system of differential equations could represent a reliable and rather simple to apply tool to design the chased trajectory, considering both restrictions driven by such a dynamical system and all the sort of perturbations presented in Section 3.1, it is clear that a much more precise and refined force model has to be implemented to correctly propagate the final trajectory. Taking notice to what it has just been said about the implementation complexity of a system of equations of motion derived from an elliptical restricted model, recalling the impossibility of neglecting the effects of the solar radiation pressure and the gravitational fields of main Solar System bodies, a different approach has to be adopted to model an acceptable complete force field.

For the purpose of this research, it has been decided to directly solve the differential equations of motion for the generic i^{th} body given the position of other N bodies, adding the force or the acceleration component induced by the

solar radiation, where the aforementioned N bodies are represented by the Sun, all the planets of the Solar System, including Pluto, and the Moon. In terms of acceleration the equation (1.5) may be written as

$$\mathbf{a} = -\frac{Gm_1}{r_{1i}^3}\mathbf{r}_{1i} - \frac{Gm_2}{r_{2i}^3}\mathbf{r}_{2i} - \dots - \frac{Gm_n}{r_{ni}^3}\mathbf{r}_{ni} \quad (3.6)$$

The vector equation (3.6) express the overall acceleration perceived by the i^{th} body, the hypothetical spacecraft. Adding the component relative to the solar radiation pressure, equation (3.5), it is possible to express the system of differential equations of motion adopted to propagate all the trajectories designed and analyzed throughout this research. In terms of acceleration the system could be expressed as

$$\mathbf{a} = -\frac{\Phi A}{mc}C_R\frac{\mathbf{r}_{1i}}{r_{1i}^3} - \frac{Gm_1}{r_{1i}^3}\mathbf{r}_{1i} - \frac{Gm_2}{r_{2i}^3}\mathbf{r}_{2i} - \dots - \frac{Gm_n}{r_{ni}^3}\mathbf{r}_{ni} \quad (3.7)$$

Where m_1, m_2, \dots, m_n are the mass values of the N bodies considered and $r_{1i}, r_{2i}, \dots, r_{ni}$ represents distance values between the aforementioned bodies and the i^{th} body. Adopting the astronomical symbols:

- Sun - \odot
- Mercury - \mercury
- Venus - \venus
- Earth - \earth
- Moon- \moon
- Mars - \mars
- Jupiter - \jupiter
- Saturn - \saturn
- Uranus - \uranus
- Neptune - \neptune
- Pluto - \pluto

It is possible to write the system of differential equations of motion, (3.7), as follows

$$\begin{aligned} \mathbf{a} = & -\frac{\Phi A}{mc}C_R\frac{\mathbf{r}_{\odot i}}{r_{\odot i}^3} - \frac{Gm_{\odot}}{r_{\odot i}^3}\mathbf{r}_{\odot i} - \frac{Gm_{\mercury}}{r_{\mercury i}^3}\mathbf{r}_{\mercury i} - \frac{Gm_{venus}}{r_{venus i}^3}\mathbf{r}_{venus i} - \frac{Gm_{\earth}}{r_{\earth i}^3}\mathbf{r}_{\earth i} - \frac{Gm_{\moon}}{r_{\moon i}^3}\mathbf{r}_{\moon i} \\ & - \frac{Gm_{\mars}}{r_{\mars i}^3}\mathbf{r}_{\mars i} - \frac{Gm_{\jupiter}}{r_{\jupiter i}^3}\mathbf{r}_{\jupiter i} - \frac{Gm_{\saturn}}{r_{\saturn i}^3}\mathbf{r}_{\saturn i} - \frac{Gm_{\uranus}}{r_{\uranus i}^3}\mathbf{r}_{\uranus i} - \frac{Gm_{\pluto}}{r_{\pluto i}^3}\mathbf{r}_{\pluto i} \end{aligned} \quad (3.8)$$

Numerical values of both bodies mass values and gravitational constant are reported in Section 1.5.

To solve the system of differential equations of motion, (3.8), a numerical integration process has been adopted; such a process is based on an explicit

Rung-Kutta (4,5) formula, the Dormand-Prince pair. It is a single-step solver in computing the solution as a time function, it needs only the solution at the immediately preceding time point [6]. Observing equation (3.8), it is clearly that precisely evaluate positions of all bodies characterizing the force model is fundamental to solve the aforementioned system. Thus it is necessary to use a computational tool whose usefulness is to provide ephemerides of desired celestial body along a defined time span, in this sense the SPICE Toolkit has been employed.

3.2.1 SPICE Toolbox

SPICE is an observing geometry information system, provided by NAIF (an acronym which stands for NASA's Navigation and Ancillary Information Facility) to assist scientists and engineers in planning and interpreting scientific observations from space-based instruments; moreover SPICE usefulness could be oriented to mission engineering tasks. The nascent SPICE system was focused on assisting scientists with data analysis tasks, but it was quickly realized by the space exploration community that the design characteristics of SPICE made it equally suitable for use in mission design, mission operations, and observation planning. Today SPICE is routinely used in all phases of planetary missions, and portions of SPICE are increasingly being used on other types of space science missions. Introducing a SPICE data overview, it is possible to identify many different type of data kernels, necessary to perform every type of analysis in SPICE environment. Table 3.4 provide a brief summary of these data files typologies. Kernels adopted in this research are reported in Section 1.5. It is now introduced a brief description of most useful tools, belonging to SPICE library, adopted to compute all the necessary celestial bodies ephemerides.

- *bodvrd* - The routine *bodvrd* supply physical data, radius and gravitational parameter values, of celestial bodies. Values reported in Section 1.5 have been obtained using this tool.
- *str2et* and *et2utc* - The routine *str2et* convert a string representing an epoch to a double precision value representing the number of TDB seconds past the J200 epoch corresponding to the input epoch; instead the routine *et2utc* perform the inverse procedure.
- *sxform* - The routine *sxform* return the state transformation matrix from one frame to another at a specified epoch.
- *spkezr* - The routine *spkezr* return the state vector, position and velocity, of a target body relative either to an observing body or a specific point like the Solar System barycenter, optionally corrected for light time (planetary aberration) and stellar aberration. It is obviously necessary to define in input the time or the time span of observation and the reference frame considered.

Recalling the system of differential equations of motion (3.8) and considering the aforementioned tools requirements, it clearly appears essential to define an inertial reference frame under which ephemerides are defined; in fact assuming a non-inertial reference frame would make lose validity to the considered equations of motion. Aiming to get a numerical solution to the (3.8) system of equations,

Logical Components	Data Files (Kernels)	Contents
Planet and Spacecraft	SPK	Space Vehicle or Target Body Trajectory (Ephemerides)
Planet	PCK	Target Body Size, Shape and Orientation
Instrument	IK	Instrument Field of View Size, Shape and Orientation
Camera-Matrix	CK	Orientation of Space Vehicle or any articulating Structure on it
Events	EK	Events Information: Science Plane, Sequence of Events and Experimenter's Notebook
Other	FK	Reference Frame Specifications
Other	LSK	Leapseconds Tabulation
Other	SCLK	Spacecraft Clock Coefficients
Other	DSK	Digital Shape Models

Table 3.4: Kernels Contents

ephemerides, under which relative distances between each celestial body and the hypothetical spacecraft are computed, refer to the J2000 reference frame centered in the Solar System barycenter. Thus it is also taking in consideration

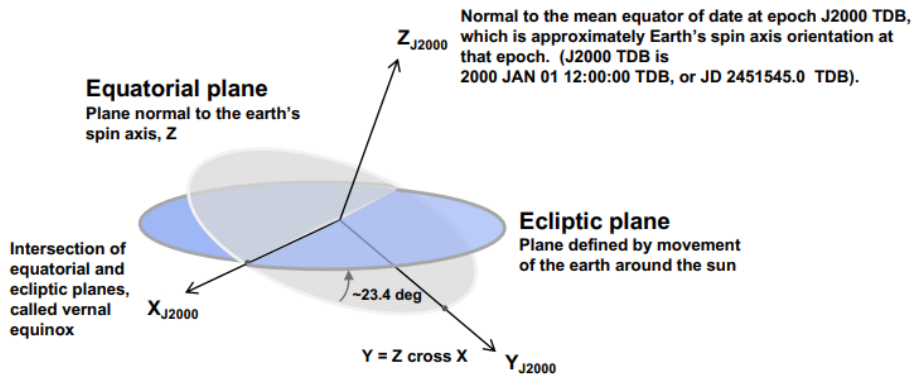


Figure 3.4: J2000 Reference Frame Representation

the Sun motion around the barycenter of the entire Solar System, even so it is slightly moving around such a point whose position is located rather close to the Sun barycenter (the Solar System barycenter could be periodically found inside the Sun volume or at a maximum distance of rather 2.5 Sun radii from the Sun barycenter itself) at low speed values of less than 20 m/s.

The definition of the J2000 reference frame is based on the Earth's equatorial plane and on the Ecliptic plane, determined from observations of planetary data. The X-direction of such a reference frame is called *vernal equinox* and represents the intersection the equatorial and ecliptic plane. The Z-direction is normal to the mean equator of date at epoch J2000 TDB, approximately Earth's spin axis orientation at that epoch (J2000 TDB is 01 JAN 2000 at 12:00:00.000 TDB). The Y-direction complete the set of three. Figure 3.4 shows a simplified representation of the axes orientation of the J2000 reference system.

3.2.2 Perturbations Effects

In order to provide a brief overview of all the perturbations effects driven both by the third bodies gravitational fields and by the solar radiation pressure, a simple simulation has been carried out in STK environment (references to this software usage provided in Section 5.3) and it is now reported. First of all an initial condition, characterized by values of epoch, position and velocity completely coherent with a quasi-periodic orbit around Sun-Earth L2, has been fixed. Subsequent to such a state point definition, the initial condition itself has been propagated for 30 days (designing the final trajectory, this time step represents the maximum interval of free propagation considered) using 5 different propagators:

- **H0 Propagator** - Only Sun and Earth gravitational fields
- **H1 Propagator** - Moon perturbation added to H0
- **H2 Propagator** - Spherical Solar Radiation Pressure added to H1
- **H3 Propagator** - Inner Solar System Planetary systems gravitational fields added to H2
- **H3 Propagator** - Outer Solar System Planetary systems gravitational fields added to H3

Figure 3.5, Figure 3.6, Figure 3.7 and Figure 3.8 highlights the effects of adopting different propagators which include different sources of perturbation.

Looking in particular to Figure 3.5 and Figure 3.6 it is possible to observe the error in terms of position using a propagator whose composition neglects the effect of third bodies perturbations (Moon and Solar System planets) and Solar Radiation Pressure; discrepancies raise exponentially to values around 8000 km, fluctuation of higher precision propagators depends mainly on mutual positions of the inner and outer planets of the Solar Systems, strictly dependent from the epoch analyzed. Error magnitude raises exponentially considering a larger time span; in fact, propagating the aforementioned initial conditions for 90 days, the position error, evaluated adopting the H4 Propagator instead of the H0 Propagator, reach values around 2e5 km.

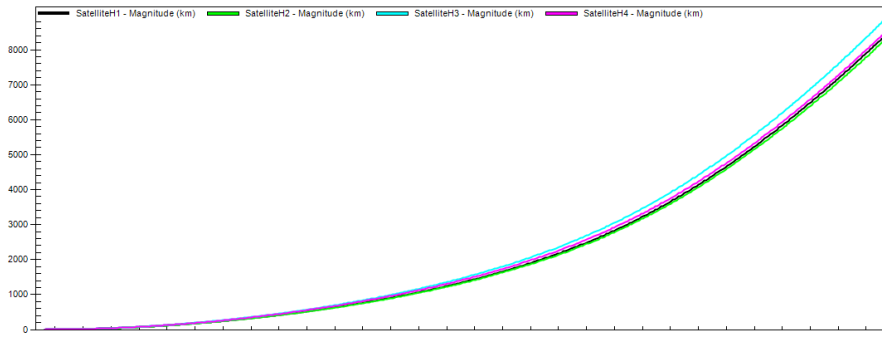


Figure 3.5: Propagators Confrontation. Distance [km] from H0 Trajectory

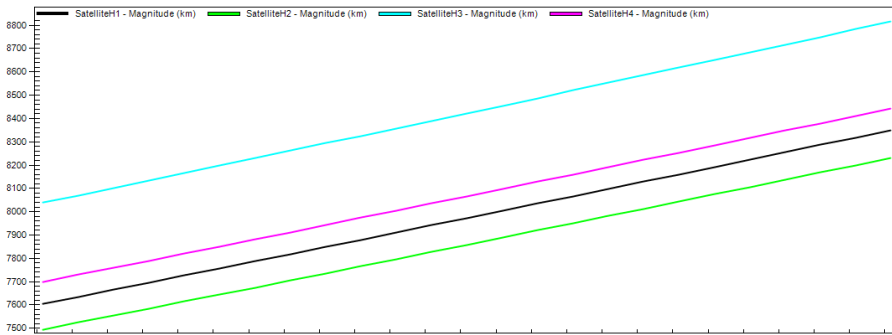


Figure 3.6: Terminal Section of Position Error Confrontation Curve

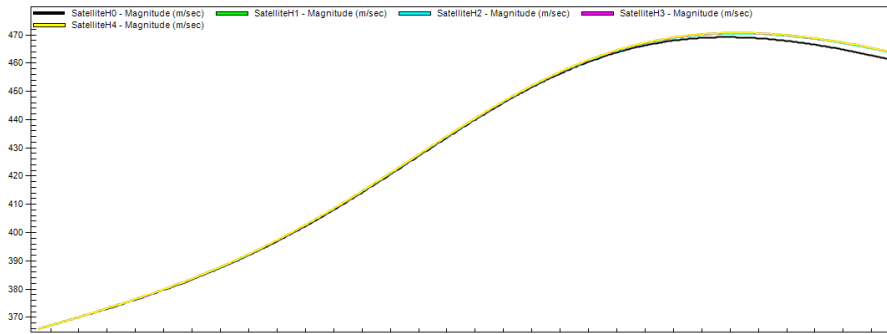


Figure 3.7: Propagators Confrontation. Velocity [m/s] (respect to the Earth)

Excluding the third body perturbation driven by the Moon from the H4 Propagator, it has been obtained the H4Mod Propagator. Making a 30 days comparison of position error, considering both H4 and H4Mod, it is possible to observe the preponderant effect of Moon perturbation over any other whose effect has been taken in consideration. Figure 3.9 show such a result. Thus, considering the Sun-Earth system, it is obviously clear and demonstrated the most relevant perturbation is driven by the Moon gravitational field. Evidently, for this analysis it has been considered the real Earth's orbit path to design

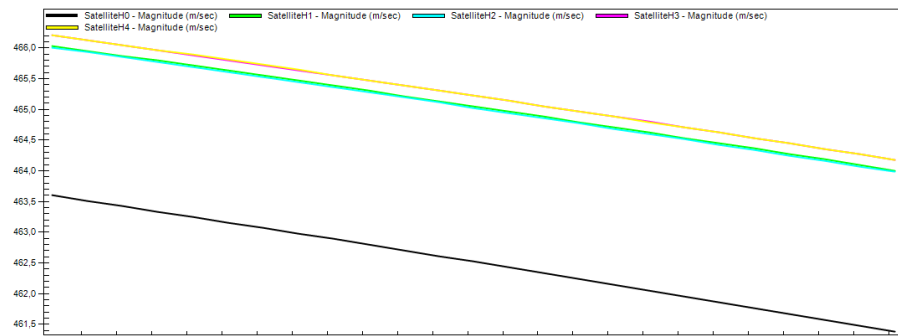


Figure 3.8: Terminal Section of Velocity Error Confrontation Curve

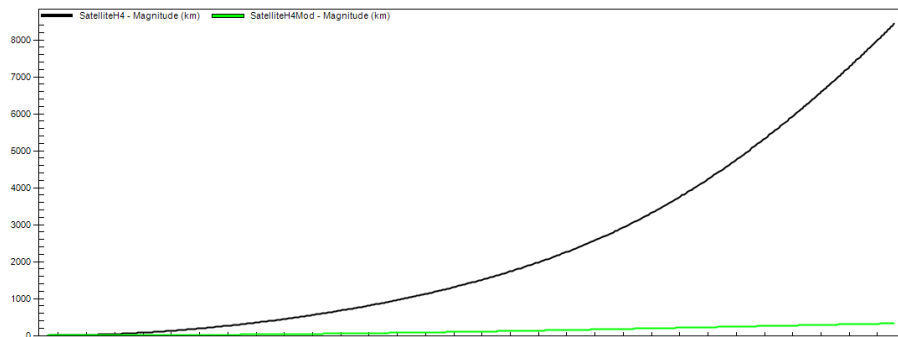


Figure 3.9: H4 and H4Mod Propagators Confrontation. Distance Magnitude [km] from H0 Trajectory

even the less accurate propagator, so restrictions in terms of orbit circularity characterizing the CR3BP have been in this sense overcome. Finally deepened considerations about Moon's perturbation are highlighted in Section 5.2.1.

Chapter 4

Complete Force Model Approach to Trajectory Optimization

This Chapter is concerned with the procedure developed to 'translate' the hypothetical trajectory designed in the context of the CR3BP, taking into consideration a quite close to reality force model. Firstly a clear overview of the numerical and mathematical tools, adopted while designing and parsing the trajectories, will be provided. Thus the most relevant aspects of the 'translation' to the complete force model algorithm will be exposed. Finally, trying to retrace an ESA Euclid's discarded trajectory, it shall try to give some validation of both the complete force model and the algorithm adopted.

4.1 Computational Approach

This Chapter will focus on the methodology used to determinate a continuous path fitted for connect the Earth to a quasi-periodic orbit around a desired Lagrangian point in a particular binary system. The approximation provided in Chapter 2 is based on the numerical solution of the system of differential equations of motion regarding the circular restricted three body problem. Whereas, adopting the complete force model proposed in Chapter 3 and then propagating the initial conditions concerning the aforementioned approximation, the solution will diverge quite rapidly.

The method developed provides improved initial conditions, at specified intervals along the entire path, taking into consideration the expanded force model; then such improved propagated trajectories can be 'patched' together for a continuous motion along the path previously drawn according to the CR3BP. Operationally, using this methodology, it is firstly attempted to define a sequence of specific points, a *mesh*, belonging to the previously designed CR3BP adimensionalized trajectory. These points shall be considered as bounds of many sub-trajectories arcs to be determined according to the designed complete force model. Thus each of these arcs is characterized by a specific initial condition, a state vector which has to be proper modified, in terms of velocity module and

direction, so that, numerical solving the equations of motion, (3.8), a trajectory connecting the initial position to the next mesh point can be designed.

All the numerical integration processes are accomplished adopting the same approach exposed in Section 2.1. Further in this Section, main features of the proposed methodology will be exposed.

4.1.1 Dimensionalize the CR3BP Solution

At this point it shall be noticed the presence of inconsistencies considering the hypothetical CR3BP Trajectory and the complete force model proposed in Chapter 2, specifically an adimensionalized trajectory has just been designed, thus it is necessary to translate it in a dimensional reference system. Such a reference system must be consistent with the equations of motion (3.8), so the trajectory propagated under the equations of the CR3BP shall be dimensionalized and translated from the synodic frame, Section 1.3, to the J2000 reference frame, centered in the Solar System barycenter, Section 3.2.1.

Recalling the planar and circular orbit constraints, concerning to the CR3BP assumptions, it is clear that, aiming to adopt a close-to-reality complete force model, seeking to dimensionalize the aforementioned trajectory, it is not possible to adopt constant values of primaries distance. Clearly this has to do with the fact that primaries orbits are elliptical, thus their mutual distance values vary as a function of time. This tallies with the need to define an epoch value to be allocated to the initial point of the supposed trajectory. By doing so, it is possible to assign, to each adimensionalized trajectory point, an epoch value, computed from the first. Obviously, these epoch values are computed considering the time values previously assigned to each CR3BP trajectory point, assuming a zero value for the first point.

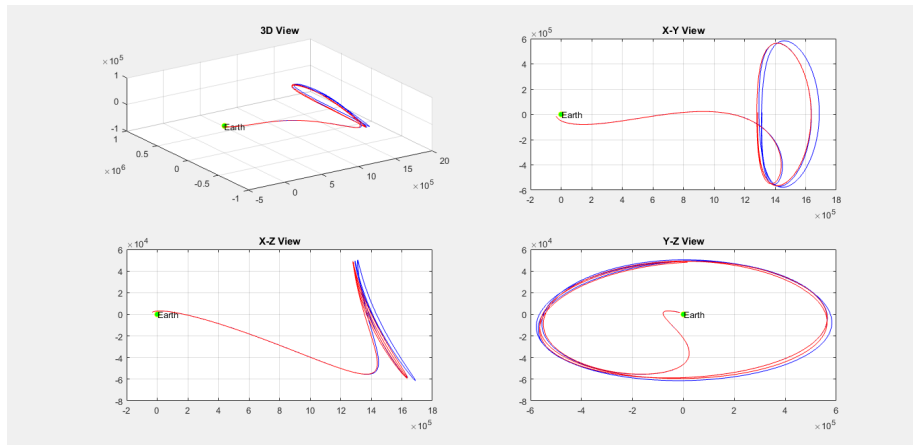


Figure 4.1: Dimensionalization Comparison. Constant Sun-Earth Distance (shaded in red); Real Sun-Earth Distance (shaded in blue). Earth Centered Synodic Ref Frame.

Once an epoch value has been assigned to each point, it is possible to dimensionalize the matching state vector computing the real primaries distance value. Such a parameter should be evaluated using the SPICE Toolbox, Section 3.2.1.

Figure 4.1 and Figure 4.2 highlight the difference found using both a constant primaries distance value and computing the evolution in time of this parameter; an arbitrary quasi-periodic orbit around the L2 Lagrangian point in the Sun-Earth system has been used to show the comparison ($A_x=2e5$ km, $A_z=5e4$ km and $\phi=180$ deg; epoch: 01 Jan 2019 00:00:00).

Clearly such an operation has no physical meaning and can't be considered as a methodology to solve the elliptical restricted three body problem. By the way, dimensionalizing the CR3BP trajectory it has been created a path to be retraced under the effect of the complete force model proposed, getting to the final solution. Lastly it has to be noticed that, referring to this dimensional path, it is only considering the position components. The final result of the dimensionalization process of the CR3BP trajectory will be a series of points, a path, deriving from this trajectory, characterized by an epoch value and three position components, expressed under the inertial J2000 reference frame (centered in the Solar System barycenter).

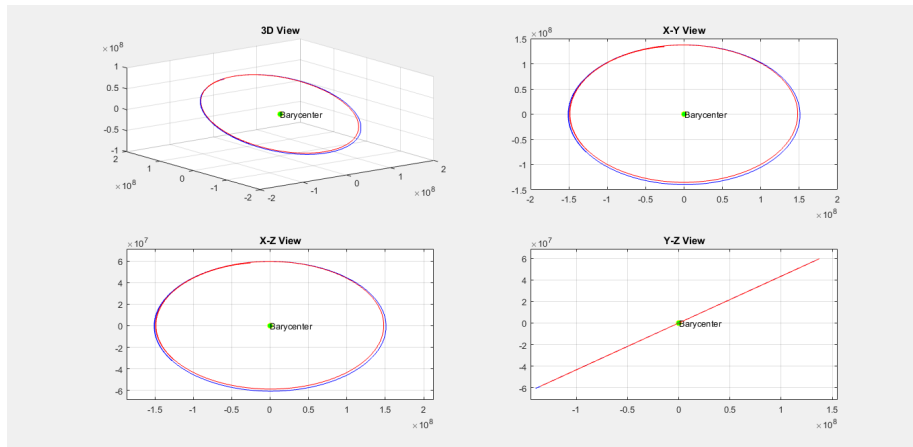


Figure 4.2: Dimensionalization Comparison. Constant Sun-Earth Distance (shaded in red); Real Sun-Earth Distance (shaded in blue). Solar System Barycenter, J2000 Ref Frame.

Having translate the CR3BP trajectory (at least in terms of position), it is now possible to point the focus on the evaluation of the trajectory arcs connecting each two consecutive mesh points. For the sake of completeness, it has to be said that the first point of the adimensionalized trajectory will represent the initial condition from which start even the propagation under the complete force model. For this reason it is necessary to dimensionalize and translate also its velocity components, first point complete state vector will be adopted as first attempt to be propagated in order design a proper first trajectory arc.

Adopting a Variable Step Size Mesh

Clearly, it is fundamental to create an optimal mesh starting from the CR3BP trajectory; it is aiming to choose the best number of trajectory's points to be considered as nodes of such a mesh. These points will define the path to be retraced under the equations of motion defined by the complete force model, thus

they represent the bounds of the trajectory arcs which have to be propagated. Basically it would be possible to consider a mesh as fit as the number of points characterizing the preliminary trajectory (the quantity and the distribution in time of such these points is determined by the numerical integration time step, Section 2.1). Clearly such a mesh would be too dense and completely useless, furthermore, as it will be explained in the next Section, the numerical approach adopted to identify the correct initial conditions, which propagation define a trajectory arc connecting the current mesh point to the next, could not converge to an acceptable solution if the time step between the two mesh points is too large. Thus an adaptive time step has been considered to define an optimal mesh; in this sense an upper limit of 30 days time step and a lower limit of 1 hour time step have been imposed. Due to the nature of the numerical procedure further exposed, there will be a much more dense mesh in the early phase of the transfer trajectory, then the time step will increase to the maximum value of 30 days in parallel to the QPO approach and up-keeping. This upper limit has been set as compromise between the need of computational cost reduction and the scientific and engineering requirements fulfillment.

4.1.2 Trajectory Arcs Construction

Given two generic consecutive mesh points it is necessary to define a numerical procedure to determine which initial condition will produce a solution to the complete force model equations of motion, resulting in a trajectory arc which connects the aforementioned mesh points. State vectors at the beginning and at the end of each interval are defined as six-dimensional target points (three position components plus three velocity components). An integrated path between two consecutive mesh points is defined as a trajectory segment. Further exposed procedure was firstly presented by K. C. Howell and H. J. Pernicka [8].

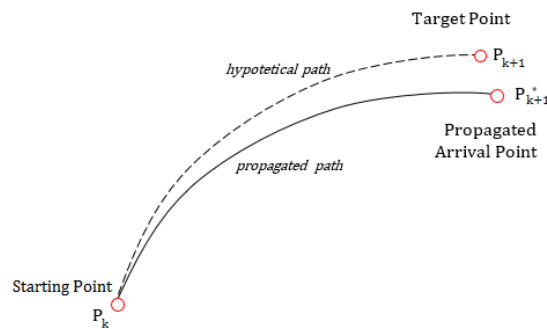


Figure 4.3: Schematic Representation of a Single Step of the Iterative Correction Process.

Once the mesh points or the target points have been determined, trajectory segments between target positions are determined modifying the velocity state vector at the beginning of the interval, trying to match the resultant trajectory segment end point with the position value at the end of the interval. This first iterative process is made using a differential corrector. Segments are patched

together, resulting in a trajectory which is continuous in position but presenting also velocity discontinuities, DV, at each mesh point. To expose an example of such a process, the method is summarized for the case of an arbitrary interval between two hypothetical mesh points separated by a certain time step. Figure 4.3 shows an hypothetical step of the iterative correction process.

The State Transition Matrix

Before entering the explanation of the correction process, it is necessary to introduce the concept of *State Transition Matrix* of partial derivatives. The function of the State Transition Matrix, STM, is to relate the coordinate variations for the times t_k and t_{k+1} , in addition such a matrix could pose cumbersome analytical expression when the equations of motion regard a much more complex and accurate force model. For the purpose of this research a particular method has been considered to compute the STM, the *Markley's Method* [7].

The Markley's method uses two different states at the times t_k and t_{k+1} , and then it evaluates the transition matrix between them by using the expression of the equations of motion. This method consists of making one approximation for the STM of the state vector based on the Taylor series expansion for a determined interval of propagation Δt . It is possible to express the differential equation of the state transition as follows

$$\frac{d}{dt} \Phi(t, t_0) = \mathbf{A}_1(t) \Phi(t, t_0) \quad (4.1)$$

Where it has been introduced the $\mathbf{A}_1(t)$ matrix, defined using the gradient matrix $\mathbf{G}(t)$

$$\mathbf{A}_1(t) = \begin{bmatrix} 0 & \mathbf{I} \\ \mathbf{G}(t) & 0 \end{bmatrix} \quad \text{and} \quad \mathbf{G}(t) = \frac{\partial}{\partial \mathbf{r}} \mathbf{a}(\mathbf{r}, t) \quad (4.2)$$

In equations (4.1) and (4.2) it has been referred to $\mathbf{r}=(x,y,z)^T$ as the Cartesian position state vector at the generic time t . The vector $\mathbf{a}(\mathbf{r},t)$ represents the acceleration of the hypothetical spacecraft; components of such a vector could be evaluated, at each time instant, through the equations of motion (3.8). $\mathbf{G}(t)$ matrix expression could be expanded as follows

$$\mathbf{G}(t) = \frac{\partial}{\partial \mathbf{r}} \mathbf{a}(\mathbf{r}, t) = \begin{bmatrix} \frac{\partial a_x}{\partial x} & \frac{\partial a_x}{\partial y} & \frac{\partial a_x}{\partial z} \\ \frac{\partial a_y}{\partial x} & \frac{\partial a_y}{\partial y} & \frac{\partial a_y}{\partial z} \\ \frac{\partial a_z}{\partial x} & \frac{\partial a_z}{\partial y} & \frac{\partial a_z}{\partial z} \end{bmatrix} \quad (4.3)$$

Thus, performing successive derivatives of the differential equation (4.1), followed by substitutions, gives the derivative of the transition matrix:

$$\begin{aligned} \frac{d^i}{dt^i} \Phi(t, t_0) &= \mathbf{A}_i(t) \Phi(t, t_0) \\ \mathbf{A}_i(t) &= \dot{\mathbf{A}}_{i-1}(t) + \mathbf{A}_{i-1}(t) \mathbf{A}_1(t) \end{aligned} \quad (4.4)$$

The dot represents the derivative with respect to the time. Developing $\Phi(t, t_0)$ in Taylor's series at $t=t_0$, using the matrices $\mathbf{A}_i(t_0)$ for $i=1, \dots, 4$ and the initial condition $\Phi(t_0, t_0) \equiv \mathbf{I}$, the transition matrix of the position and velocity obtained after some simplification [7] may be written as

$$\Phi(t, t_0) \sim \begin{bmatrix} \Phi_{rr} & \Phi_{rv} \\ \Phi_{vr} & \Phi_{vv} \end{bmatrix} \quad (4.5)$$

$\Phi(t, t_0)$ is a 6x6 matrix where, considering that $\Delta t \equiv t - t_0$ and $\mathbf{G}_0 \equiv \mathbf{G}(t_0)$,

$$\begin{aligned}\Phi_{rr} &= \mathbf{I} + (2\mathbf{G}_0 + \mathbf{G})\frac{(\Delta t)^2}{6} \\ \Phi_{rv} &= \mathbf{I}\Delta t + (\mathbf{G}_0 + \mathbf{G})\frac{(\Delta t)^3}{12} \\ \Phi_{vr} &= (\mathbf{G}_0 + \mathbf{G})\frac{\Delta t}{2} \\ \Phi_{vv} &= \mathbf{I} + (\mathbf{G}_0 + 2\mathbf{G})\frac{(\Delta t)^2}{6}\end{aligned}\quad (4.6)$$

Having introduced the concept of State Transition Matrix and having also provided a method to evaluate it, according to the complete force model proposed, it is now possible to proceed in the explanation of the iterative correction process.

Iterative Correction Process

Looking again to Figure 4.3, aiming to find a trajectory segment which connects the starting and the arrival points, it is necessary to define the proper initial condition, in terms of velocity, which, once propagated along the $t_k - t_{k+1}$ time span, provides the required result. Further it will refer to the situation shown in Figure 4.3 as an example to illustrate the generic iterative correction process.

The first guess for the initial point state vector is $X_k = \{x_k, y_k, z_k, u_k, v_k, w_k\}^T$, and vector states associated with the other target points are X_{k+1} and X_{k+1}^* . Clearly if $k=0$, in other words considering the first trajectory segment, the first guess in terms of velocity is equal to the velocity value at the first point of the CR3BP trajectory, properly dimensionalized and translated in the J2000 reference frame. The first segment is computed by numerically integrating P_k , along with the transition matrix, for the time $t_k - t_{k+1}$ to the point P_{k+1}^* . In general, the state values at P_{k+1}^* will not equal the target values at P_{k+1} . A differential correction process is used to modify the velocity components at P_k to meet the position requirement at P_{k+1} . The vector relationship can be written as follows

$$\delta X_{k+1}^* \simeq \Phi(t_{k+1}^*, t_k) \delta X_k + \left. \frac{\delta X}{\delta t} \right]_{P_{k+1}^*} \delta(t_{k+1}^* - t_k) \quad (4.7)$$

The three scalar equations in (4.7) contain four unknown: changes in the velocity components, δu_k δv_k δw_k , and change in the segment time, $\delta(t_{k+1} - t_k)$. There are many solutions to such a problem. However a rearranged linear form of the scalar equations could be expressed as follows

$$L\mathbf{c} = \mathbf{b} \quad (4.8)$$

Where

$$L = \begin{bmatrix} \Phi_{14} & \Phi_{15} & \Phi_{16} & u \\ \Phi_{24} & \Phi_{25} & \Phi_{26} & v \\ \Phi_{34} & \Phi_{35} & \Phi_{36} & w \end{bmatrix} \quad \text{evaluated at } P_{k+1}^* \quad (4.9)$$

$$\mathbf{c} = \{\delta u_{P_k}, \delta v_{P_k}, \delta w_{P_k}, \delta(t_{k+1}^* - t_k)\}^T$$

$$\mathbf{b} = \{\delta x_{P_{k+1}}, \delta y_{P_{k+1}}, \delta z_{P_{k+1}}\}^T$$

Elements Φ_{ij} are elements of the aforementioned 6x6 State Transition Matrix. The last three scalar equations of (4.7) are not used. Assuming that all the unknowns in \mathbf{c} have equal importance, a result from linear algebra states the solution to (4.8) with the smallest Euclidean norm is given by

$$\mathbf{c} = L^T(LL^T)^{-1}\mathbf{b} \quad (4.10)$$

Once the vector \mathbf{c} of velocity variations at P_k has been evaluated, the integration is restarted at t_k considering the modified initial state and proceeds for the new time interval. Such a process has to be iterated until the position P_{k+1}^* converge to the position P_{k+1} within some small tolerance (as example, for the purpose of this research, a tolerance of 1 km has been set). The following trajectory segment is computed following the same steps, using as initial guess the arrival point state vector, X_{k+1} , of the previous segment. The two segments are now patched; in calculation of both segments, starting and arrival positions are fixed, and the just explained iterative process corrects velocity so that the resulting path is continuous in position, but not in velocity. This process is repeated for all the trajectory segments bordered by the selected mesh points.

As it is previously said, such a process only guarantees a path continuous in position, in fact, at each junction point, a certain velocity discontinuity arise. Such a DV has to be provided by the spacecraft, thus it represents an infinite maneuver which has to be performed to continue traveling along the charted trajectory. The overall sum of these maneuvers somehow represents the cost in terms of propellant budget of the mission; taking also notice that every single maneuver complicates the entire mission, it is necessary to minimise the number of these impulsive burns. Thus it is clearly fundamental to drastically reduce the number of mesh points considered, discarding any of them which is unnecessary. Figure 4.4 shows a representation of the final result of the iter-

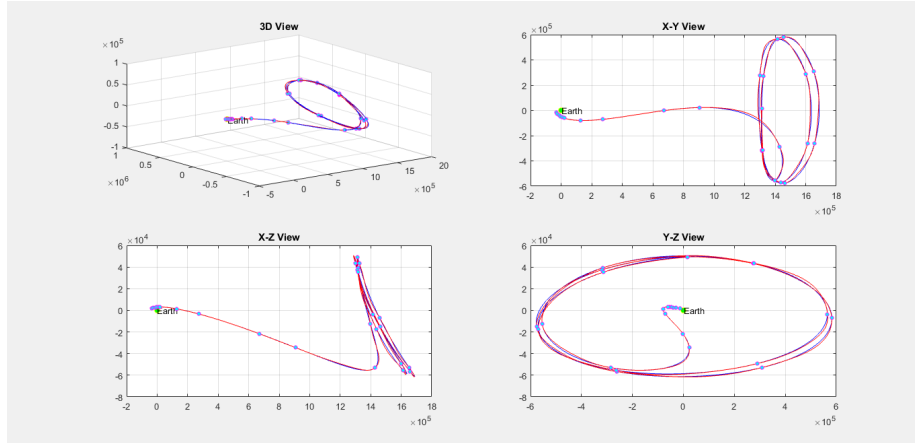


Figure 4.4: Final Corrected Trajectory Representation. CR3BP Trajectory at Variable Primary Distances Dimensionalization (shaded in blue), Complete Force Model Trajectory (shaded in red), Mesh Points (cyan dots). Earth Centered Synodic Ref Frame.

ative process applied over the entire CR3BP trajectory. The final trajectory, propagated considering the complete force model is shaded in red; an arbitrary

quasi-periodic orbit around the L2 Lagrangian point in the Sun-Earth system has been used to show the comparison ($A_x=2e5$ km, $A_z=5e4$ km and $\phi=180$ deg; epoch: *01 Jan 2019 00:00:00*). As it was anticipated, the resulting mesh of boundary points is much more dense in the Earth-Moon system proximity. This is due to the higher intensity and variability of the proposed force model in such this region. However such an elevated number of maneuver points has to be avoided, especially when the considered maneuver is performed too much close to the Earth system (injection precision requirements could be too far out to reach, due to the stronger effect of the Earth-Moon gravitational fields). Section 5.3 will concern the trajectory optimization process to sensitively reduce the number of maneuvers to be planned. Further results will be exposed in the next Chapter.

4.2 Algorithm Validation

It is now illustrated the strategy adopted to perform a preliminary validation of the entire aforementioned process adopted to design a trajectory connecting the Earth and a quasi-periodic orbit around a generic Lagrangian point. In this regard, it has been considered, as reference solution, a discarded ESA's Euclid [11] trajectory (further information about this mission are reported in Section 1.4). The aim of this validation process is to recreate such an Euclid type trajectory, starting from a preliminary design phase, under the CR3BP equations of motion, and then modifying this solution to meet the complete force model constraints. Further in this Section it will refer to the reference Euclid trajectory as RET.

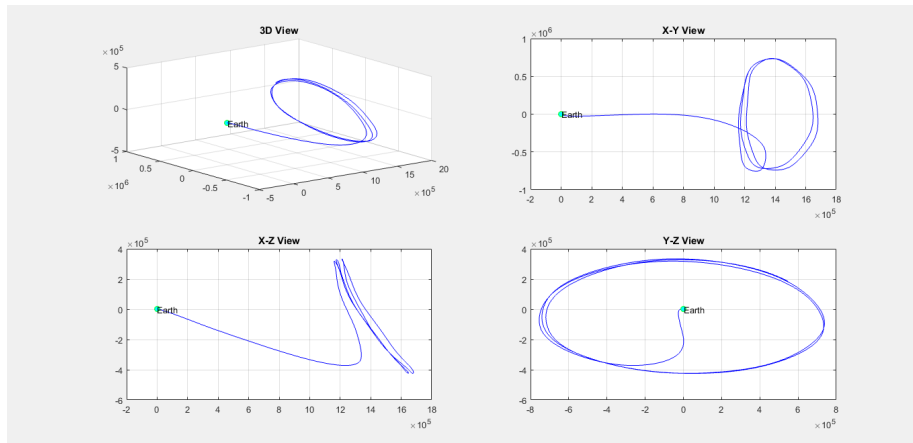


Figure 4.5: Reference Euclid Trajectory (RET). Earth Centered Synodic Reference Frame

Only available sources, regarding RET, are a complete set of ephemerides, computed in the synodic Earth-centered reference frame, from which it has been possible to draw a simple representation reported in Figure 4.5.

CR3BP Preliminary Design

Firstly it is necessary to properly define the geometric characteristics of the CR3BP quasi-periodic orbit which it is trying to recreate. The considered Euclid's orbit around the Sun-Earth L2 libration point is a Lissajous type quasi-periodic orbit. Furthermore it is possible to observe, from Figure 4.5, that such a QPO is characterized by large amplitude values, in addition these values seems to be pretty similar and ranging from $3e5$ km to $4e5$ km. Recalling considerations made in Chapter 2, the insertion phase angle value still has to be defined; looking to the transfer phase shape and the insertion in QPO location, Figure 4.5, a 180 deg insertion phase angle value has been adopted.

An analysis made by trial and error has been accomplished, thus, to retrace the RET, it has been selected a CR3BP trajectory ending in a QPO of $A_x=3.2e5$ km, $A_z=3.4e5$ km and $\phi=180$ deg. Figure 4.6 shows a geometrical confrontation between the RET and the aforementioned proposed trajectory.

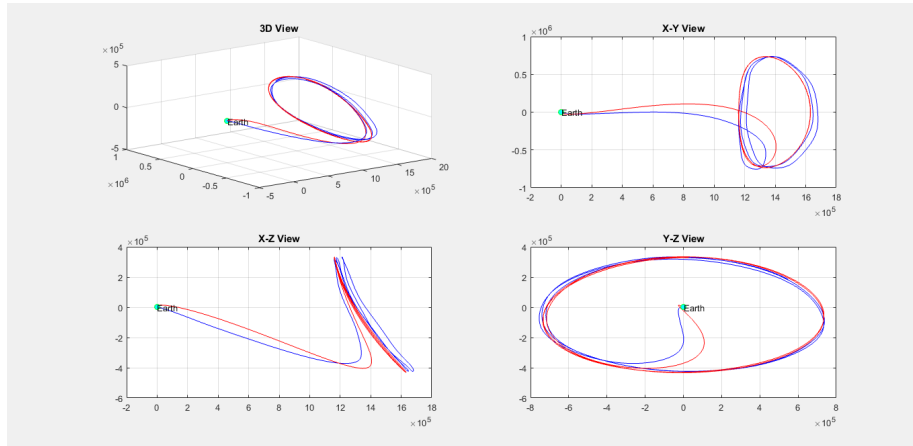


Figure 4.6: RET (shaded in blue). Computed CR3BP Trajectory (shaded in red)

It is important to notice that the designed trajectory has been built under the CR3BP equations of motion and further dimensionalized adopting a variable Sun-Earth distance value. Instead the RET is a trajectory propagated according to the complete force model equations of motion, thus such a confrontation has to be considered only useful to narrow down the analysis space and select a proper preliminary trajectory to be modified under the complete force model equations of motion.

Complete Force Model Design

It has been previously said that, aiming to compute the final trajectory, it is necessary to define an epoch value from which the propagation has to be initiated. Taking as reference the epoch values characterizing the RET, a rounded initial time has been selected to design the trajectory of comparison. The selected initial epoch is the 3rd of November, 2017. In Figure 4.8 it is possible to observe the trajectory resulting from the correction process illustrated previously in this Chapter (shaded in red).

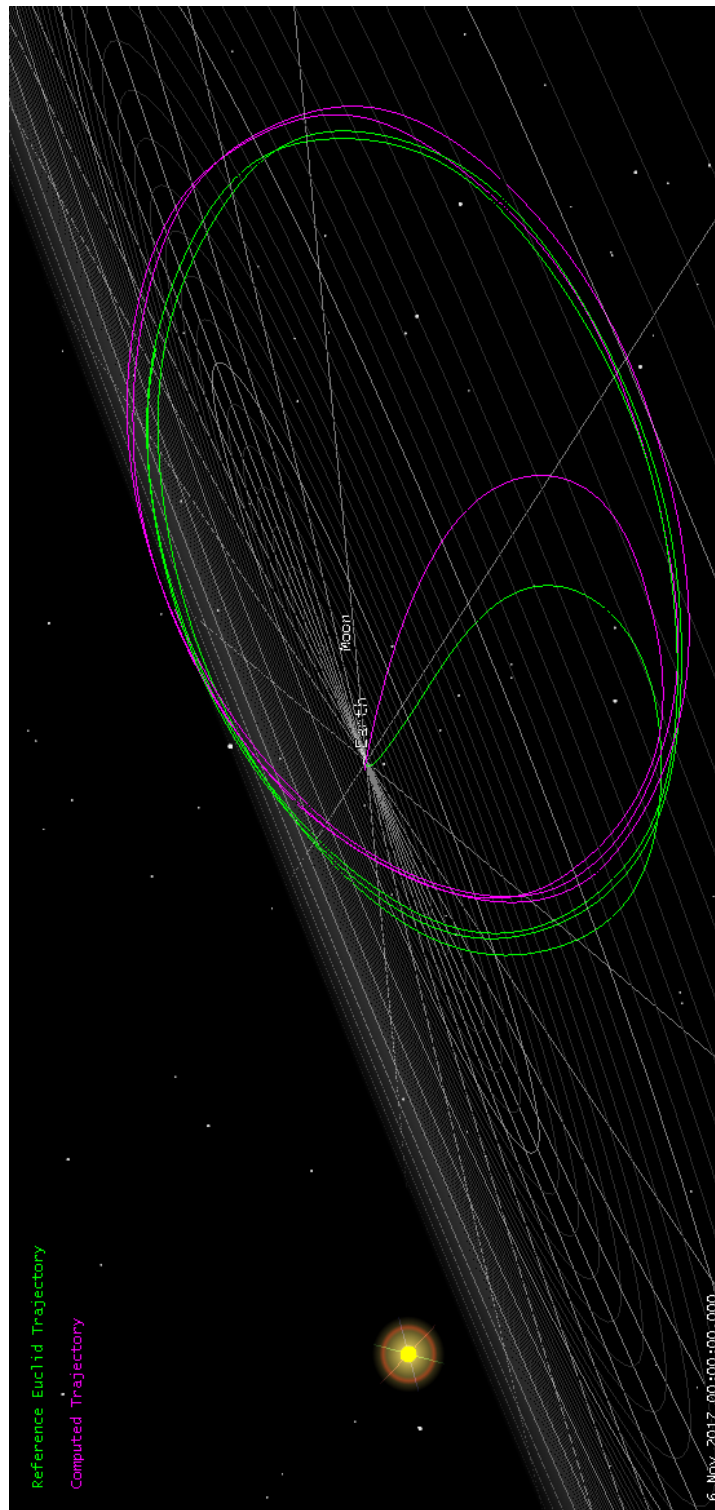


Figure 4.7: STK representation of both RET and computed trajectory.

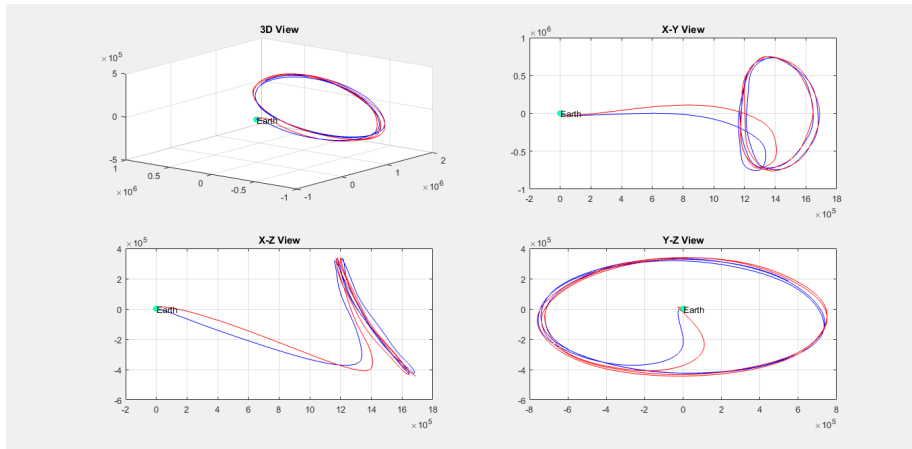


Figure 4.8: RET (shaded in blue). Final Corrected Trajectory (shaded in red)

Such a trajectory has clearly been propagated under the complete force model equations of motion, Chapter 3. As it is possible to see from Figure 4.8, the computed final trajectory is pretty similar to the RET. In particular the quasi-periodic orbit around the Sun-Earth L2 libration point is very much like the RET corresponding phase. Moreover some views from the Figure 4.8 highlight even slightly differences between the two transfer phases. However, for what concerns the transfer phase, different shapes could be obtained simply varying the minimal distance value from Earth which it is trying to achieve. As example the aforementioned final trajectory starts from an altitude over the Earth surface of approximately $1e4$ km. Anyway such a shape difference could be neglected observing that the transfer phase inserts the hypothetical spacecraft in the QPO in a similar manner, considering both the RET and the computed trajectory; moreover they present approximately the same transfer time from the Earth to the insertion in QPO.

This final solution, present a DV budget of approximately 400 m/s (the sum of all the velocity discontinuities along the complete path). This value could be lowered adopting an ignition sequence optimization strategy (such a methodology will be exposed in depth in Section 5.3). An optimized DV budget of approximately 150 m/s could be finally achieved. Considering the geometric conformity of the RET and the computed trajectory, whose DV budget appears to have an acceptable value, if compared with that characterizing similar trajectories, it may be concluded that the proposed methodology, adopted to design a trajectory under a complete force model, is valid and applicable.

Chapter 5

Results

In order to provide a clear overview of research achievements, main features of evaluated trajectories are shown in this chapter. First of all geometric characteristics will be highlighted, then these will be related to some propellant budgeting consideration; for this purpose some response surfaces will be assembled steering research objective towards an optimization problem in terms of Delta-V necessities.

5.1 Trajectories Found

According to Chapter 4, the generic final trajectory propagated considering complete force model, comes out from a baseline path well defined by the integration of the differential equations of motion and by the analytical solution of CR3BP. In particular the geometrical definition of the quasi-periodic orbit around the libration point derives from a specific analytical solution. In this sense, referring to the Lissajous solution to the CR3BP, once few parameters (x-axis amplitude, z-axis amplitude, time of propagation) are selected, a single Lissajous periodic orbit is determined. The following step is to find a numerical solution to the CR3BP rather similar to this Lissajous orbit. Such a numerical solution is achieved through a numerical integration process, so correctly varying the initial conditions evaluated considering the analytical solution, it is possible to get a numerical solution close enough to the aforementioned Lissajous orbit. Proceeding in the dissertation it is referred to final trajectories as:

$$TXXX - ZZZ$$

Where:

- XXX Refers to x-axis amplitude of Lissajous Orbit [1e3 km]
- ZZZ Refers to z-axis amplitude of Lissajous Orbit [1e3 km]

5.1.1 Nominal Periodic Orbit Selection

The code and the relative procedure developed to find suitable trajectories could manage large typologies, in terms of geometric traits, of Lissajous orbits around both L1 and L2 libration point in Sun-Earth System or Earth-Moon System;

nevertheless the focus will be pointed on three different quasi-periodic orbits around L2 in Sun-Earth System, due to scientific significance of this orbit class, ascertained during the state of the art analysis of mission involving periodic orbit around Lagrangian points. QPOs are propagated for one year after the end of nominal transfer phase; these orbits are:

- T200-050
- T200-010
- T300-050

They have been selected after preliminary and rough evaluation phase considering only the stability of the numerical solution to the differential equations of CR3BP; moreover geometries considered are similar to one of the proposed hypothetical relative to Euclid trajectory, benchmark solution of the study.

5.1.2 Variables domain

Given the nominal QPO, two other variables have been considered: the insertion angle on QPO and the launch date. First it is necessary to consider the insertion angle on the quasi-periodic orbit found; this variable refers to the phase angle of the analytical Lissajous orbit, assuming 0 degrees in case of insertion at the furthest point from the Earth, in xy plane, of QPO and 180 degrees for the closest point (it is considered an orbit around L2 in Sun-Earth system). Once the phase angle is selected the code can evaluate the transfer trajectory from an undefined Earth departure orbit (further analysis could concern about the merging operation of transfer phase and launch phase) through a process of backward integration. The coupling of transfer trajectory and QPO gives the baseline final trajectory. Then it is needed to define a launch Epoch relative to the first point of the transfer phase in order to evaluate the final trajectory. This will be propagated considering the proposed complete force model (time parameter is fundamental to obtain correct ephemerides of solar system perturbing bodies, giving a correct solution of the N-body problem).

Finally there are four different variables defining the complete solution; given one nominal periodic orbit solution, Section 5.1.1, it has been defined a simple domain characterized by two parameters: insertion phase angle, IPA, values span from 135 degrees to 225 degrees with 15 degrees step (the Earth-pointing arc), and launch date which values vector contains the first and the fifteenth day of every month of 2019. Referring to the launch date vector, the analysis will take in consideration a time span of one year, this assumption is justified by the duration of the revolution motion of the Earth around the Sun. The perturbation driven by the elliptical shape of Earth's orbit (CR3BP considered circular orbits) is characterized by a periodic nature and presents rather the same value after one complete Earth's revolution. Considering a time step of 15 days gives the possibility of take in consideration the revolution motion of the Moon around the Earth; again will arise a periodic perturbation driven by the elliptical shape of Moon's orbit. This step value permits to achieve a good comprehension of the behaviour of the solutions field over the variables domain, without increasing computational costs. No more contributions have been taken into account modeling the variables domain as a matter of fact that

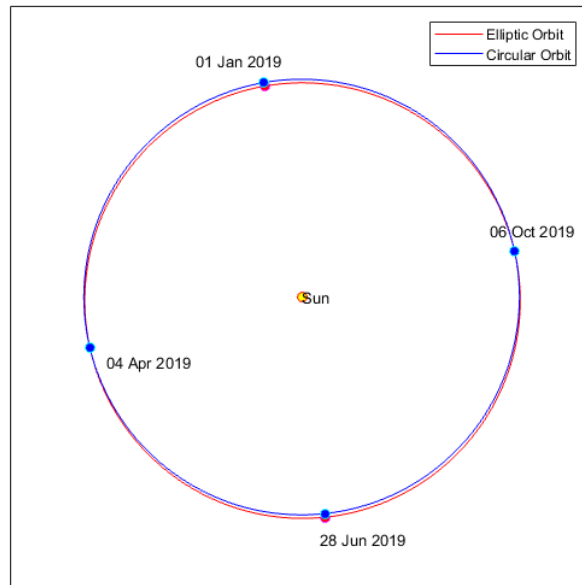


Figure 5.1: Earth's Orbit around the Sun

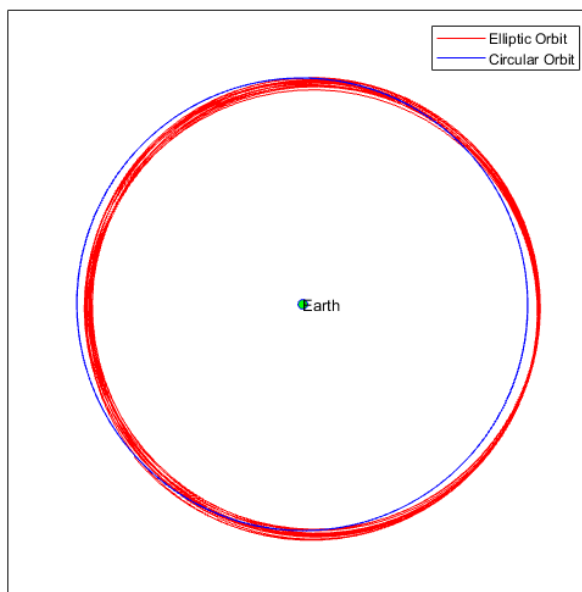


Figure 5.2: Moon's Orbit around the Earth

Sun, Moon and Earth contributions to the N-body problem solution are preponderant respect to the other bodies gravitational field. Underlying relevance of aforementioned time span, in Figure 5.1 and Figure 5.2 respectively the Earth's orbit around the Sun and the Moon's orbit around the Earth are shown. Each orbit is evaluated starting from a launch epoch between the first of January 2019 to the first of January 2020. Each position vector derive from ephemerides data calculated using Spice toolkit. As reference, to compute circular orbits it has been considered following values:

- Earth's Orbit Radius - 1,4960E+8 km
- Moon's Orbit Radius - 3,8440E+5 km

In Figure 5.3 it is possible to see a simple representation of the variables domain through which the final trajectory research activity will be driven. Each point represents a single trajectory characterized by the QPO geometry (equal over the domain) and specific values of insertion angle and launch date.

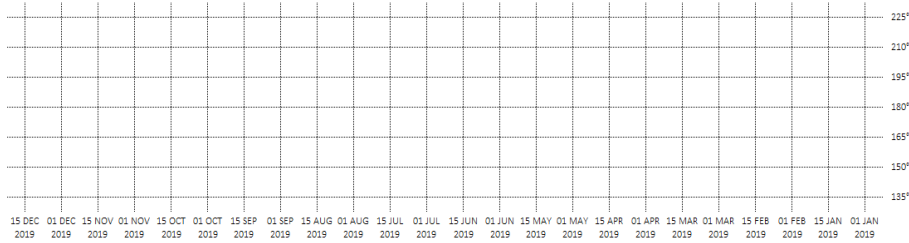


Figure 5.3: Domain of Final Trajectory Variables

5.1.3 CR3BP Solution

The baseline path of the final complete model trajectory is marked by an adimensionalized numerical solution of the CR3BP, therefore this first sketchy result is completely independent from the time variable. Reminding consideration of Chapter 2, the adimensionalized solution derives from an orbital model which considers the Earth in an exact circular motion around the barycenter of the two-body Sun-Earth system. Then the adimensionalization parameter is equal to the Astronomical Unit, the distance between Earth and Sun centers of mass:

$$AdimensionalizationParameter = 1,4960E + 8km$$

Analyzing the trajectory obtained considering the CR3BP model, it is possible to distinguish two different phases. Firstly, the transfer phase starts from an altitude, over the Earth surface, lower than 30000 km (independently from the trajectory built, this altitude value is a constraint imposed by preliminary settings of the code) and reaches the quasi-periodic orbit, QPO. The second phase is represented by the QPO itself, propagated for 360 days. The insertion in QPO, the connection between these two 'sub-trajectories', is strictly characterized by the insertion angle value considered. This parameter affects both the construction of the QPO and the research operation of the transfer trajectory. Once a precise insertion phase angle value is selected, initial conditions,

regarding the backward integration procedure, aiming to the transfer trajectory definition, are determined. In particular it was found a strictly dependence from the insertion angle value for what concerns the capability of the code to find trajectories which approach much closer the Earth. Choosing higher values of insertion angle allows to easily achieve a transfer trajectory which starts from altitudes lower than 10000 km.

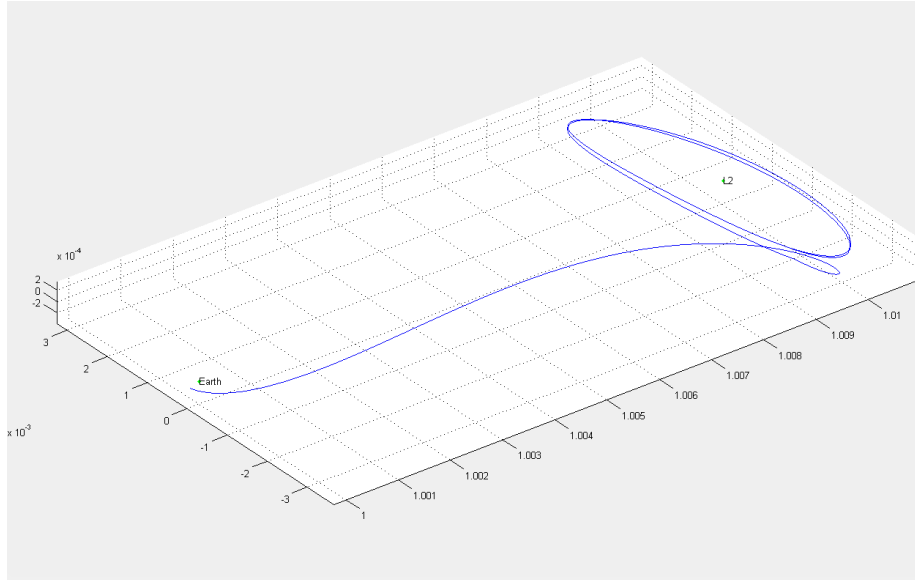


Figure 5.4: T200-050, Insertion Phase Angle in QPO 135, CR3BP propagation

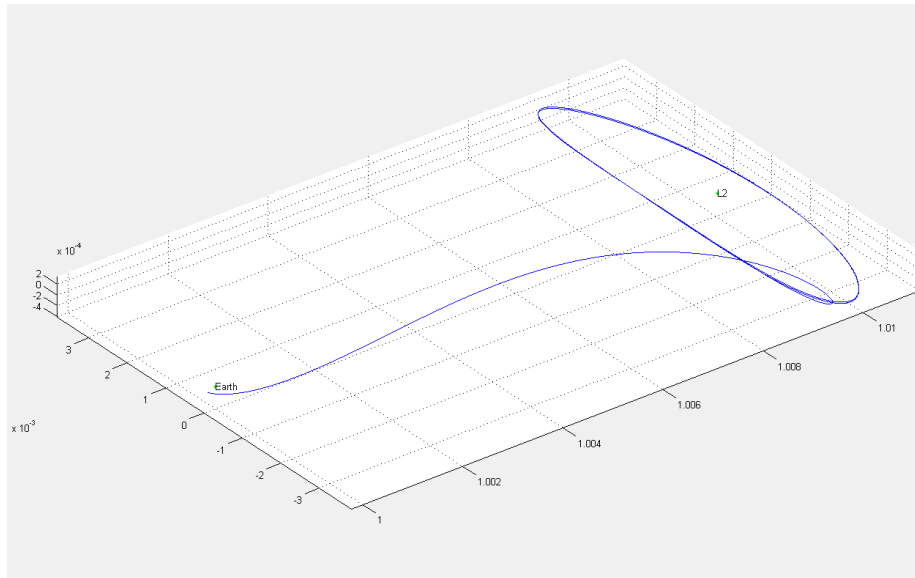


Figure 5.5: T200-050, Insertion Phase Angle in QPO 180, CR3BP propagation

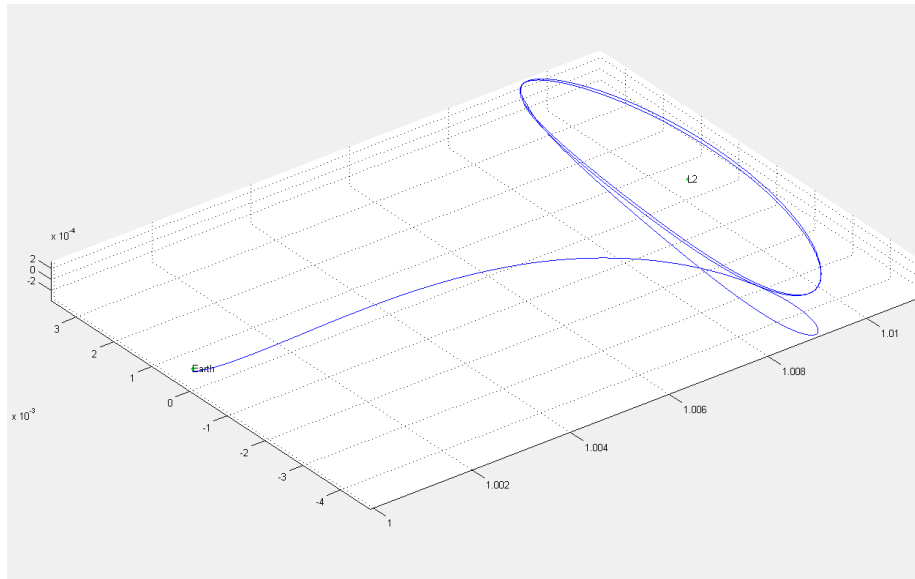


Figure 5.6: T200-050, Insertion Phase Angle in QPO 225, CR3BP propagation

In order to underline these differences, it's now taken into account the trajectory T200-050 propagated according to CR3BP; in Figure 5.4, Figure 5.5 and Figure 5.6 are shown variations of T200-050 depending on different insertion phase angle values. Plots are obtained in Matlab environment.

Graphic results confirm what has just been assessed, the trajectory T200-050 characterized by 225 degrees insertion angle shows a closer Earth-approach than the other two, which are rather similar in this sense. There are clear geometric differences between the trajectories evaluated, specifically they diverge from each other in terms of amplitude of quasi-periodic orbit, even though the analytical solution is the same; it depends on the convergence of numerical solution which is conditioned by the assumption of a significant value of z-axis amplitude of Lissajous analytical periodic solution. It has to be taken in consideration that the variables domain exploration will ignore approach-to-Earth performances of different trajectories, as a matter of fact that, in this sense, results could be improved well-defying and optimizing the launch phase.

Results achieved considering the CR3BP model are slightly meaningful, in fact it hasn't been assumed yet the effect of considering the Earth in an elliptic orbit around the barycenter of the Sun-Earth system; in fact, contrary to circular simplification, the mutual distance between the two main bodies would change; moreover, aiming to a closer to reality solution, it has to be considered the effect of perturbations of third bodies and solar radiation pressure.

5.1.4 Complete Force Model Solution

According to what has been said in Chapter 3, the complete force field which distinguishes the space around Earth and Sun-Earth collinear libration points, L1 and L2, is variable in time, due to non circularity of Earth's motion around Solar system barycenter and to the presence of the Moon, Figure 5.7.

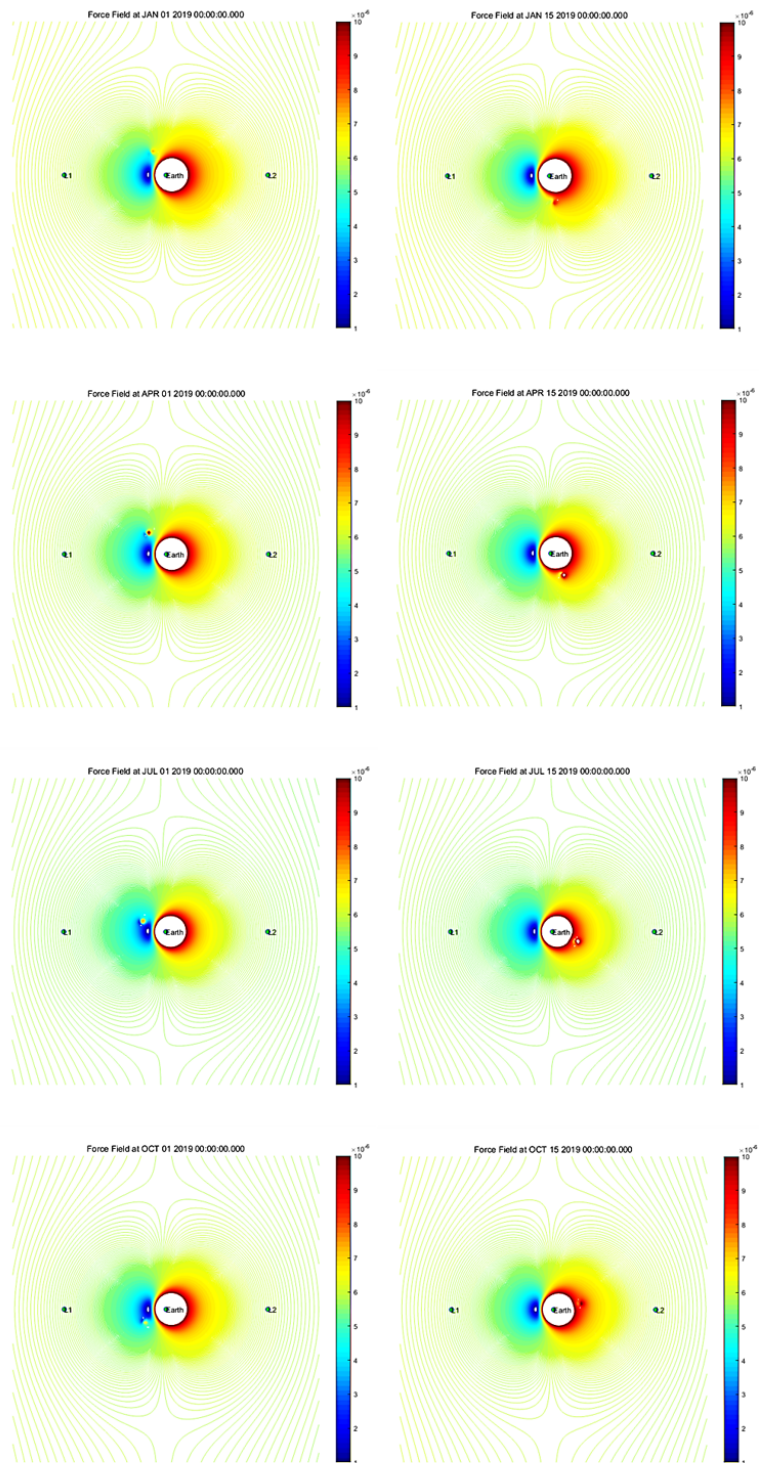


Figure 5.7: Complete Force Field representation for a representative Epoch span, L1 and L2 positions are approximated and based on CR3BP

Earth' satellite revolution introduces non negligible irregularities in Sun-Earth force field; the elliptic orbit considered for the Earth revolution and the presence of the Moon as a third body are the most relevant perturbations of circular restricted three body problem, then it is necessary to take these aspects into account converting the baseline CR3BP solution to the final trajectory.

The first step in order to get the final solution is to introduce a correct mesh for the baseline trajectory. This meshing operation allows to consider only few points of the initial path, based on CR3BP equations of motion. Then the mesh points will be linked towards a differential corrector acting on the initial state vector, obtaining a multiple arc trajectory propagated according to the complete force field. Sudden variations of acceleration field intensity could affect the convergence of the differential corrector solution, in other words, two points too much separated in time could not be connectable using a single arc, due to aforementioned acceleration variations; otherwise, considering too many points, a too dense mesh, entail a large computational cost and above all a large number of impulsive maneuvers, increasing DV budget, to overtake the velocity discontinuities between two consecutive arcs.

It's clearly necessary to consider a variable mesh. For this purpose it has been taken into account a mesh spanning from a 30 days step between two consecutive points, to a 60 minutes step. Closer step are related to the early transfer phase, where the Earth-Moon gravitational field contributions to local acceleration are greater then any other, whereas a larger step could be considered escaping from Earth's sphere of influence and during up-keeping operations in QPO orbit. Figure 5.8 represents a sample of the meshing operation result, it's evident the higher density of points in the region closer to the Earth. Once a

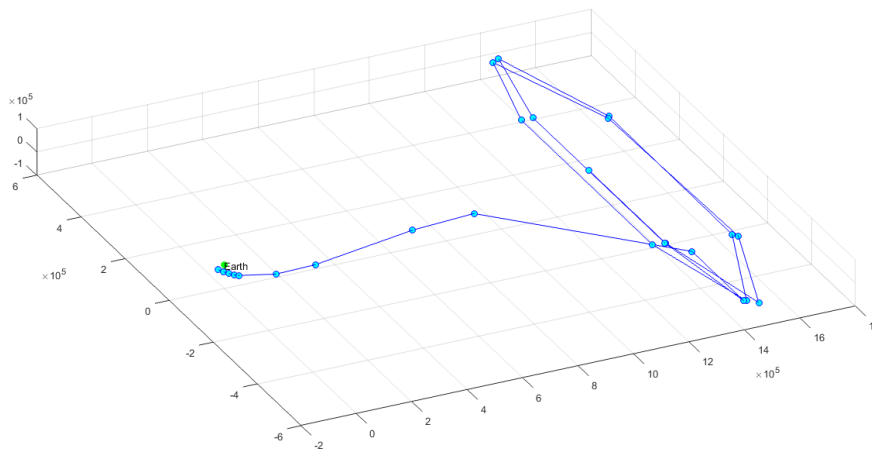


Figure 5.8: Mesh Points for T200-050 Trajectory, launch date 15 MAR 2019, Insertion Angle 180

mesh-based path has been established, through an operation of differential correction of the state vector at any mesh point (Chapter 4), required to guarantee continuity at every between-arc connection, it is possible to propagate all the intermediate initial conditions according to the complete force model system of differential equations. Some final trajectories are shown; in Figure 5.9, Figure 5.10 and Figure 5.11 it is possible to observe a graphic representation of T200-

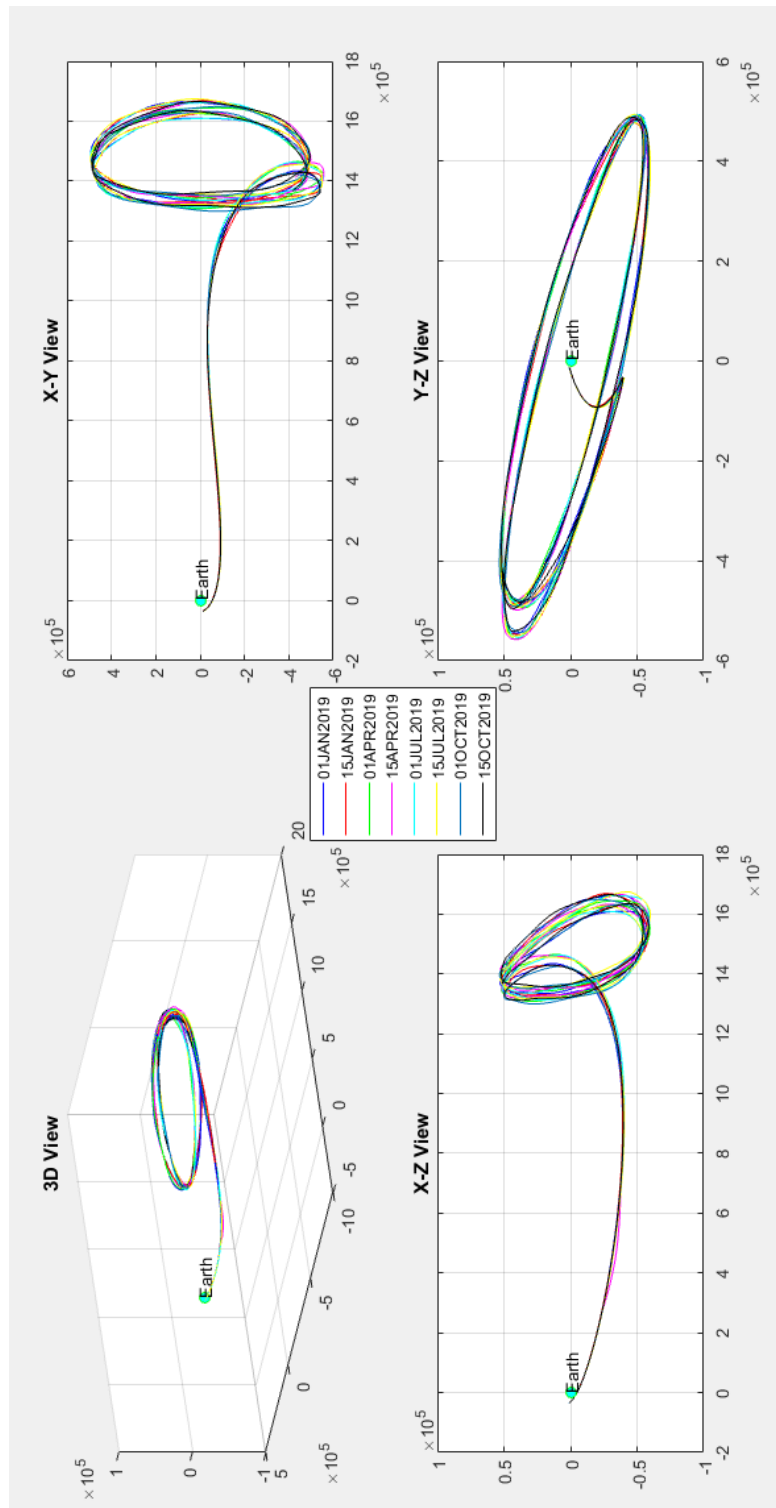


Figure 5.9: Different views of T200-050 propagated considering the complete force model and different launch epoch values, insertion angle in QPO value 135

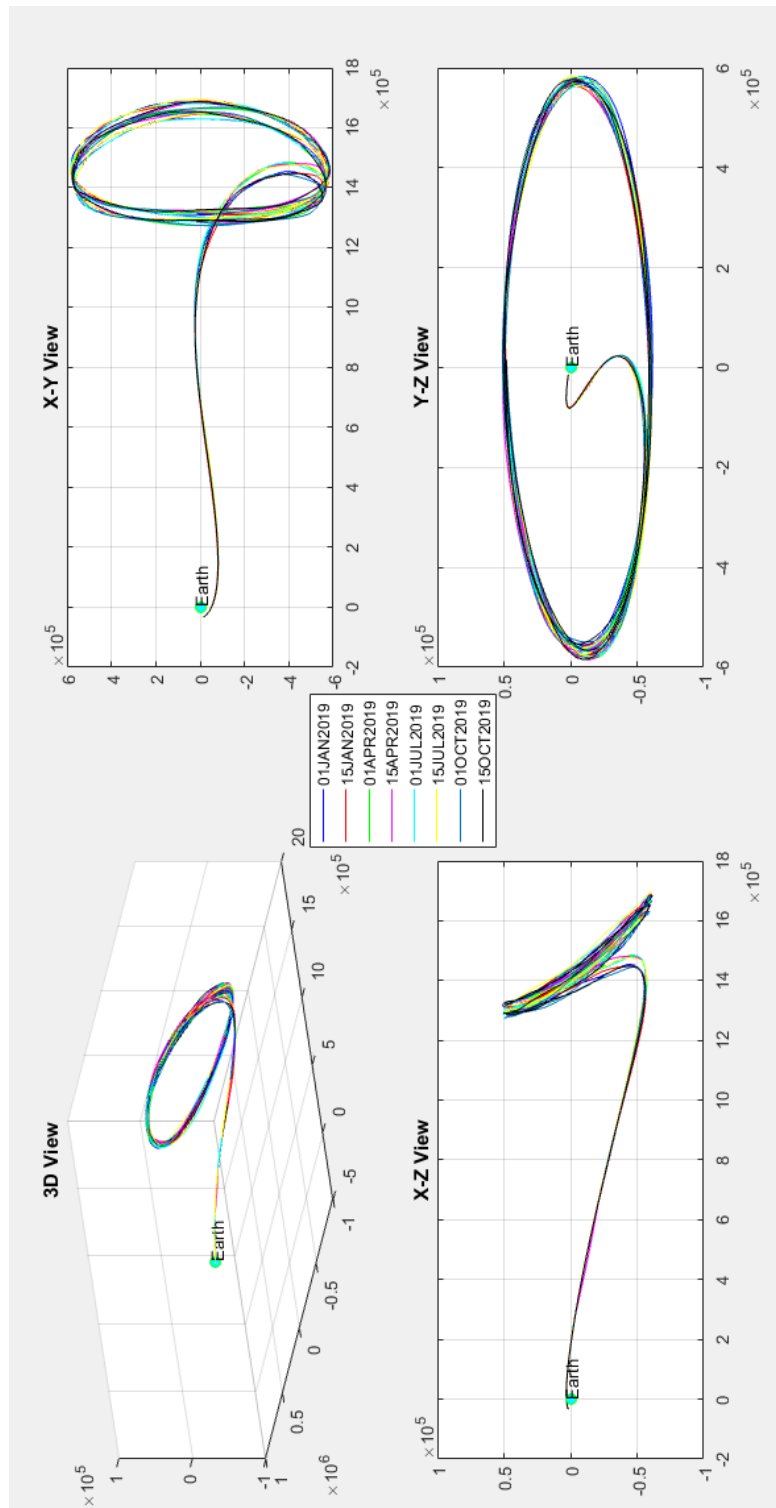


Figure 5.10: Different views of T200-050 propagated considering the complete force model and different launch epoch values, insertion angle in QPO value 180

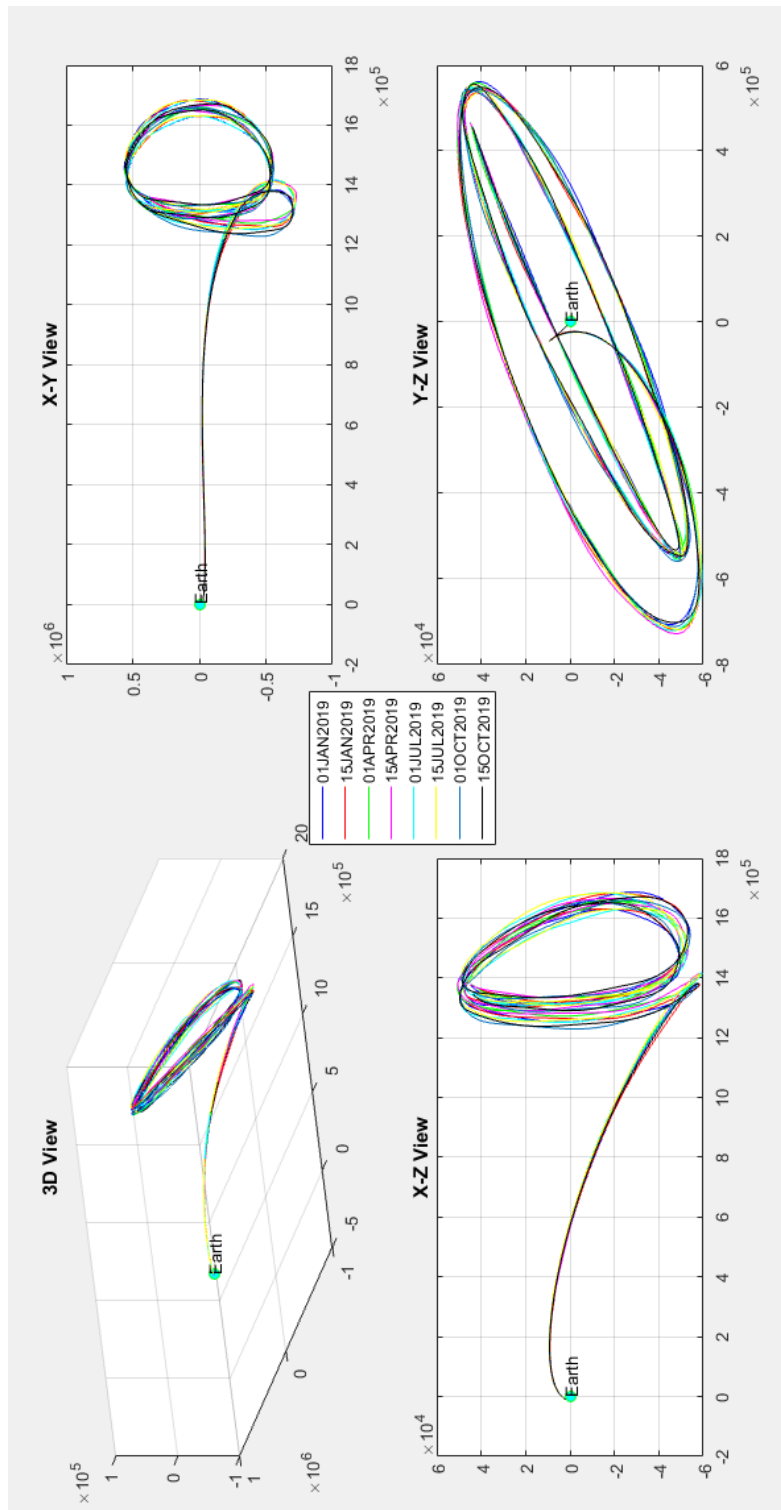


Figure 5.11: Different views of T200-050 propagated considering the complete force model and different launch epoch values, insertion angle in QPO value 225

050 trajectory, considering an insertion angle in QPO of respectively 135, 180 and 225 degrees propagated starting from different Epoch values.

As it has been previously said, main geometric differences come varying insertion angle, whereas variation of launch date parameter would entail significant variations in DV consumption. Following on from considering a time-variable mesh as baseline path, evaluating trajectories at different epochs imply that these will be characterized by different primary points due to variations in force model caused by different main bodies mutual position, depending on time parameter; these different points are linked by different trajectory arcs, however, meshes are completely generated from the CR3BP solution which is time independent, so any primary point belong to this unique trajectory, justifying minimum differences in shape spotted driving the analysis at different launch epoch values. Later in this Chapter will be examined in depth physical and geometric characteristics relative to trajectory T200-050; the analysis has been driven in STK environment.

5.2 Response Surfaces based on preliminary DV budget

For what has been said in Section 5.1.4, final trajectories found are the result of an assembly operation of many arcs, each patch point of these sections is characterized by the presence of certain discontinuity in terms of velocity. In order to overcome these irregularities a series of impulsive maneuvers, located at every patch point, is planned; each of them provides a change of velocity vector precisely fitted to void the discontinuity; Figure 5.12.

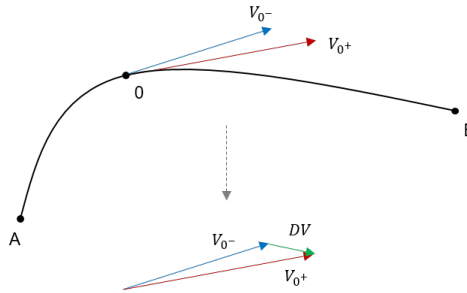


Figure 5.12: Graphical velocity discontinuity representation

It is clear that the sum of these maneuvers will represent a rough estimation of DV amount that the probe has to provide during his mission. Further improvements could drive the analysis to consider the effect of finite thrust and consequently to optimize time, modulus and direction of injections in order to couple two or many maneuvers and reduce the overall final DV cost.

5.2.1 DV budget estimation

Taking as reference the trajectory T200-050, evaluated considering an insertion angle in QPO of 180 degrees and as starting epoch the 15th of March 2019

at midnight, in this paragraph will be given an overview of the evaluated DV budget. Table 5.1 shows each DV modulus and related components expressed in the J2000 reference system (centered in the solar system barycenter), moreover the transfer phase and the QPO distinction has been highlighted. DV values are expressed in [m/sec]. Later in Section 5.2, it will be shown that even if the

Phase	Time of Ignition	DV (x)	DV (y)	DV (z)	DV
TRN	15 MAR 2019 01:00	3.4315	2.7089	1.4905	4.6190
TRN	15 MAR 2019 02:00	1.7045	2.9571	1.5558	3.7511
TRN	15 MAR 2019 03:00	0.4802	2.5202	1.2943	2.8736
TRN	15 MAR 2019 04:00	2.6009	5.2126	2.6285	6.3910
TRN	15 MAR 2019 16:00	5.7776	0.8979	0.5260	5.8705
TRN	16 MAR 2019 16:00	20.8553	7.5095	4.8575	22.6922
TRN	21 MAR 2019 16:00	32.1496	5.7517	4.5849	32.9803
TRN	26 MAR 2019 16:00	0.7093	5.8971	3.3989	6.8433
TRN	25 APR 2019 16:00	0.8567	2.4207	1.4234	2.9360
TRN	25 MAY 2019 16:00	5.8334	1.3602	0.1892	5.9929
TRN	24 JUN 2019 16:00	9.6357	1.9336	0.0620	9.8280
QPO	24 JUL 2019 16:00	0.8088	2.3407	1.8472	3.0895
QPO	23 AUG 2019 16:00	2.9345	6.6260	2.4636	7.6541
QPO	22 SEP 2019 16:00	0.9116	0.2968	0.5360	1.0984
QPO	22 OCT 2019 16:00	0.3923	0.6172	0.1327	0.7433
QPO	21 NOV 2019 16:00	5.3765	4.9539	2.5786	7.7519
QPO	21 DEC 2019 16:00	7.3940	3.3535	0.5734	8.1391
QPO	20 JAN 2020 16:00	2.5825	4.0702	0.7128	4.8727
QPO	19 FEB 2020 16:00	1.7713	4.9539	2.4088	5.7863
QPO	20 MAR 2020 16:00	1.0347	2.2523	0.6664	2.5667
QPO	19 APR 2020 16:00	2.6085	2.8771	1.7725	4.2689
QPO	19 MAY 2020 16:00	8.0102	0.9227	0.1221	8.0641
QPO	18 JUN 2020 16:00	6.7816	7.1932	2.6227	10.2279
Total DV estimation : 169.0406 [m/s]					

Table 5.1: Estimated DV

trajectory above mentioned presents really good results in terms of DV budget, actually ,in this sense, it is not the best which has been obtained, nevertheless it will be taken as an example in order to underline the effect of Moon perturbation.

Perturbation driven by the Moon

As it is possible to see from Table 5.1 two mesh points, the sixth and the seventh, respectively placed at 16 MAR 2019 16:00 and 21 MAR 2019 16:00, present higher values of DV corrections respect to the average of the others characterizing the trajectory taken into exam. Further analysis have shown that this behaviour strictly depends on the gravitational effect of the Moon. Perturbations driven by this body haven't been considered finding baseline solution, in fact, for this purpose, only the gravitational effect of Sun-Earth system has been taken into account, coherently with the CR3BP model. Figure 5.13 shows the weight of gravitational effect of both Sun and Earth over the total amount of force per unit of mass perceived by the probe. The force values are obtained

considering the complete force model, Chapter 3. It is clear that the trajectory section considered is distinguished by a sinusoidal pattern around values close to unit. These deviations are due to the Moon's gravitational effect, the probe, crossing regions delimited by mesh points 6 and 7, comes closer to the Moon. Actually, the probe, moving away from the Earth, keeps its distance from the Moon rather fixed, due to the particular combination of its trajectory and the Moon's orbit itself. This mutual motion increases Moon's perturbation to the CR3BP model, in fact, in this condition, Moon's gravitational field becomes less negligible respectively to the Earth and Sun fields. The perturbation caused by the presence of a fourth body to the CR3BP model solution is more important in this phase than in any other. This aspect forces the algorithm to find a more expensive solution, in terms of DV, to connect consecutive points. Further improvements could drive the analysis to consider a narrow and dense time span in order to optimize the launch Epoch and avoid negative contributions driven by Moon proximity. Taking as reference the time span considered in

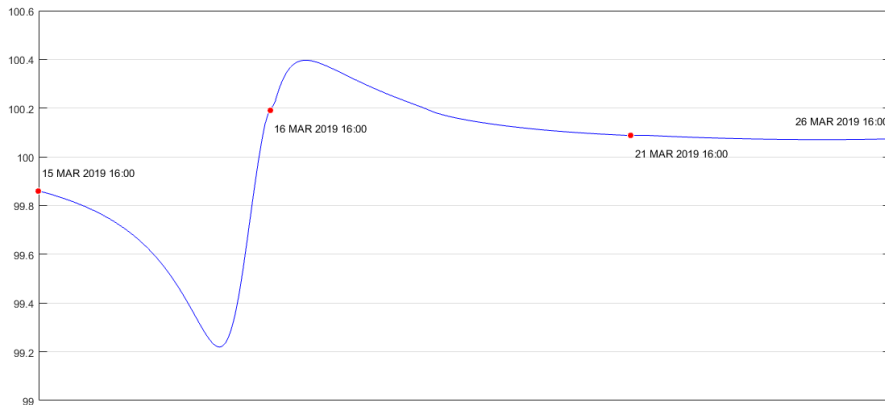


Figure 5.13: Percentage weight of Sun-Earth combined gravitational effect over total force per unit of mass perceived by the probe, evaluated according to the complete force model

the previous analysis, the trajectory section between 15 MAR 2019 16:00 and 26 MAR 2019 16:00, Figure 5.14, enlightens the condition which drives an increasing perturbation effect of Moon's gravitational attraction. As a matter of fact, during the period taken into exam, the probe moves away from the Earth, increasing constantly its distance from the planet, but remains rather at same distance from the Moon. The combined effect of these two conditions makes the attractive force contribution given by the satellite not negligible. During this phase the gravitational attractive force of the Moon weights on the complete force model for about 1-2%. Using the STK environment it is possible to have a clear representation of what has beforehand been discussed about; in Figure 5.15 it is possible to observe the evolution in time of mutual position of Earth, Moon and the hypothetical probe considered.

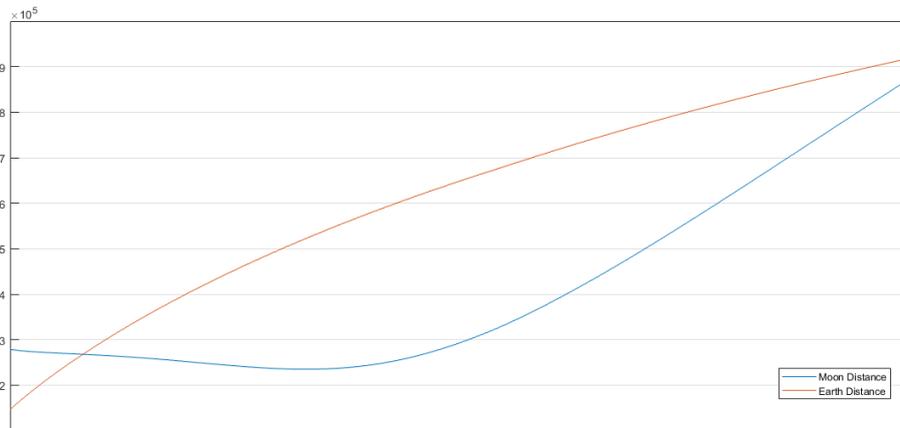
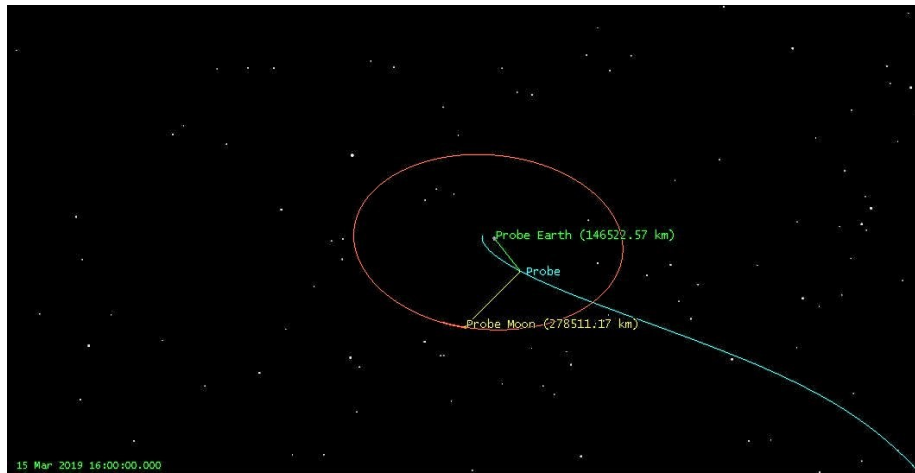


Figure 5.14: Probe distance from Earth and Moon, spanning from 15 MAR 2019 16:00 to 26 MAR 2019 16:00

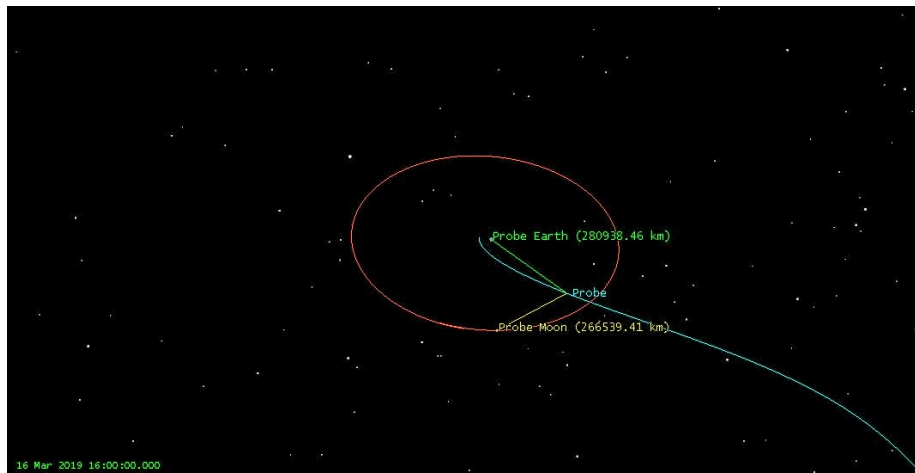
5.2.2 Building Response Surfaces

Owing to the procedure illustrated in this research, once geometrical parameters of the quasi-periodic orbit around the collinear libration point, L2 point in Sun-Earth system as benchmark, has been selected, the resulting QPO orbit, propagated considering the CR3BP model, is to be considered as the only univocal aspect which characterize the final result. It's necessary to introduce two more parameters to completely define the conclusive trajectory: the phase angle of insertion in the QPO, which determines the transfer phase, and the launch epoch, affecting the force model, in terms of gravitational body mutual position, where the probe will be included.

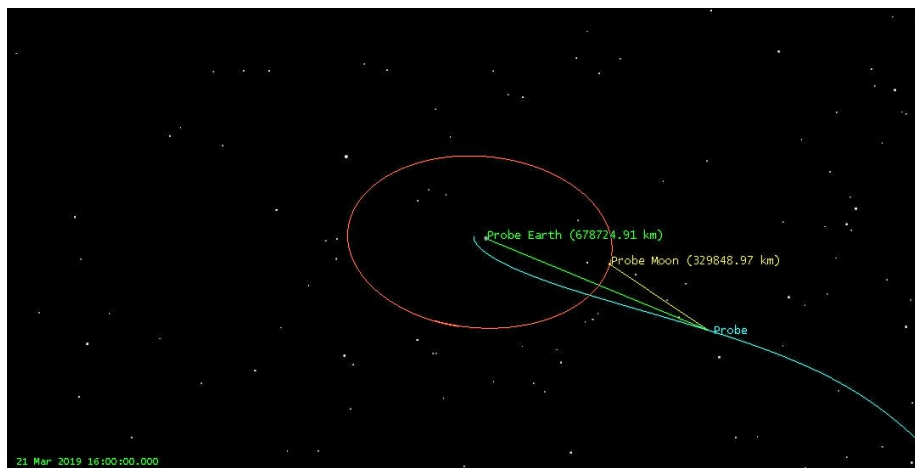
These variables define uniquely the final trajectory and they have been evaluated as design variables in an optimization process to find the solution characterized by lowest DV needs. Because of the impracticability of defining a function which relate the aforementioned trajectory characteristics and its DV budget, it has been necessary to resort to a statistic methodology. *Response Surface Methodology* (RSM) explores the relationships between several explanatory variables and one or more response variables. The method was introduced by George E. P. Box and K. B. Wilson [1]. The main idea of RSM is to use a sequence of designed experiments to obtain an optimal response, therefore a copious number of analysis have been performed in order to assign a rough DV estimation to every trajectory figuring out from the points considered building the variables domain, Section 5.1.2. Then the variables domain mesh has been tightened adding query points every 24 hours along the 'epoch axis' and every one single degree step along the 'phase angle axis'; the interpolated value at a single query point is thus based on a cubic interpolation of the values at neighboring grid points in each respective dimension. The interpolation is based on a cubic spline using not-a-knot end conditions. Such a response surface permits to better identify best directions of DV optimization, pointing to the most performant values of launch epoch and insertion phase angle; once an optimal region is located, more experiments could be driven considering a limited span. A similar method will reduce the computational cost of the analysis without



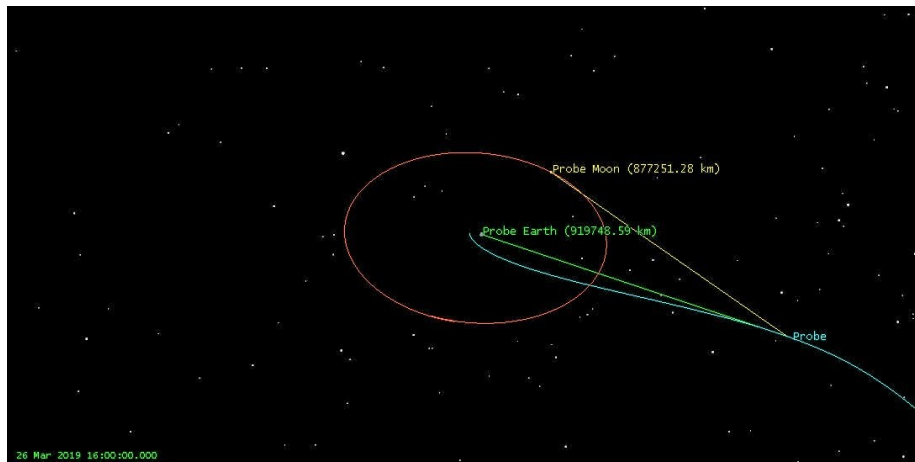
(a) 15 MAR 2019 16:00



(b) 16 MAR 2019 16:00



(c) 21 MAR 2019 16:00



(d) 26 MAR 2019 16:00

Figure 5.15: STK Visualization of relative positions of Earth, Moon and Probe at different mesh point epochs

significant lacks of information due to a bad conditioned variables pool.

Figure 5.16, 5.17 and 5.18 show the resulting response surfaces regarding three different baseline trajectories: T200-050, T200-010 and T300-050 respectively. According to 5.1.2 the analysis span along the entire 2019, considering the launch epoch variable, and between values of 135 degrees and 225 degrees, considering the insertion phase angle. Diagrams shown refer to *Day OTY* as value on y-axis, this variable concerns to the number of days past after the first of January 2019; furthermore *IPA* refers to the value of insertion phase angle considered. Along z-axis is reported the DV value relative to the single trajectory analyzed, expressed in m/s. These solutions have been chosen in order to figure out how the geometrical characteristics of target quasi periodic orbit influence the DV budget of the mission, in other words the aim of such a multiple analysis is to establish which type of QPO is more stable and is less affected by force model perturbations.

First of all it will be taken into account the response surface relative to T200-050, the benchmark solution, a trajectory characterized by a QPO build over a baseline Lissajous orbit with an x-axis amplitude of 200000 km and a z-axis amplitude of 50000 km; this surface is shown in Figure 5.16. Taking into consideration the diagram reporting level surfaces, it is possible to identify some remarkable regions. Foremost fundamental differences in terms of overall correction maneuvers cost are caused by variations of launch epoch; fixing the time variable and changing only the insertion phase angle value, less DV variations are registered. Two main regions of low DV cost come to notice. The first is placed between the day 50 and day 100 of 2019, approximately this time span refers to the month of March, in particular values of DV lower than 200 m/s are obtained considering insertion phase angles next to 135 degrees and 180 degrees. Solution proposed in Section 5.2.1 is just part of this region. Then increasing launch epoch values, moving forward through the year, a region of solutions characterized by elevated values of DV budget figures out. Nearby the

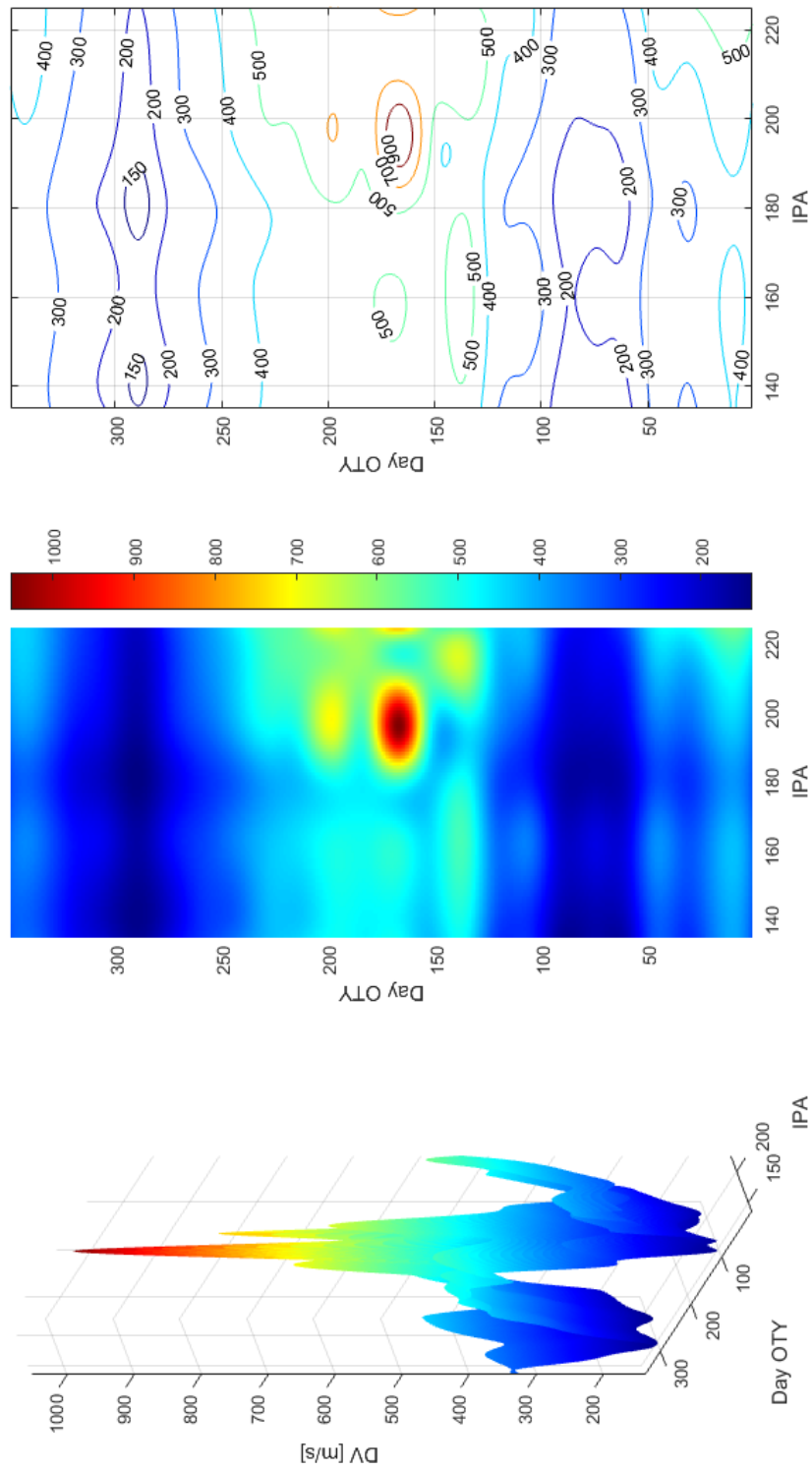


Figure 5.16: Response Surface, Trajectory T200-050

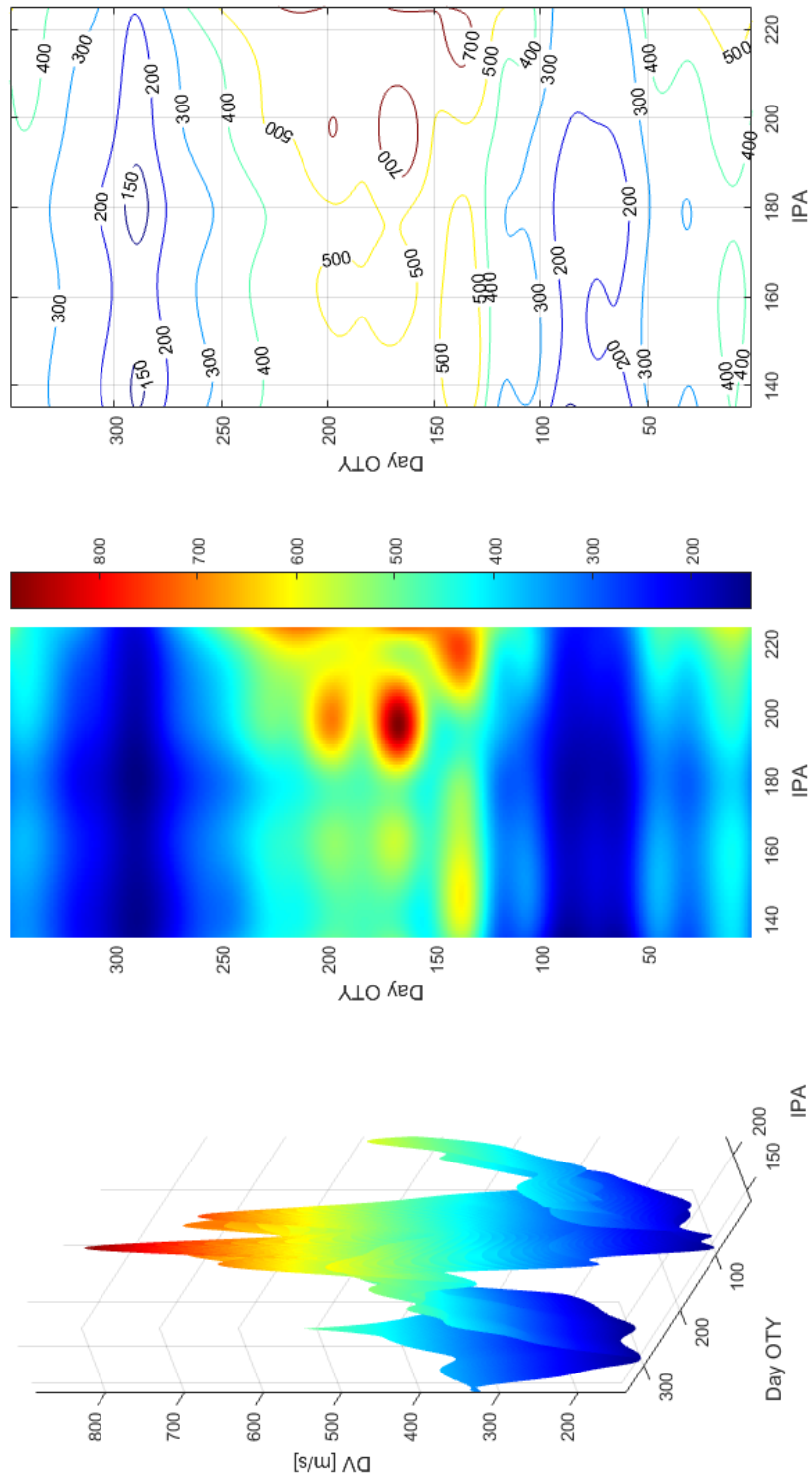


Figure 5.17: Response Surface, Trajectory T200-010

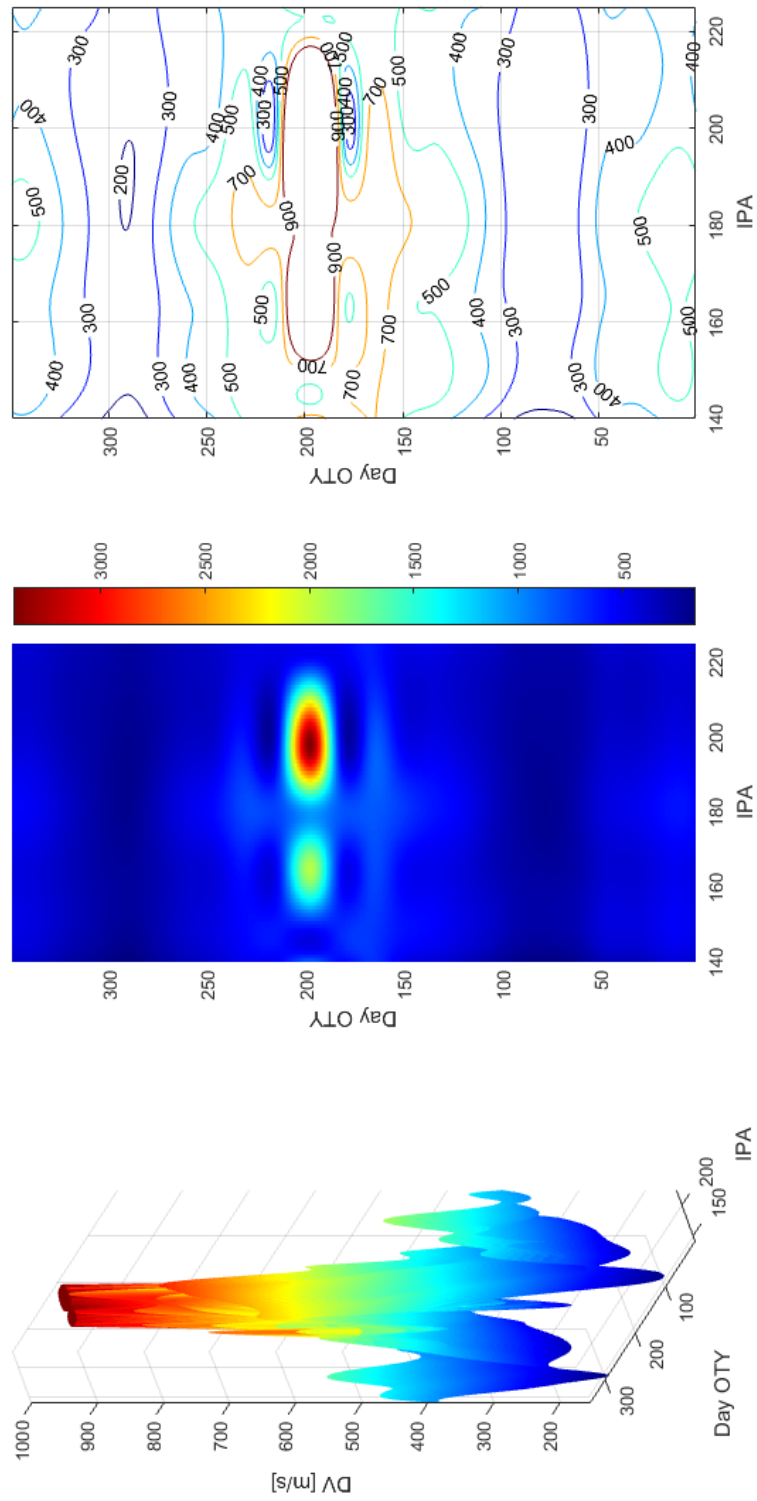


Figure 5.18: Response Surface, Trajectory T300-050

160th day of the year, it is possible to notice a particular region of variables domain presenting really low quality solution, DV values over 400 m/s, and a singularity up to 1 km/s due to badly conditioned launch epoch and transfer geometry affected by unfavorable mutual position of Sun, Earth and in particular Moon, which pass really close to the hypothetical probe. Going forward through the year another low overall maneuvers cost region comes out nearby day 300 of 2019; starting the mission during the second half of October could permit to reach really low values of DV budget, lower than 150 m/s considering again insertion phase angles next to 135 degrees and 180 degrees.

Paying now attention to Figure 5.17, relative to trajectory T200-010, it comes out that results found are pretty closer to them highlighted by the precedent analysis of T200-050. Regions of low and high DV budget are strictly the same in terms of both launch epoch and insertion phase angle; only remarkable difference is the magnitude of singularity registered at day 165 and phase angle 195, considering the aforementioned nature of this discontinuity, strictly related to punctual position of the Moon, it is possible to consider the response surfaces relative to T200-050 and T200-010 almost equivalent.

Lastly it is necessary to consider Figure 5.18 and the response surface regarding T300-050. In this case it is clear that final estimation of DV values are certainly higher than the beforehand mentioned cases. Analyzing the diagram reporting level surfaces, it comes out that considering quasi periodic orbits and relative transfers, geometrically similar to the T300-050 benchmark, drives the overall cost of the mission through higher average values along the time span of launch epoch; moreover in this case, larger portion of elevated DV singularity occurs. The nature of the discontinuity is always similar to the previously mentioned, however in this case the magnitude of the singularity is completely out of scale reaching values up to 3 km/s.

In Table 5.2 best solutions, relatively to baseline trajectory T200-050, are reported. Further in Section 5.2.3 they will be taken in consideration as objective of a deepened optimization process, aiming to reduce negative effects of Moon perturbation during the first phase of transfer to QPO.

Baseline Trajectory T200-050			
Launch Epoch	Insertion Phase Angle	DV [km/s]	Transfer [days]
15MAR2019	135	0.1705	90
15MAR2019	180	0.1690	120
15OCT2019	135	0.1520	90
15OCT2019	180	0.1378	120

Table 5.2: Best solution found, Trajectory T200-050

5.2.3 Final Optimization

Two different variables could be the objective of the last optimization process. Firstly an analysis of the time variable, the launch epoch, will be conducted in order to avoid main negative effects of Moon's perturbation; once a refined launch epoch will be obtained, the focus will move to the geometrical variable, the insertion phase angle. Lastly a completely refined solution, the optimized

trajectory, will be attained and in Section 5.3 will be simulated and further analyzed using the AGI's STK simulation tool.

It is necessary to remark that such an optimization process could be driven in different directions. The problem of finding suitable trajectories could be affected by multiple constraints dictated by scientific necessities or mission objectives, thus, for many reasons, the solution characterized by the lowest DV value could be useless or unsuitable. Nevertheless, due to the academic and theoretical purpose of this research, the refinement procedure will aim to search the global minimum over the variables domain.

Launch Epoch, avoid Moon perturbation

Referring to what has been discussed about in Section 5.2.1, in the first phase of transfer trajectory, the perturbation due to the Moon's gravitational attraction could not become negligible, causing an increase in terms of maneuvers entity to overcome this discontinuity in the force field. To precisely select the launch epoch could improve performances, however this problem is really sensitive to minimal variations of the initial conditions, thus it is necessary to consider a thicker time span than the one previously used. In this paragraph results reported in Table 5.2 will further be investigated and, keeping constant their geometrical characteristics, the analysis will span 10 days before and 10 days after the original launch epoch. Two days step will be adopted aiming to find better solutions in terms of overall maneuvers cost. Figure 5.19, 5.20, 5.21 and Figure 5.22 report results of the additional analysis operation.

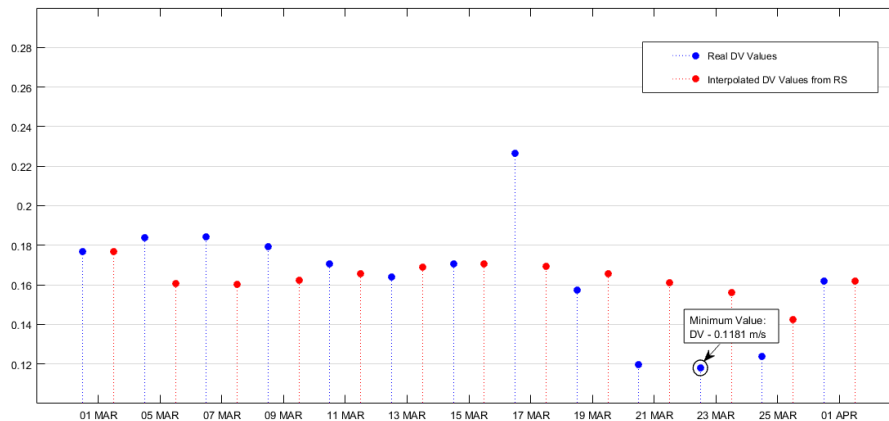


Figure 5.19: Overall DV values for T200-050, insertion phase angle 180 degrees; launch epoch spans from 01 MAR 2019 to 01 APR 2019

First of all focus must be pointed on differences between real DV values evaluated during the optimization process and interpolated values coming from response surfaces; the initial span of 15 days doesn't accomplish at all to precisely model the behaviour of the problem response, nevertheless it's adequately thick to locate regions of local minimum and maximum over the variables domain without worsening computational cost. Analyzing the achieved results it is possible to identify refined solutions regarding the four trajectories further analyzed (Table 5.2), resume of the optimized trajectories is shown in Table 5.3. By

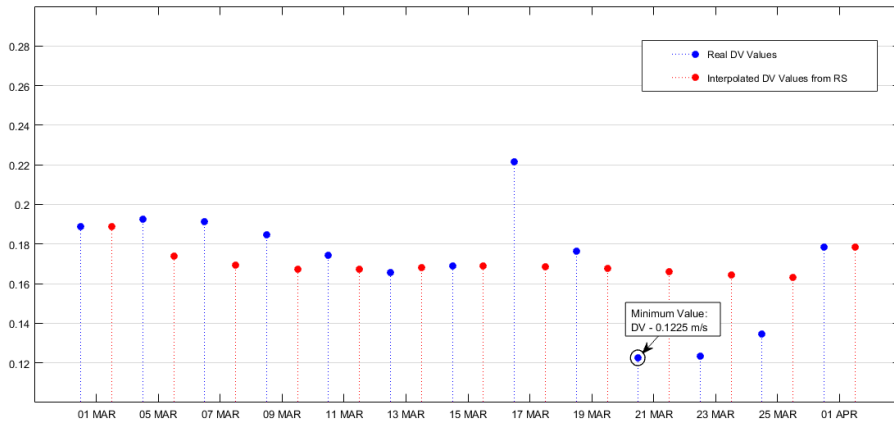


Figure 5.20: Overall DV values for T200-050, insertion phase angle 135 degrees; launch epoch spans from 01 MAR 2019 to 01 APR 2019

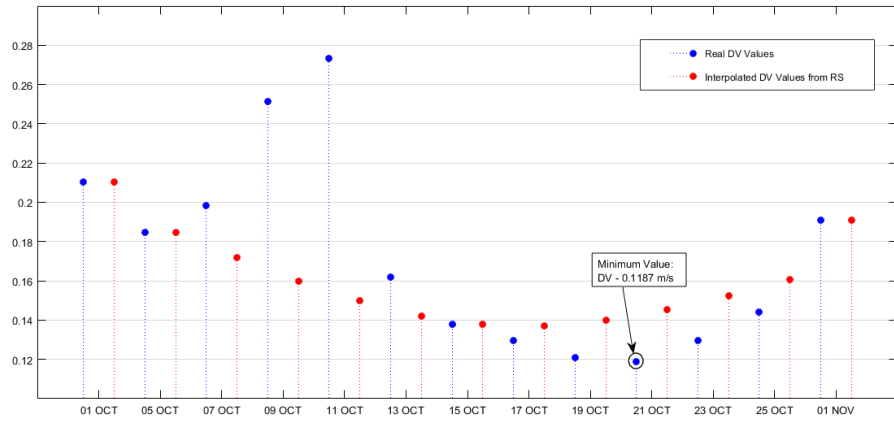


Figure 5.21: Overall DV values for T200-050, insertion phase angle 180 degrees; launch epoch spans from 01 OCT 2019 to 01 NOV 2019

reducing the time step between two consecutive values of launch epoch, it has been possible to take notice of effects due to the Moon gravitational force on the probe motion; to reduce performance losses in terms of DV, it is important to select an opportune value of the time variable, aiming to avoid disadvantageous configuration of Earth-Moon system and to avoid too much closer approach to the Earth' satellite.

This additional optimization process has reduced the overall maneuvers cost of considered trajectories by 30% in some cases, despite they were just best solutions of previous analysis. Further improvements could be attained reducing again the timestep or considering a larger number of solutions extrapolated from response surfaces, however considering the goodness of the achieved results and the nature of this research, trajectories displayed in Table 5.3 are considered properly refined and optimal for what concerns the launch epoch selection. Referring to these optimized solutions, it is possible to notice that the first (23 MAR 2019; IPA 135) and the fourth (21 OCT 2019; IPA 180) present almost

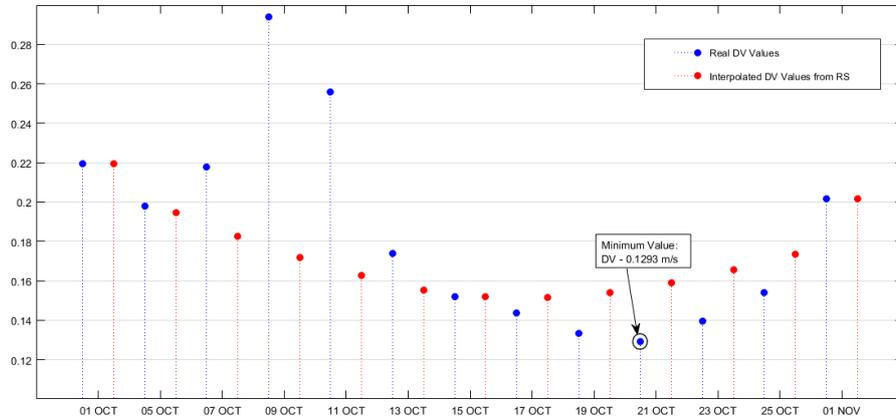


Figure 5.22: Overall DV values for T200-050, insertion phase angle 135 degrees; launch epoch spans from 01 OCT 2019 to 01 NOV 2019

the same value of DV budget, 0.118 m/s, which is the minimum value reached, thus both trajectories could be considered as the equivalent global minima of the domain.

Baseline Trajectory T200-050			
Launch Epoch	Insertion Phase Angle	DV [km/s]	Transfer [days]
23MAR2019	135	0.1181	90
21MAR2019	180	0.1225	120
21OCT2019	135	0.1293	90
21OCT2019	180	0.1187	120

Table 5.3: Refined solutions achieved optimizing the launch epoch, Trajectory T200-050

Insertion Phase Angle, transfer phase enhancement

The last step consists in precisely select the insertion phase angle in QPO. This variable doesn't affect particularly the nature of the consequent quasi periodic orbit (considering minimal deviations from the reference value), but could drive significant differences in geometrical characteristics of the transfer portion of the complete trajectory. These differences come out from the high sensitivity of the problem to the initial conditions, thus changing by few degrees the insertion phase angle could modify substantially the overall DV budget of the entire trajectory considered. Variations from reference values could scatter the attainments of the time variable optimization process. In this sense it is recommended to select all baseline trajectories, selecting insertion phase angle values, that will be objectives of response surfaces construction and then select a worthwhile launch epoch. Response Surfaces previously found could be considered affordable to such a theoretical purpose, nevertheless it is suggested to decrease the step between insertion phase angle values to obtain a more precise tool to investigate the variables domain; critically higher computational costs

have pushed away this type of analysis, however minimum values aforementioned could be considered really close to what has to be the optimal solution, in this sense dissimilarities are negligible.

5.3 STK Simulation

In this Section refined solutions evaluated in Section 5.2.3 will be simulated in the STK environment. The aim of such an activity is first to use the Astrogator tool with the purpose of validate the result obtained in terms of overall DV budget, secondly, to analyze trajectories found and better contextualize them. Systems Tool Kit (formerly Satellite Tool Kit), often referred to by its initials STK, is a physics-based software package from Analytical Graphics, Inc. that allows the user to perform complex analysis of ground, sea, air, and space assets, and share results in one integrated solution. At the core of STK is a geometry engine for determining the time-dynamic position and attitude of objects ("assets"), and the spatial relationships among the objects under consideration including their relationships or accesses given a number of complex, simultaneous constraining conditions. Using STK it is possible to perform multiple analysis and extrapolate report about physical condition, attitude, position et alii about multiple objects.

For what concerns to this research, once a refined solution has been evaluated, its ephemerides has been computed and imported in STK environment. The software uses the ephemerides data to create a *satellite object* describing the desired trajectory. Once this procedure has been accomplished, it is possible to start the simulation and get all sort of information desired. Figure 5.23, Figurefig:finalsim2 and Figure 5.25 show best trajectories assembled; further in this Chapter it will be referred to these as:

- PT135: baseline CR3BP trajectory T200-050, launch epoch at 23 MAR 2019 and insertion phase angle 135 degrees.
- PT180: baseline CR3BP trajectory T200-050, launch epoch at 21 OCT 2019 and insertion phase angle 180 degrees.

5.3.1 Result Validation

The aim of this Section is to validate results obtained in terms of DV budget and geometrical conformity concerning both PT135 and PT180. To do this a validation procedure has been designed by means of the STK's Astrogator tool. In particular the Astrogator tool can manage independently an analysis procedure designed to target the necessary instant maneuver, starting from a defined state vector, to reach, for instance, a selected point in the space with a certain tolerance. Thus the analysis is structured as follows: first of all every mesh point of considered trajectories will be imported in STK environment, actually, to start the propagation, the state vector of the first mesh point is needed, then Astrogator will connect autonomously each mesh point, creating trajectory arcs and planning instant maneuvers at these connection points. For this purpose, the software's propagator takes count of main Solar system bodies gravitational

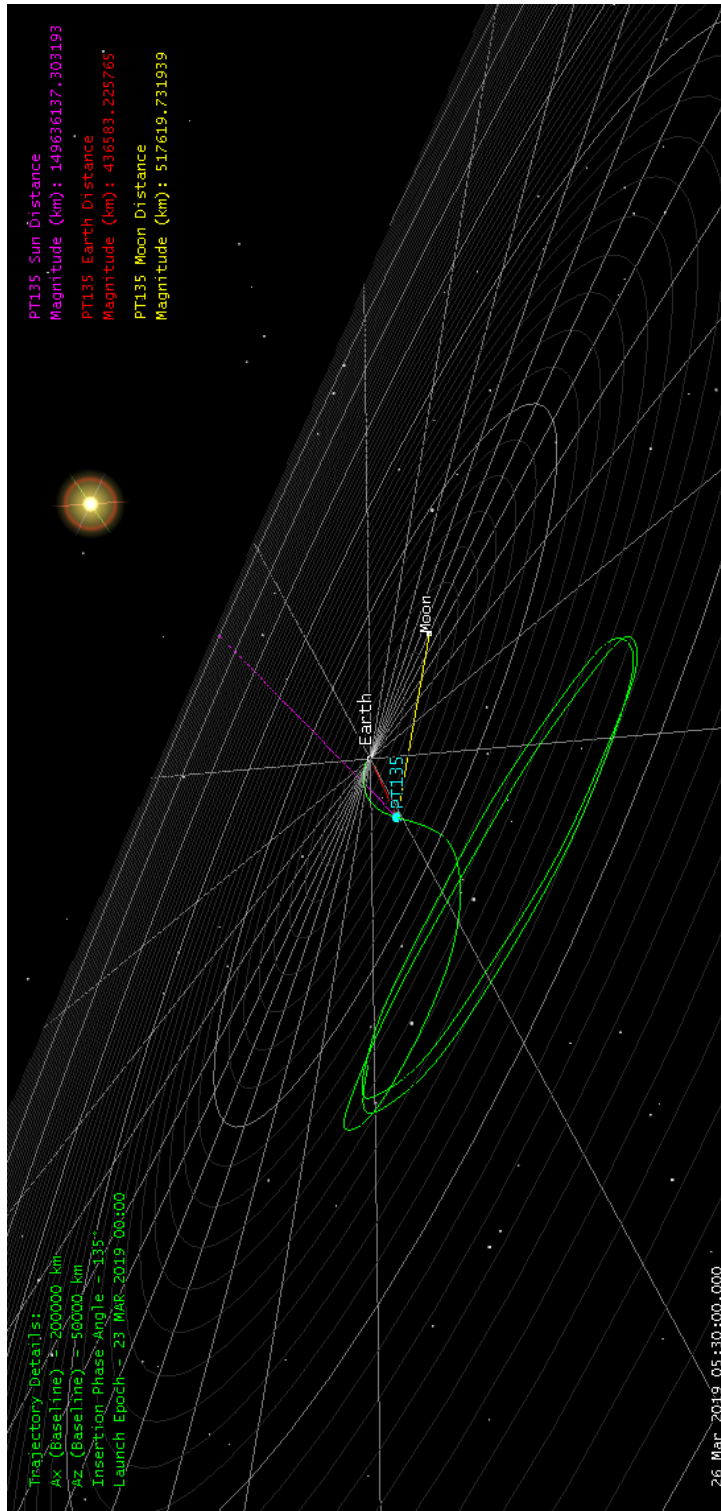


Figure 5.23: Simulation of PT135 trajectory

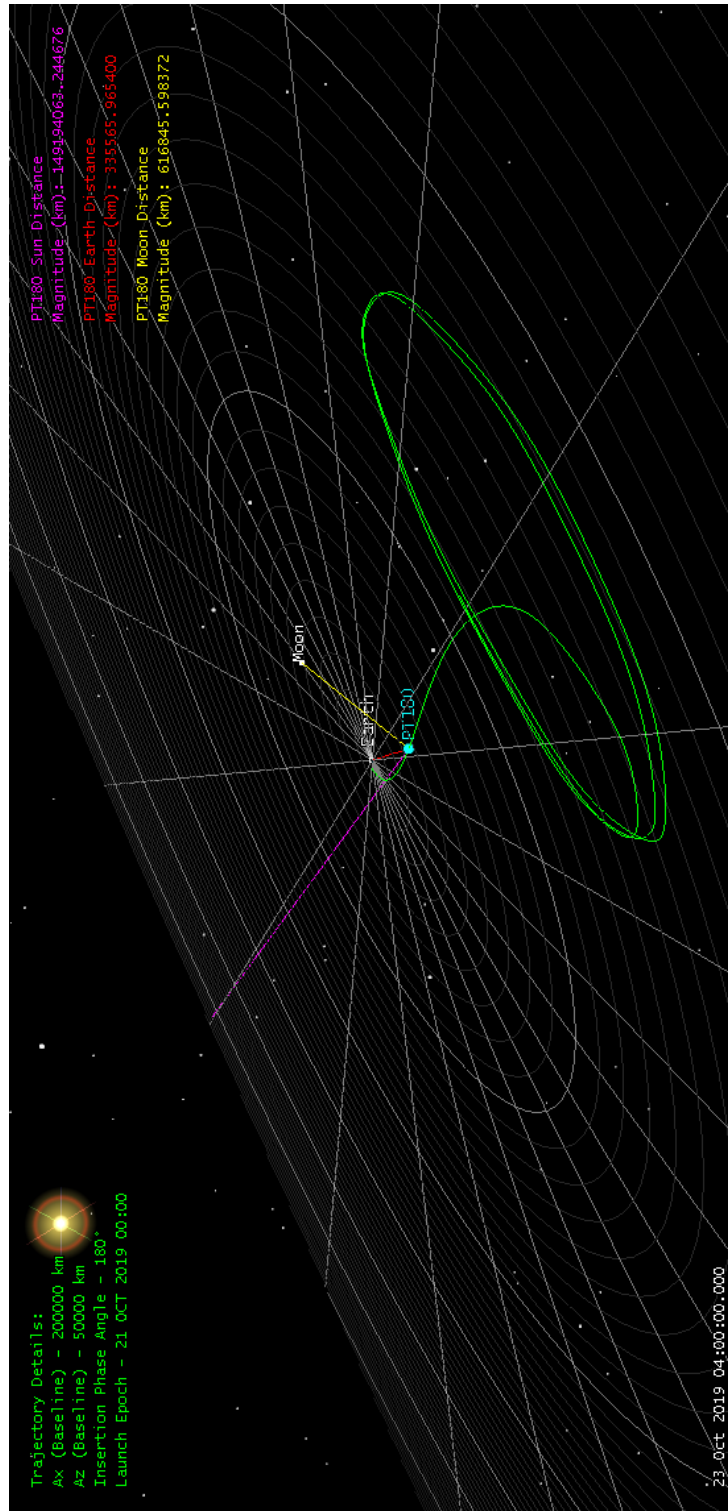


Figure 5.24: Simulation of PT180 trajectory

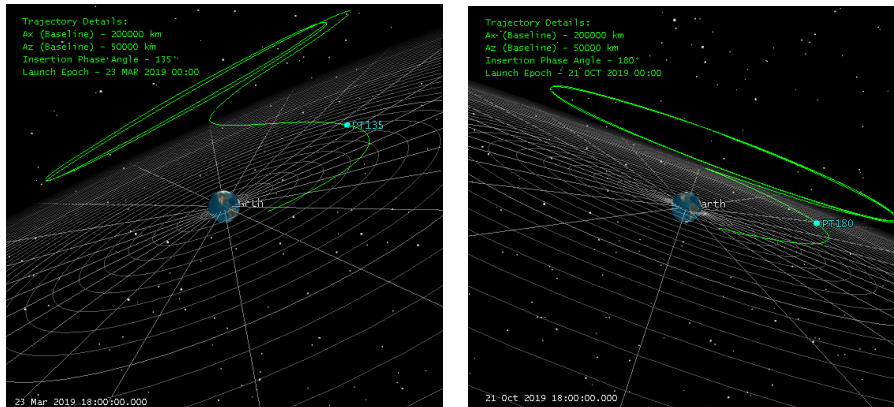


Figure 5.25: Different Views of Simulated PT135 and PT180

force, additionally also the solar radiation pressure is considered by means of a spherical solar radiation pressure model. Notice that the conformity between the complete force model introduced in Chapter 3 and the internal STK propagation tool has been guaranteed. Thus, the designed validation procedure, will collect the resulting DV values, comparing these with reference evaluated values of PT135 and PT180. Besides the geometric conformity between the aforementioned trajectories and the Astrogator simulation will be verified. Validation results will be shown simultaneously for both PT135 and PT180 referring firstly to DV budget considerations, then the focus will be pointed on the trajectory correspondence.

DV Budget Validation

Table 5.4 and Table 5.5 show the DV budget confrontation between values regarding the aforementioned PT135 and PT180 and the relative trajectories built and simulated using Astrogator. For each ignition point are reported maneuvers DV magnitudes of both evaluated trajectory and the simulated equivalent, then it has been calculated the percentage deviation of the simulated value from the reference one. DV values are expressed in [m/s]. Achieved results by means of STK simulation highlight the effectiveness of evaluated performances, as regards the optimal trajectories found, in terms of overall DV budget. In fact both single maneuvers magnitude and the total budget estimation present values of percentage error lower than 1% respect to both PT135 and PT180 parameters. Actually, considering both cases, it is possible to observe that the first maneuver magnitude, is characterized by a deviation more significant than the others, even if this deviation remain below the 5%. This singularity is due to the particular proximity to the Earth. At such these distances the perturbation caused by the Earth oblateness and its non-spherical gravitational field becomes non negligible. In this sense differences between gravitational models adopted by STK and the designed force model (Chapter 3), could generate such an error, higher than everyone else, but still negligible considering the purpose of this research.

Time of Ignition	PT135 DV	Astrogator DV	Percentage Error
23 MAR 2019 01:00	1.7174	1.7501	+1.8685
23 MAR 2019 02:00	1.3149	1.3172	+0.1746
23 MAR 2019 03:00	0.9705	0.9760	+0.5635
23 MAR 2019 04:00	2.1211	2.1274	+0.2961
23 MAR 2019 16:00	0.9139	0.9148	+0.0984
24 MAR 2019 16:00	5.6581	5.6576	-0.0088
29 MAR 2019 16:00	10.9959	10.9961	+0.0018
03 APR 2019 16:00	12.8069	12.8105	+0.0281
03 MAY 2019 16:00	6.0251	6.0324	+0.1210
02 JUN 2019 16:00	9.0496	9.0544	+0.0530
02 JUL 2019 16:00	17.5984	17.6045	+0.0347
01 AUG 2019 16:00	6.1643	6.1687	+0.0713
31 AUG 2019 16:00	6.8385	6.8427	+0.0614
30 SEP 2019 16:00	4.1856	4.1927	+0.1693
30 OCT 2019 16:00	2.1075	2.1134	+0.2792
29 NOV 2019 16:00	5.8436	5.8457	+0.0359
29 DEC 2019 16:00	5.0975	5.1020	+0.0882
28 JAN 2020 16:00	6.7350	6.7397	+0.0697
27 FEB 2020 16:00	5.9400	5.9435	+0.0589
28 MAR 2020 16:00	2.1514	2.1597	+0.3843
27 APR 2020 16:00	2.7250	2.7326	+0.2781
27 MAY 2020 16:00	1.1666	1.1661	-0.0429
Total DV estimation	118.1269	118.2460	+0.1007

Table 5.4: DV Budget Validation, PT135

Geometric Conformity

The focus is now pointed on geometric characteristics of simulated trajectories. It's important to verify that the propagated multiple arcs don't separate from the reference trajectory which it is trying to retrace. In this sense in Figure 5.26 and Figure 5.27 are shown mutual distances between two hypothetical probes traveling along the simulated and the reference trajectories PT135 and PT180. As it is possible to observe, this deviation remains under 10 km considering both cases. It is possible to assert that the simulated result essentially coincides with trajectories previously built, PT135 and PT180. Discontinuities in diagrams come across each time of ignition where the two trajectories obviously coincide and the mutual distance between probes is zero. These discontinuities are due to the time step considered to plot diagrams. It has been considered a step value of one hour, in such a time period, probes cover much larger space than the relative distance between them, thus this results in a discontinuity in distance evolution when probes' trajectories coincide, exactly at ignition points.

These results validate the goodness and the practicability of PT135 and PT180 in addition to the correctness of the procedure presented by this research aiming to the construction of an hypothetical transfer to a periodic orbit around collinear libration point L2 in Sun-Earth system and its up-keeping.

Time of Ignition	PT180 DV	Astrogator DV	Percentage Error
21 OCT 2019 01:00	0.5628	0.5482	-2.6633
21 OCT 2019 02:00	0.5033	0.5032	-0.0199
21 OCT 2019 03:00	0.4115	0.4092	-0.5621
21 OCT 2019 04:00	0.8191	0.8169	-0.2693
21 OCT 2019 16:00	0.9430	0.9429	-0.0106
22 OCT 2019 16:00	6.9963	6.9969	+0.0086
27 OCT 2019 16:00	11.8111	11.8123	+0.0102
01 NOV 2019 16:00	7.3582	7.3531	-0.0694
01 DEC 2019 16:00	4.4644	4.4570	-0.1660
31 DEC 2019 16:00	7.9610	7.9600	-0.0126
30 JAN 2020 16:00	4.1053	4.1116	+0.1532
29 FEB 2020 16:00	12.6751	12.6758	+0.0055
30 MAR 2020 16:00	1.5894	1.5925	+0.1947
29 APR 2020 16:00	3.8368	3.8383	+0.0391
29 MAY 2020 16:00	3.0389	3.0424	+0.1150
28 JUN 2020 16:00	10.3953	10.3940	-0.0125
28 JUL 2020 16:00	6.3964	6.3931	-0.0516
27 AUG 2020 16:00	3.6985	3.6964	-0.0568
26 SEP 2020 16:00	0.7437	0.7497	0.8003
26 OCT 2020 16:00	5.4313	5.4298	-0.0276
25 NOV 2020 16:00	4.2393	4.2316	-0.1820
25 DEC 2020 16:00	10.2286	10.2262	-0.0235
24 JAN 2021 16:00	10.4883	10.4834	-0.0467
Total DV estimation	118.6975	118.6645	-0.0278

Table 5.5: DV Budget Validation, PT180

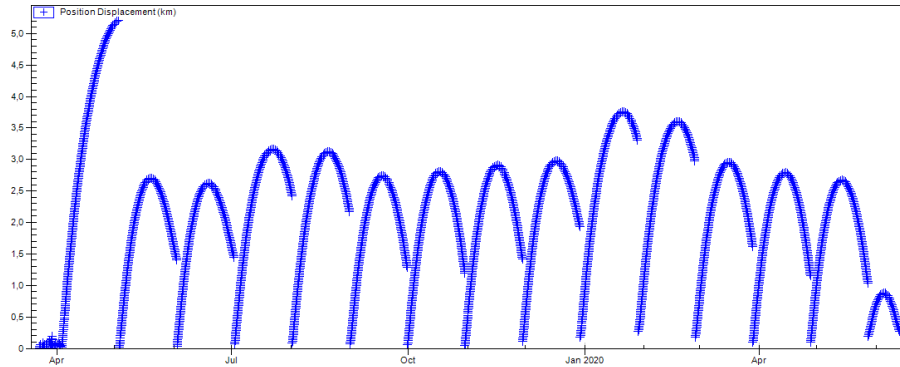


Figure 5.26: Deviation between PT135 and the related simulated trajectory

5.3.2 Analysis Report

STK gives the possibility of extrapolating all sort of physical data regarding many objects belonging to the contemplated scenario. Therefore will be presented the main characteristics of PT135 and PT180 coming out from STK simulation; pointing in particular on mutual distances between the hypothetical probe traveling along the considered trajectory and the main bodies which are

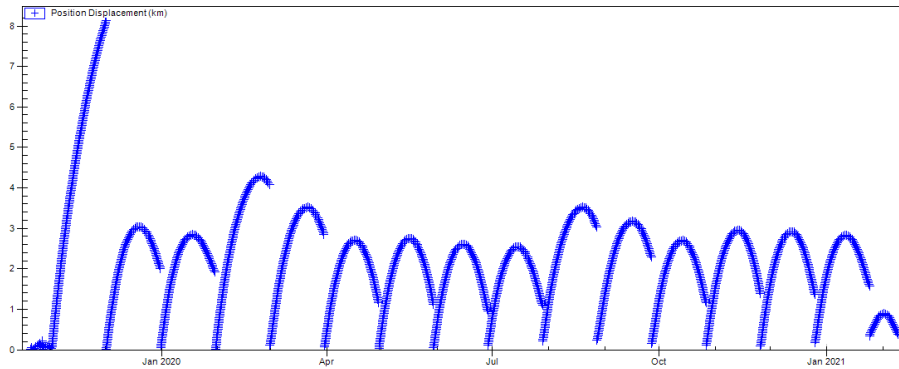


Figure 5.27: Deviation between PT180 and the related simulated trajectory

perturbing the force field, Sun, Earth and Moon. Secondly will be reported the evolution of the acceleration magnitude perceived by the probe, in particular this aspect will be related to mutual position of system’s main bodies.

Main Bodies Distances

Figure 5.28 and Figure 5.29 show distances values from Sun, Earth and Moon regarding the beforehand mentioned probe, for what concerns PT135 and PT180.

First of all, looking at diagrams shown in Figure 5.28 and Figure 5.29, it’s

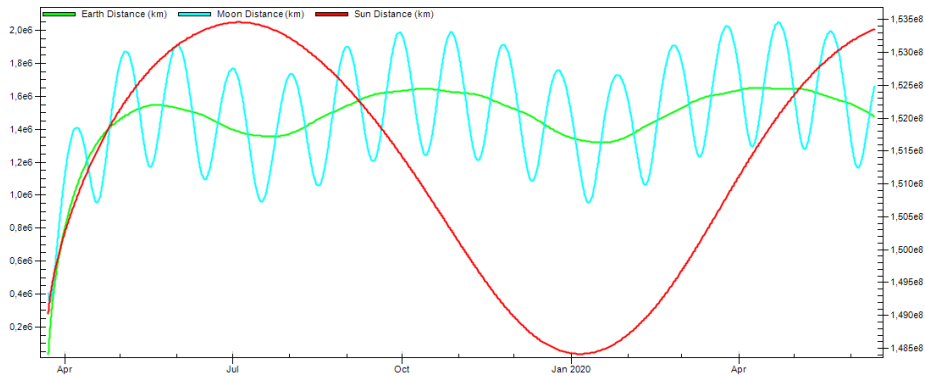


Figure 5.28: Distances Values Evolution, PT135

clear the sinusoidal behaviour of the evolution of Sun distance value; trajectories PT135 and PT180 are strictly related to the Earth’s revolution motion, thus it is expected an year-long periodicity for what concerns mutual position between Earth and Sun. Considering that these two bodies essentially define the considered force field, the choice of analyzing the time variable, the launch epoch, over a year period is justified. Secondly, paying attention to Earth distance and Moon distance trends, it is possible to observe that evaluating both PT135 and PT180 cases, the Earth is always much closer to the probe than the Moon until it reaches a distance from the Earth of about $1e6$ km. This value represents essentially the radius of the Earth’s sphere of influence. Thus, from this point, even if the Moon could be closer to the probe than the Earth, it’s

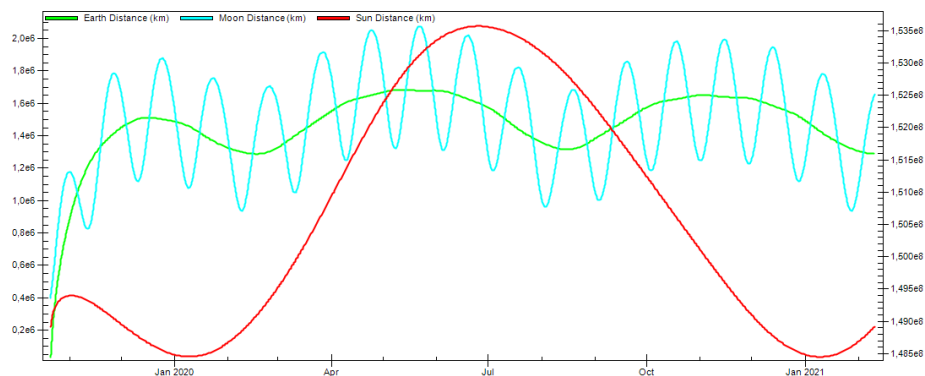


Figure 5.29: Distances Values Evolution, PT180

too much distant from the trajectory considered to be taken in consideration as a critical perturbation to the force field, which is still mainly defined by the Sun-Earth system gravitational field. What has just been said agrees with arguments fully investigated in Section 5.2.3.

Acceleration Magnitude

Figure 5.30 and Figure 5.31 show acceleration magnitude values regarding the beforehand mentioned probe, for what concerns PT135 and PT180. Dia-

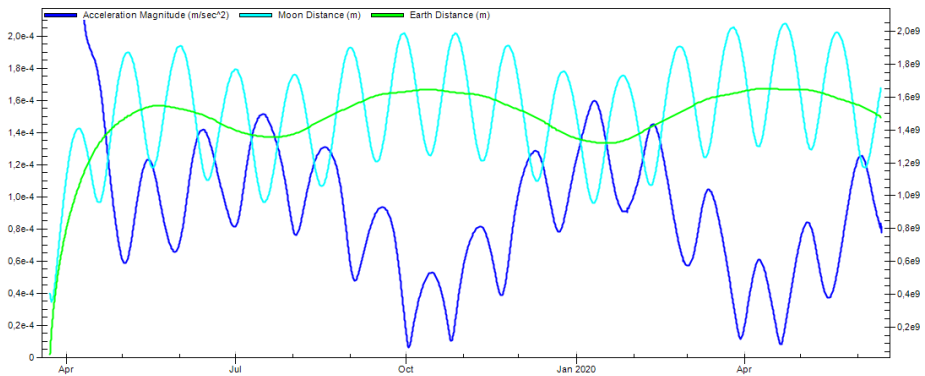


Figure 5.30: Acceleration Values Evolution, PT135

grams report again distances evolution from Earth and Moon, these variables are useful to analyze the acceleration trend. As it is possible to observe from the diagrams shown, considering both reference trajectories, acceleration values decrease rapidly escaping from the Earth. This drastic drop, Figure 5.32, stops once the acceleration reaches values swinging between 0.2 mm/sec^2 and 0.01 mm/sec^2 . This range is defined by the position of the hypothetical probe in the Sun-Earth system, in other words the magnitude of the acceleration, the entity of the force field, is essentially sized by the Earth and Sun gravitational attraction. However it is very interesting to point out that the acceleration evolution, after the main initial drop, presents a two-way sinusoidal nature. Firstly, acceleration values swing due to the motion of the Earth; as it is possible to observe

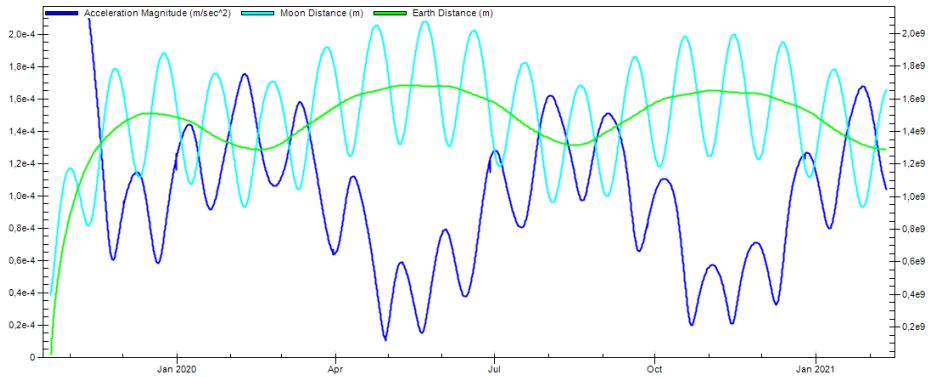


Figure 5.31: Acceleration Values Evolution, PT180

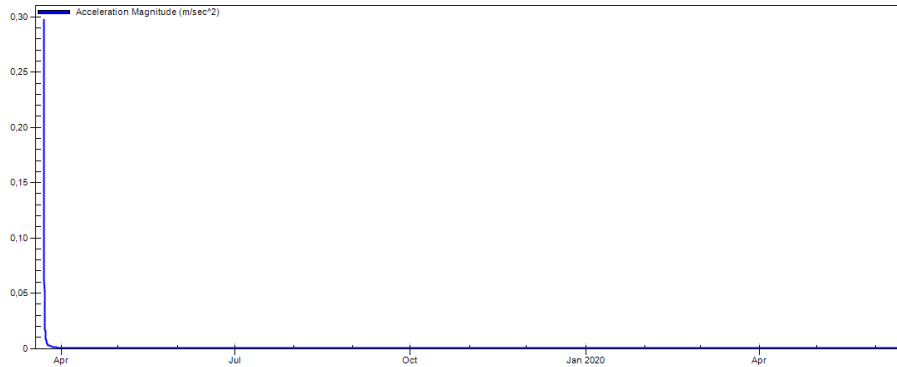


Figure 5.32: Acceleration Values Evolution, enlarged visual; from this diagram it is possible to observe the initial drop

from diagrams in Figure 5.30 and in Figure 5.31 the trend presents a peak when the Earth is much closer and vice versa. A second sinusoidal trend nestles in the first, this one is due to the Moon motion; again the acceleration raises to a local maximum when the probe is closer to the Moon. Obviously the Moon presence doesn't substantially affect the overall acceleration magnitude, it causes oscillations around a trend defined mainly by the Sun-Earth gravitational field.

5.3.3 Ignition Sequence Optimization

Analyzing the evaluated DV budget, it is possible to notice that the first section of the transfer phase is generally characterized by a large number of ignitions at low level of DV magnitude. First of all a good trajectory must consider the least possible number of corrections. Moreover, during the initial phase of the trajectory, higher values of acceleration affect the probe's motion, due to the Earth's gravitational field, so lower DV couldn't be attained considering the precision needed. To overtake these problems an analysis of the ignition sequence has been accomplished examining both PT135 and PT180. Some ignitions will be merged selecting only fewer mesh points where apply trajectory corrections. Choosing the optimal mesh points where plan new maneuvers is fundamental, as a matter of fact that the overall DV budget could drastically increase scaling

Time of Ignition	PT135 DV	Corrected DV
23 MAR 2019 01:00	1.7174	-
23 MAR 2019 02:00	1.3149	-
23 MAR 2019 03:00	0.9705	-
23 MAR 2019 04:00	2.1211	-
23 MAR 2019 16:00	0.9139	6.4419
24 MAR 2019 16:00	5.6581	-
29 MAR 2019 16:00	10.9959	-
03 APR 2019 16:00	12.8069	-
03 MAY 2019 16:00	6.0251	7.3375
02 JUN 2019 16:00	9.0496	9.0544
02 JUL 2019 16:00	17.5984	17.6045
01 AUG 2019 16:00	6.1643	6.1687
31 AUG 2019 16:00	6.8385	6.8427
30 SEP 2019 16:00	4.1856	4.1927
30 OCT 2019 16:00	2.1075	2.1134
29 NOV 2019 16:00	5.8436	5.8457
29 DEC 2019 16:00	5.0975	5.1020
28 JAN 2020 16:00	6.7350	6.7397
27 FEB 2020 16:00	5.9400	5.9435
28 MAR 2020 16:00	2.1514	2.1597
27 APR 2020 16:00	2.7250	2.7326
27 MAY 2020 16:00	1.1666	1.1661
Total DV estimation	118.1269	93.1801

Table 5.6: DV Budget Comparison, PT135

badly the mesh point sequence. Once this new sequence is selected, using again the STK Astrogator tool, it is possible to propagate the modified trajectory and evaluate the overall DV budget. Table 5.6 and Table 5.7 show corrected DV budget taking in exam both PT135 and PT180.

As it is possible to observe, modified trajectories present less correction points during the transfer phase. Anyway overall DV budget value is rather similar to them previously evaluated, even lower. The ignition sequences have been modified in order to optimize the transfer phase, whereas the up-keeping phase in the quasi-periodic orbit remain strictly the same in both cases. The generic QPO is characterized by low values of acceleration, so even low DV magnitude could be achieved without lack of precision. Furthermore even if higher time step between subsequent ignition points are feasible, analyzing precedent missions constraints, it is clear that taking as reference a period of 30 days between two corrections represents a good compromise between the objective of reduce the overall DV budget and the need of satisfy scientific mission requirements. Corrected trajectories are similar and geometrically coherent with PT135 and PT180, differences in terms of ephemerides are negligible. Obviously these modified trajectories are obtained modifying the initial conditions of the transfer phase respect to the original. Considering PT135 it is necessary to consider a velocity variation, respect to initial condition of the transfer phase, of 3.75 m/s magnitude; considering PT180 a variation of 0.85 m/s occurs. However these

Time of Ignition	PT180 DV	Corrected DV
21 OCT 2019 01:00	0.5628	-
21 OCT 2019 02:00	0.5033	-
21 OCT 2019 03:00	0.4115	-
21 OCT 2019 04:00	0.8191	-
21 OCT 2019 16:00	0.9430	-
22 OCT 2019 16:00	6.9963	6.3719
27 OCT 2019 16:00	11.8111	-
01 NOV 2019 16:00	7.3582	-
01 DEC 2019 16:00	4.4644	3.9892
31 DEC 2019 16:00	7.9610	7.9600
30 JAN 2020 16:00	4.1053	4.1116
29 FEB 2020 16:00	12.6751	12.6758
30 MAR 2020 16:00	1.5894	1.5925
29 APR 2020 16:00	3.8368	3.8383
29 MAY 2020 16:00	3.0389	3.0424
28 JUN 2020 16:00	10.3953	10.3940
28 JUL 2020 16:00	6.3964	6.3931
27 AUG 2020 16:00	3.6985	3.6964
26 SEP 2020 16:00	0.7437	0.7497
26 OCT 2020 16:00	5.4313	5.4298
25 NOV 2020 16:00	4.2393	4.2316
25 DEC 2020 16:00	10.2286	10.2262
24 JAN 2021 16:00	10.4883	10.4834
Total DV estimation	118.6975	96.0108

Table 5.7: DV Budget Comparison, PT180

variations could be transferred to the hypothetical launch phase, which is not taken in consideration for the purpose of this research.

Conclusions

The design procedure proposed seems to provide significant results in terms of trajectory design and optimization. The obtained trajectories demonstrate geometric conformity and comparable overall cost to the ones that have been previously adopted, Section 1.4.

Results from Chapter 5 indicate that it is possible to optimize, alongside the investigation of the particular variables domain designed, both the transfer phase and the station-keeping in the quasi periodic orbit aiming to reduce the DV budget in terms of number and overall cost of the planned maneuvers. The resulting response surfaces highlight particular low DV areas in terms of departure epoch, this depends from the periodically variations of mutual positions of Earth and Sun. Furthermore, it has been identified the strong influence of the Moon gravitational field on the very first portion of the transfer phase. The launch epoch has revealed itself as the dominant variable in terms of trajectory optimization, the effect of the geometry of QPO insertion is clearly concrete, but less preponderant.

The adoption of a simulation software has validate both the complete force model proposed in this research and the design process developed to obtain the particular trajectories object of this work. In addition, this validation process, has provided further analysis from which it has been possible to better optimize the overall ignition sequence, by reducing the overall DV cost of 15%-20% from previous results.

Finally, a further optimization step could be achieved properly designing the launch phase, better defining the strategy of insertion in the transfer phase.

Bibliography

- [1] G. E. P. Box and K.B. Wilson. “On the Experimental Attainment of Optimum Conditions”. In: *Journal of the Royal Statistic Society B-13.1* (1951), pp. 1–45.
- [2] James R. Newman. “Commentary on Isaac Newton”. In: *The World of Mathematics 1* (1956).
- [3] V. Szebehely and G. E. O. Giacaglia. “On the Elliptic Restricted Problem of Three Bodies”. In: *Astronomical Journal* 69 (1964), pp. 230–235.
- [4] V. Szebehely. *Theory of Orbits: The Restricted Problem of Three Bodies*. Academic Press, 1967. ISBN: 9780124124318.
- [5] D. D. Mueller R.R. Bate and J. E. White. *Fundamentals of Astrodynamics*. Dover Publications Inc., 1971. ISBN: 9780486600611.
- [6] J. R. Dormand and P. J. Prince. “A family of embedded Runge-Kutte formulae”. In: *J. Compl. Appl. Math.* 6 (1980), pp. 19–26.
- [7] F. L. Markley. “Approximate Cartesian State Transition Matrix”. In: *Journal of the Astronautical Sciences* 34 no. 2 (1986), pp. 161–169.
- [8] K. C. Howell and H. J. Pernicka. “Numerical Determination of Lissajous Trajectories in the Restricted Three Body Problem”. In: (1987).
- [9] David A. Vallado. *Fundamentals of Astrodynamics and Applications*. The McGraw-Hill Companies, 1997. ISBN: 9781881883142.
- [10] M.Marcote E. Canalias G.Gomez and J.J.Masdemont. *Assessment of Mission Design Including Utilization of Libration Points and Weak Stability Boundaries*. Department de Matematica Aplicada, Universitat Politecnica de Catalunya and Department de Matematica Aplicada, Universitat de Barcellona., 2004.
- [11] ESA Website. *Euclid*. URL: <http://sci.esa.int/euclid/>.
- [12] ESA Website. *Gaia*. URL: <http://sci.esa.int/gaia/>.
- [13] ESA Website. *Herschel*. URL: <http://sci.esa.int/herschel/>.
- [14] ESA Website. *Lisa Pathfinder*. URL: <http://sci.esa.int/lisa-pathfinder/>.
- [15] ESA Website. *SOHO*. URL: <http://sci.esa.int/soho/>.
- [16] JPL Website. *Solar System Dynamics*. URL: <https://ssd.jpl.nasa.gov/>.